

Chapter 5

Spin Transfer Torque

韩伟

量子材料科学中心

2016年11月15日

Outline

1. Spin transfer torque

2. Spin orbit torque and spin Hall effect

3. Spin orbit torque and Rashba-Edestein effect

Review of last class

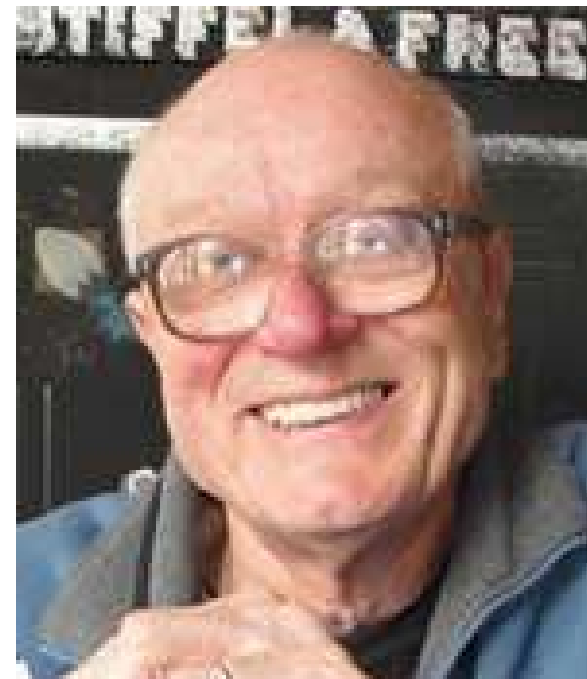
- 1. Theory and observation of spin transfer torque**
- 2. Spin transfer torque and spin pumping**
- 3. Spin transfer torque in MTJ and Domain wall motion**
- 4. Spin transfer torque in domain wall motion**
- 5. Thermal spin transfer torque**
- 6. Pure Spin current transfer torque**

Review of last class

John Slonczewski



Luc Berger



This class

1. Spin orbit torque

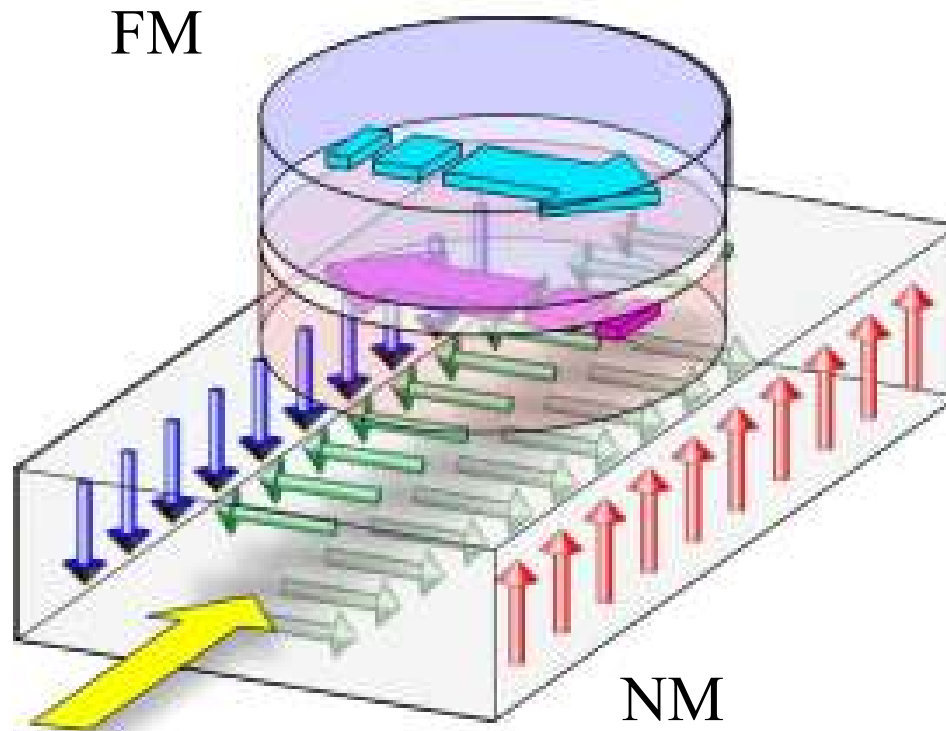
2. Spin Hall effect

3. Rashba-Edelstein effect

Outline

1. Spin orbit torque

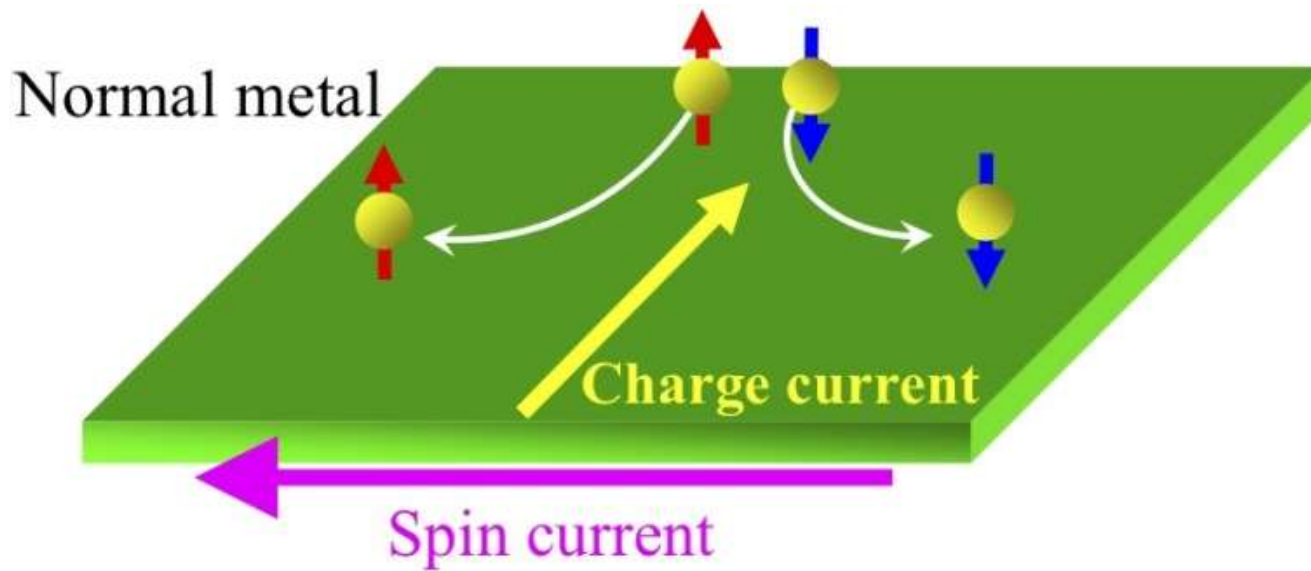
Spin orbit torque



$$\tau_{ST} = \frac{\hbar}{2} \hat{m} \times (\hat{\sigma} \times \hat{m})$$

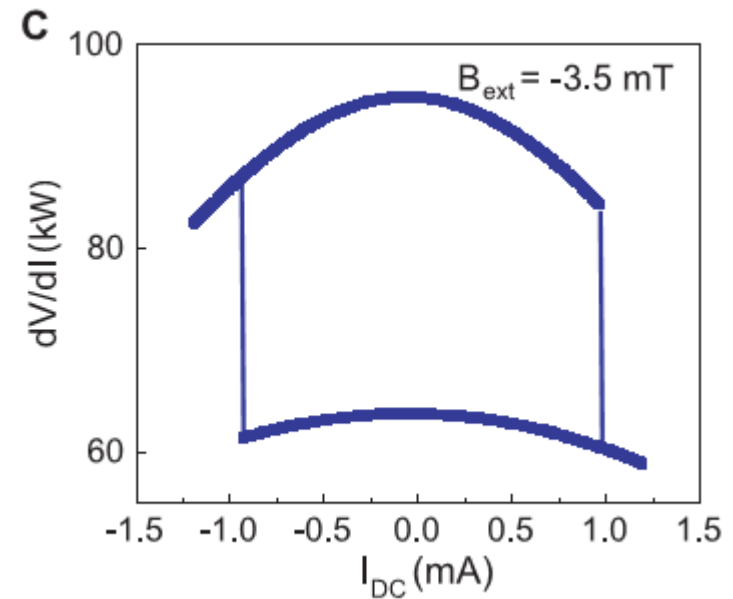
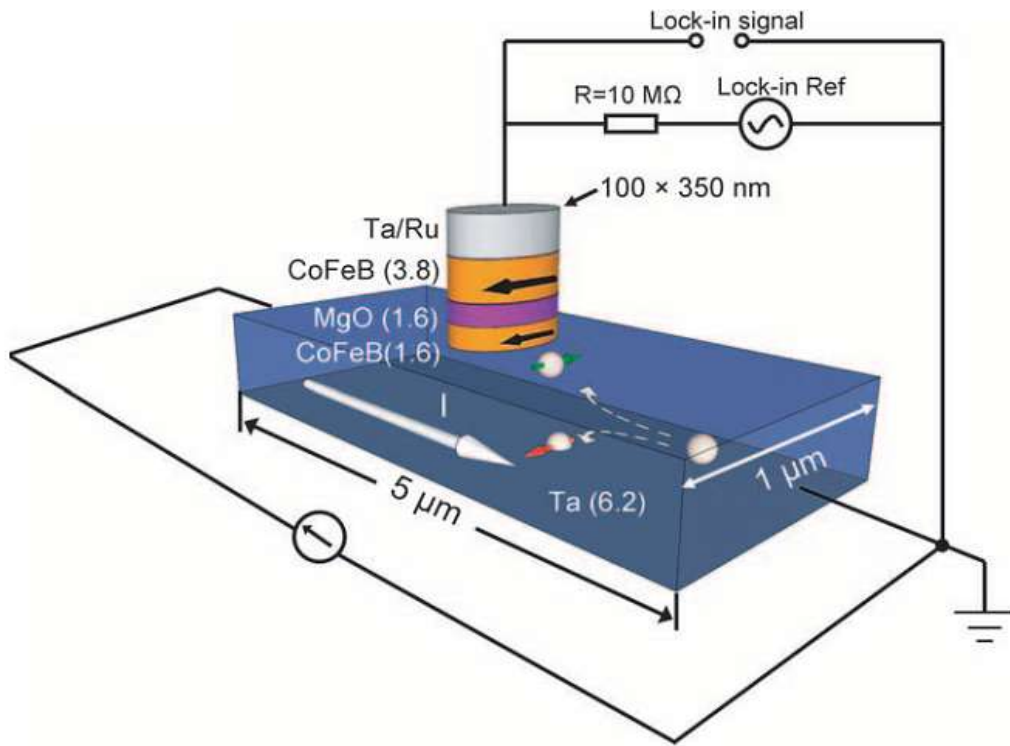
Spin orbit torque

Spin Hall effect



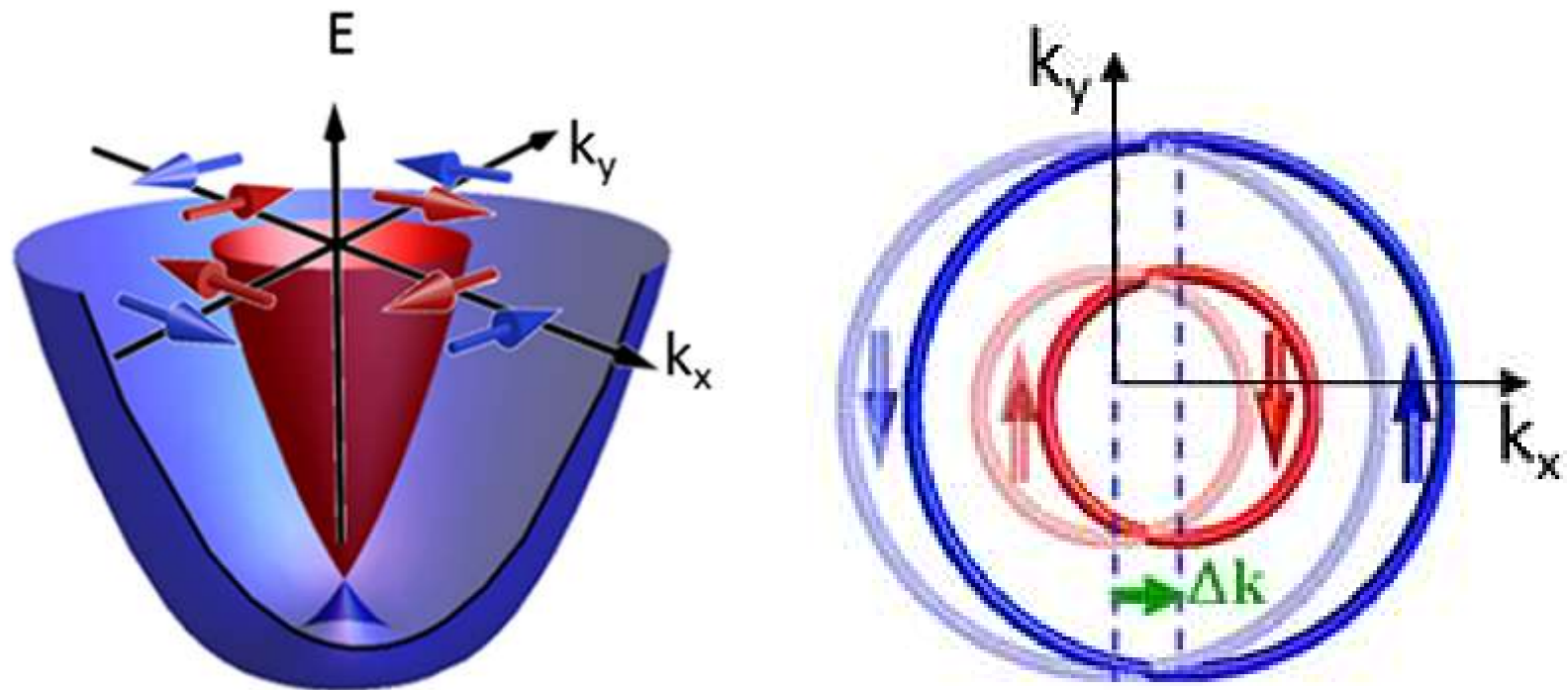
D'yakonov, M. I. & Perel', J. Exp. Theor. Phys. Lett. 13, 467-469, (1971).
Hirsch, J. E. Phys. Rev. Lett. 83, 1834-1837, (1999).
Zhang, S. Phys. Rev. Lett. 85, 393-396, (2000).

Spin orbit torque



Liu, et al, Science (2012)

Spin orbit torque

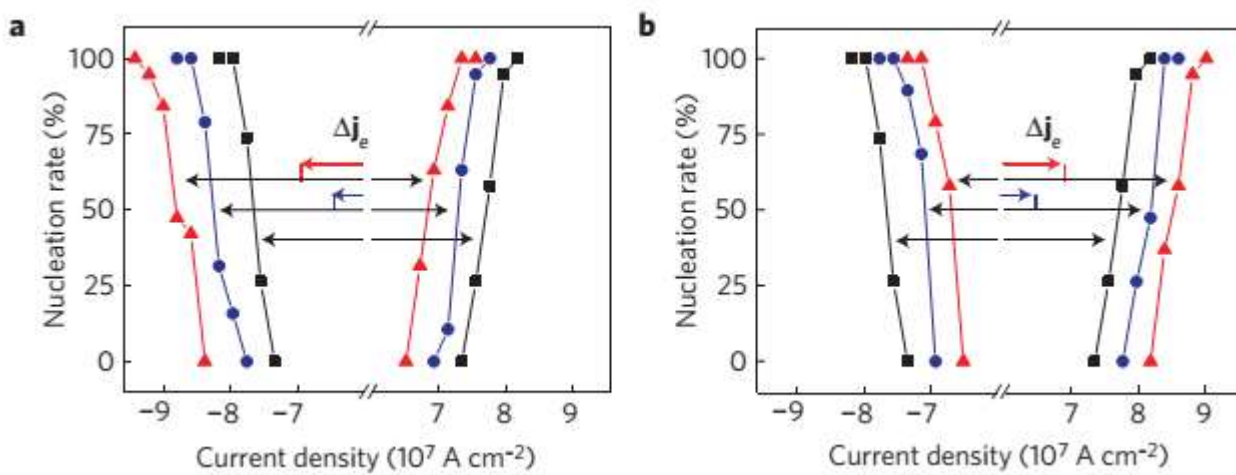
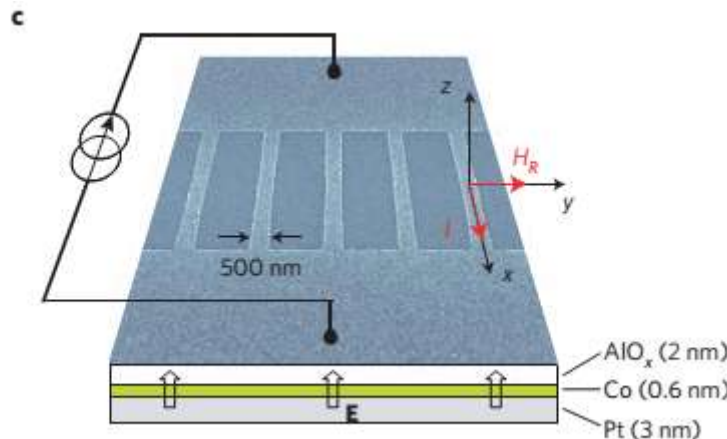


V. M. Edelstein, Solid State Commun. 73, 233 (1990)

A. Manchon, et al, Nat. Mater. 14, 871 (2015)

J. C. R. Sánchez, et al, Phys. Rev. Lett. 116, 096602 (2016)

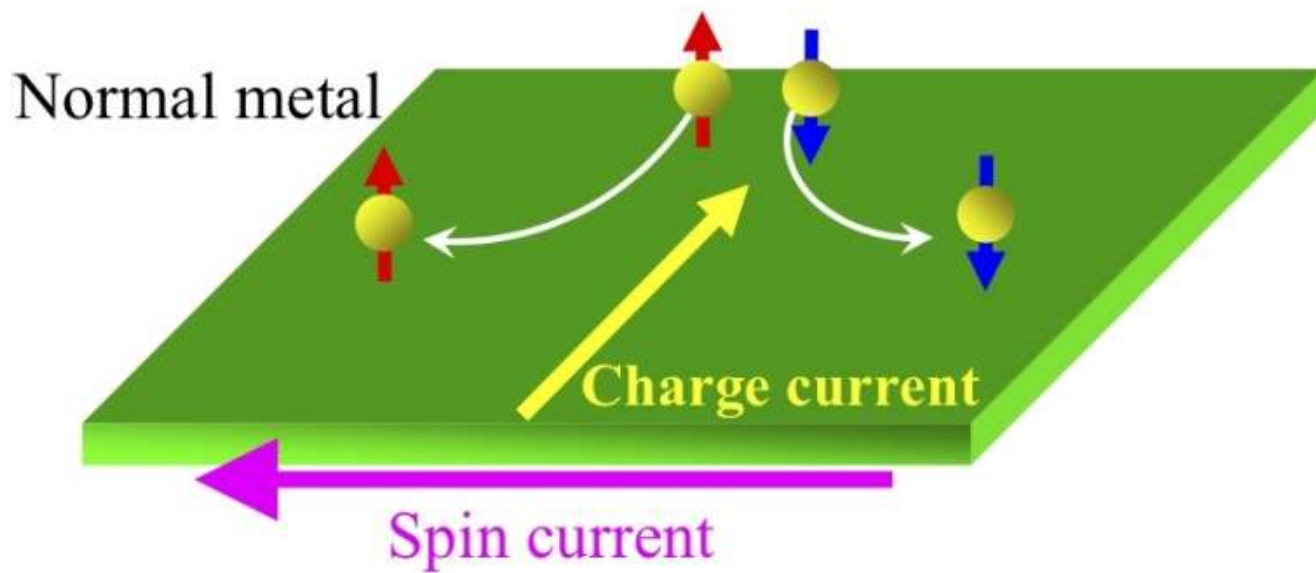
Spin orbit torque



Outline

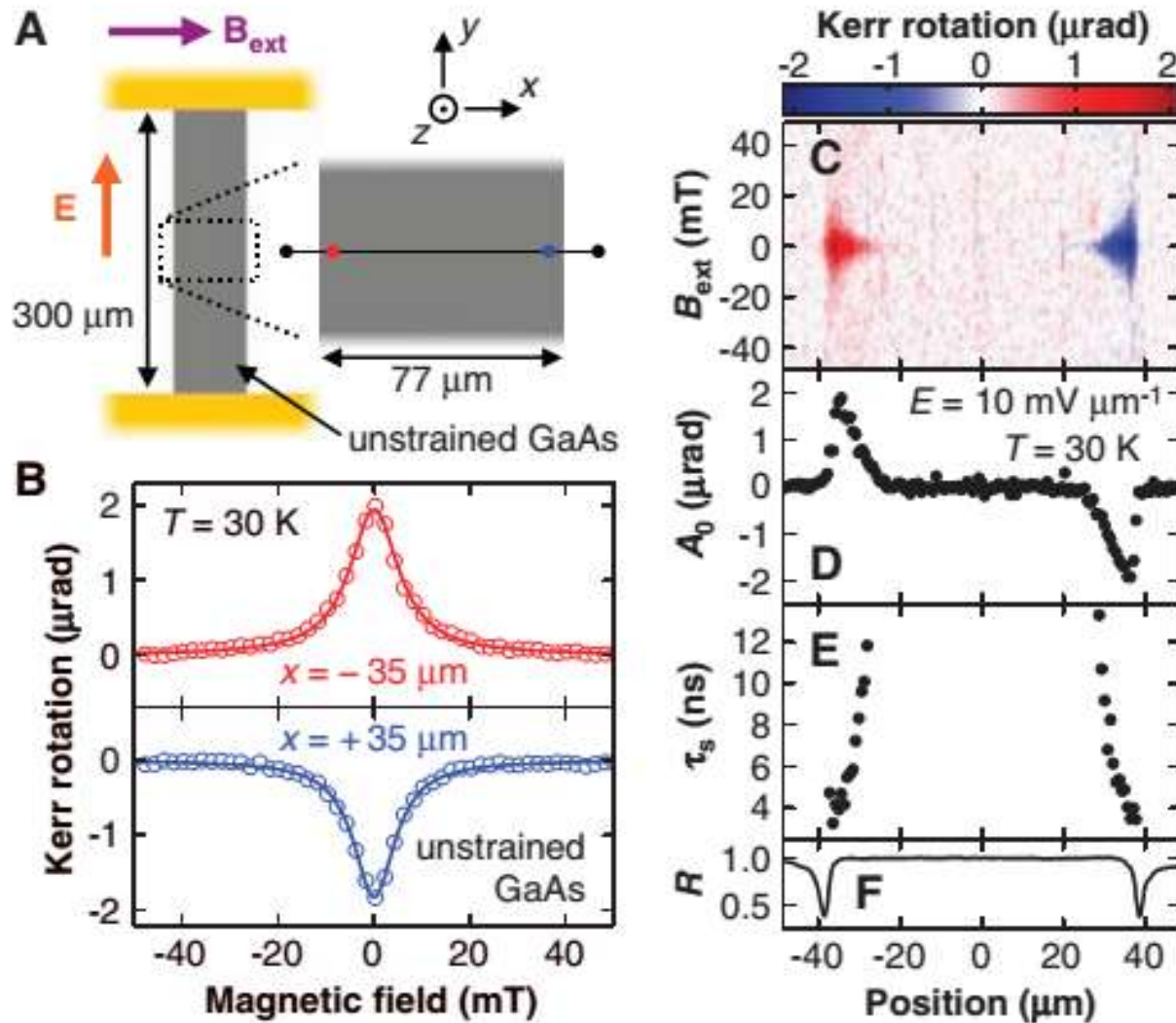
2. Spin Hall effect

Spin Hall effect



D'yakonov, M. I. & Perel', J. Exp. Theor. Phys. Lett. 13, 467-469, (1971).
Hirsch, J. E. Phys. Rev. Lett. 83, 1834-1837, (1999).
Zhang, S. Phys. Rev. Lett. 85, 393-396, (2000).

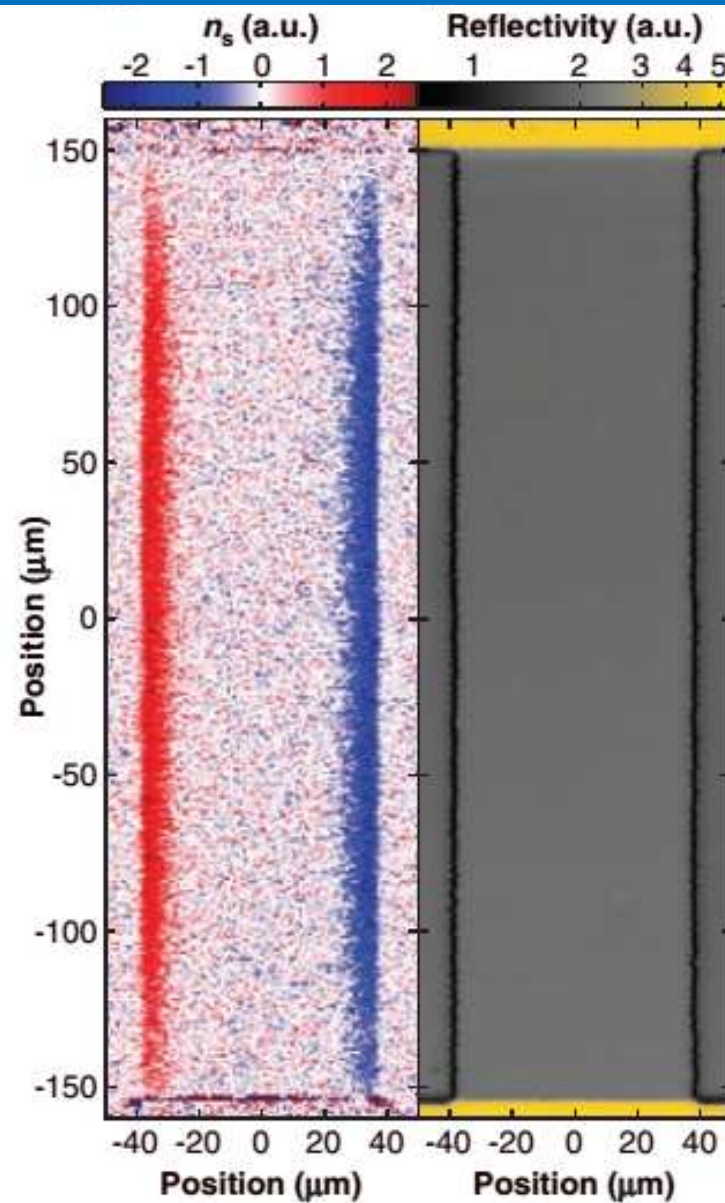
First observation of SHE



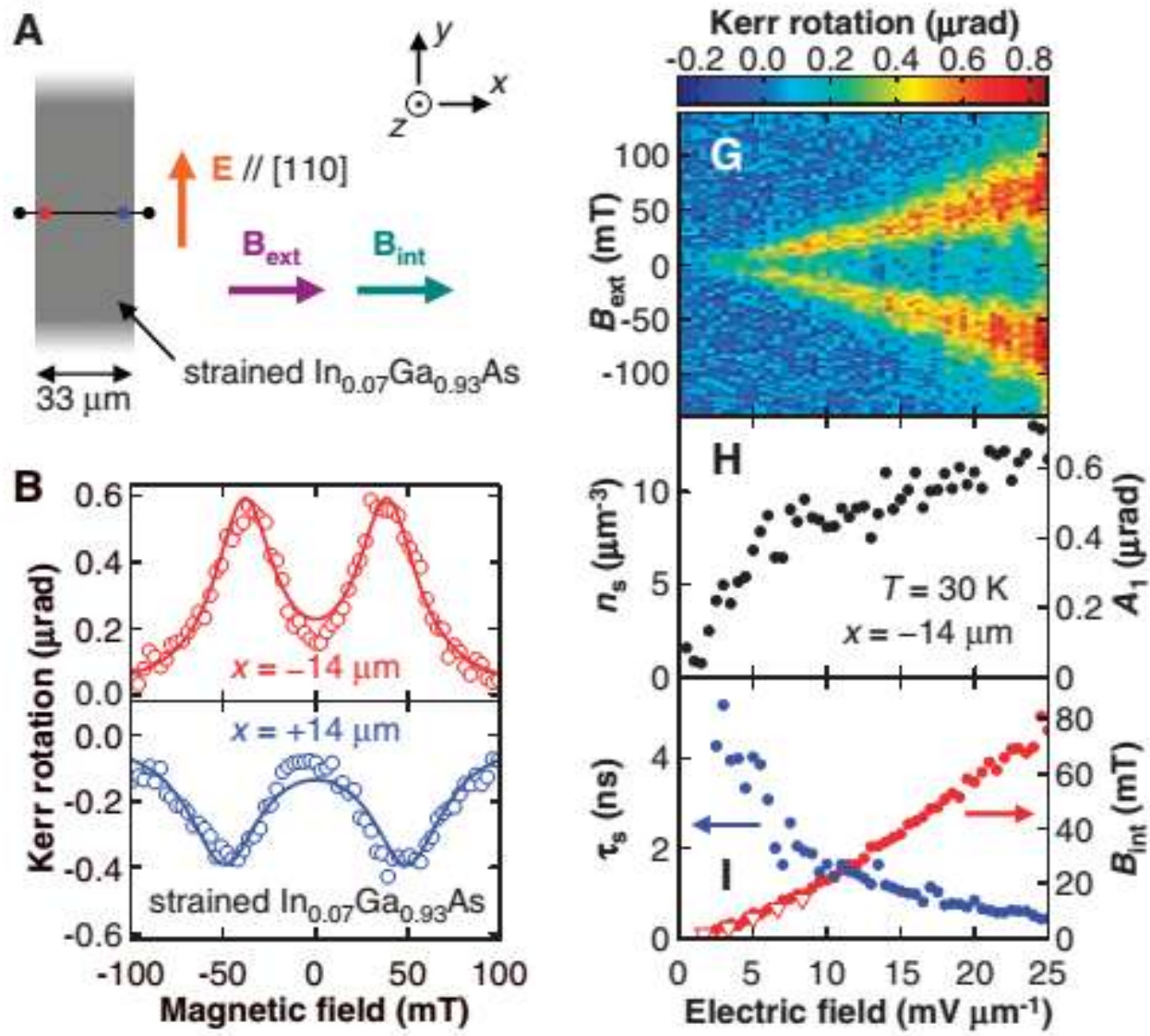
Kato, et al, Science (2004)

14

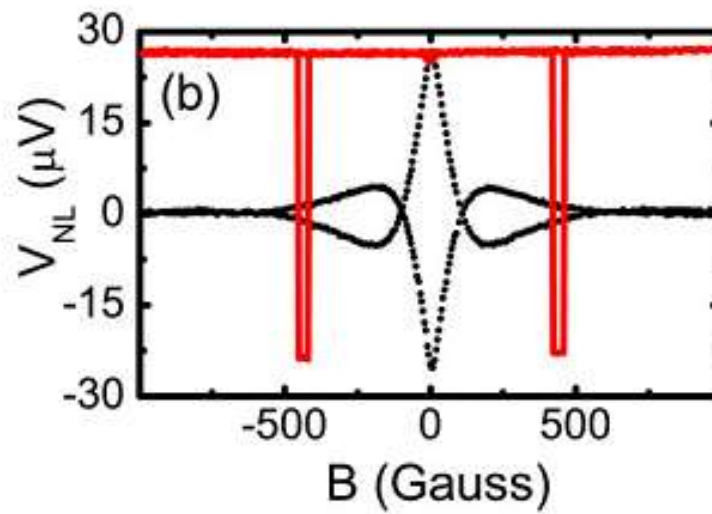
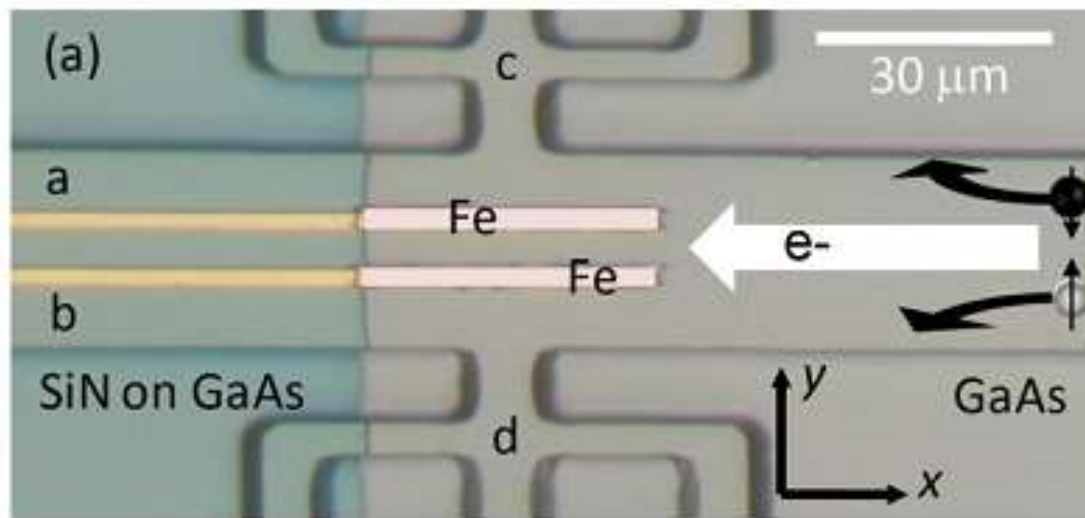
First observation of SHE



First observation of SHE

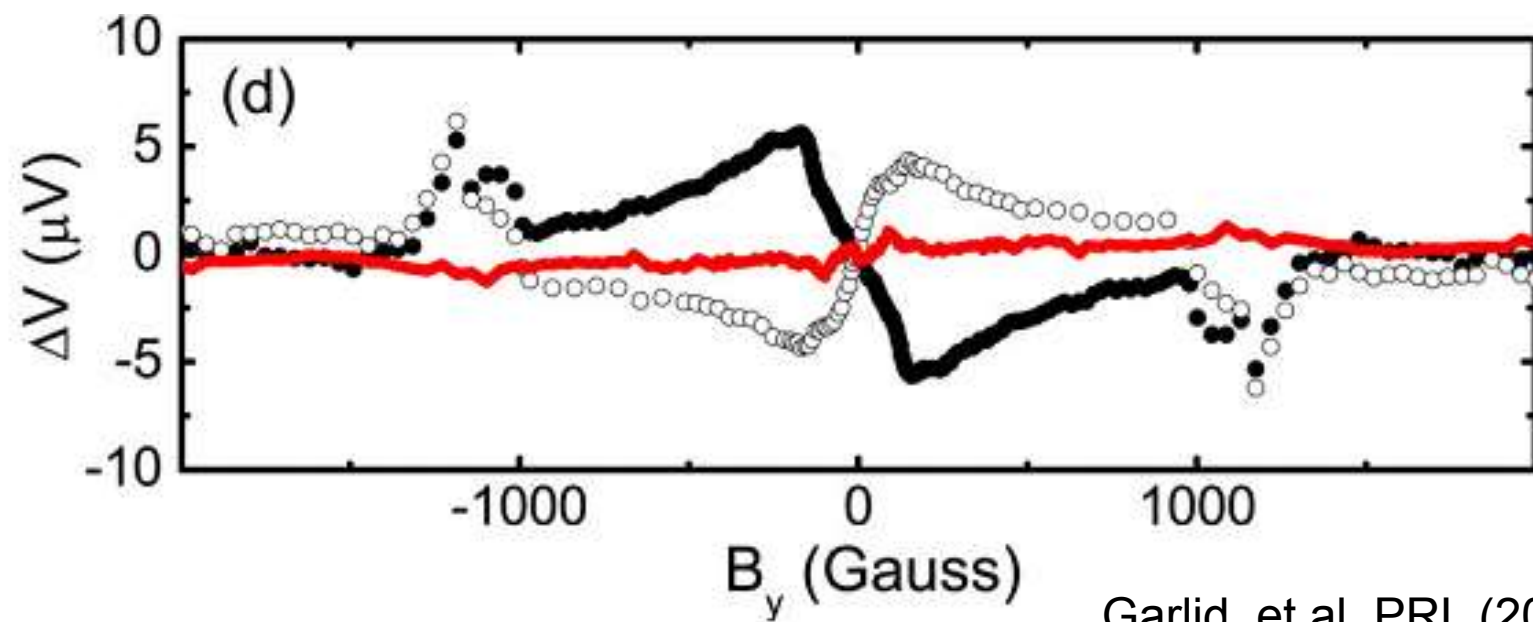
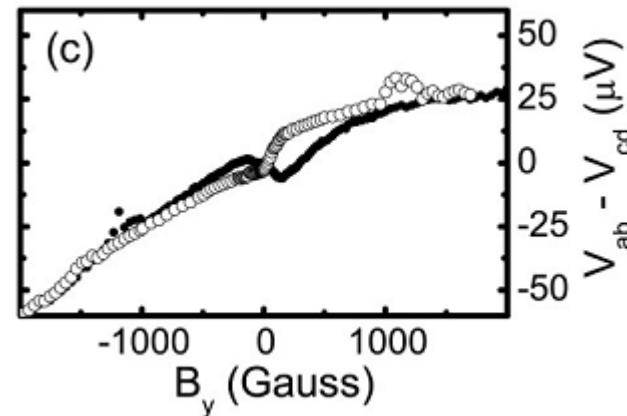
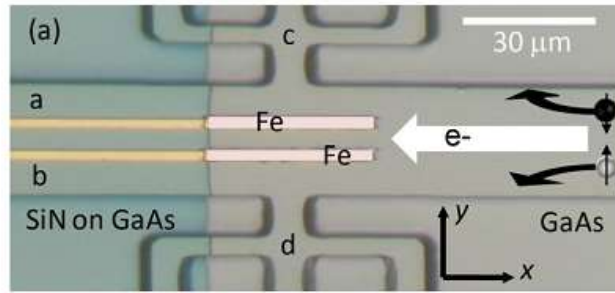


Electrical measurement



Garlid, et al, PRL (2010)

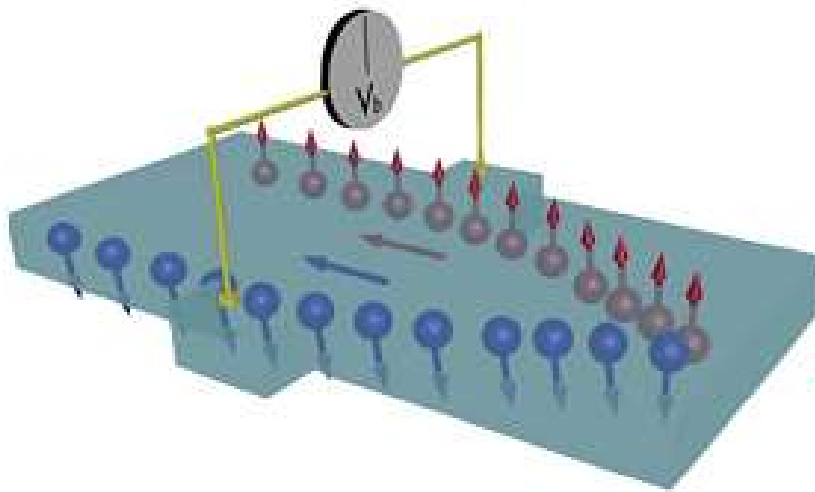
Electrical measurement



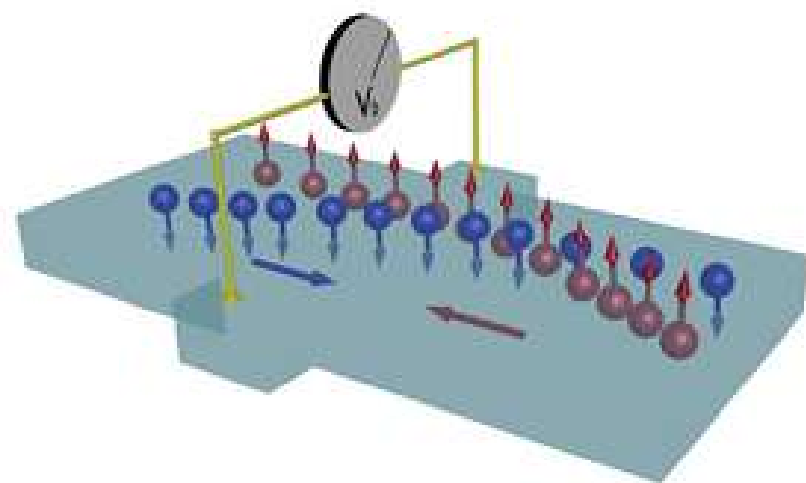
Garlid, et al, PRL (2010)

SHE vs ISHE

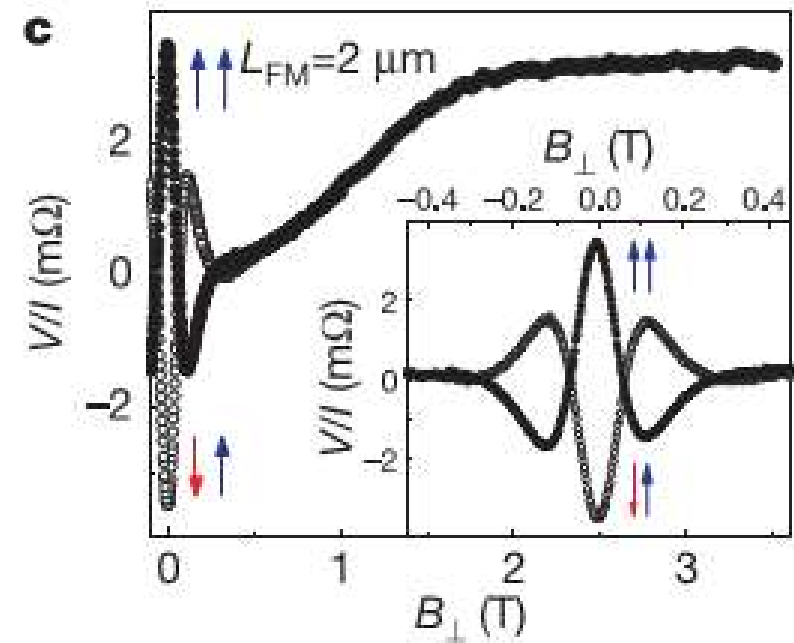
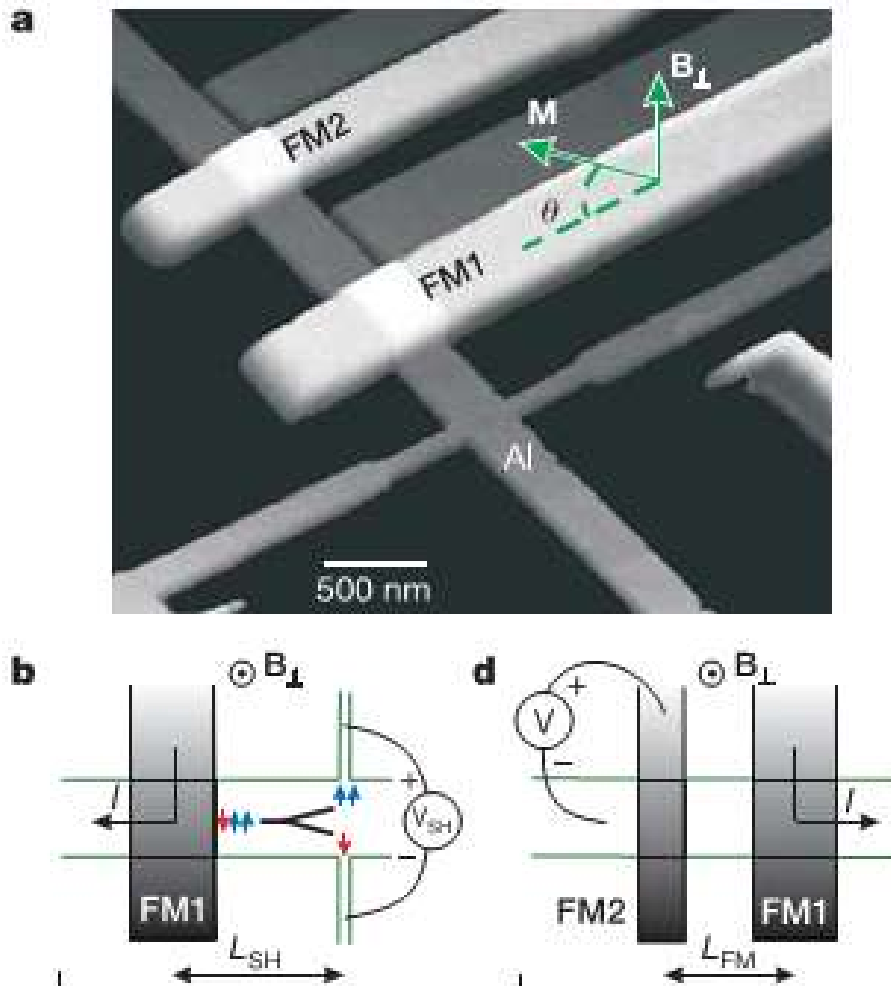
SHE
non-magnetic



ISHE
non-magnetic

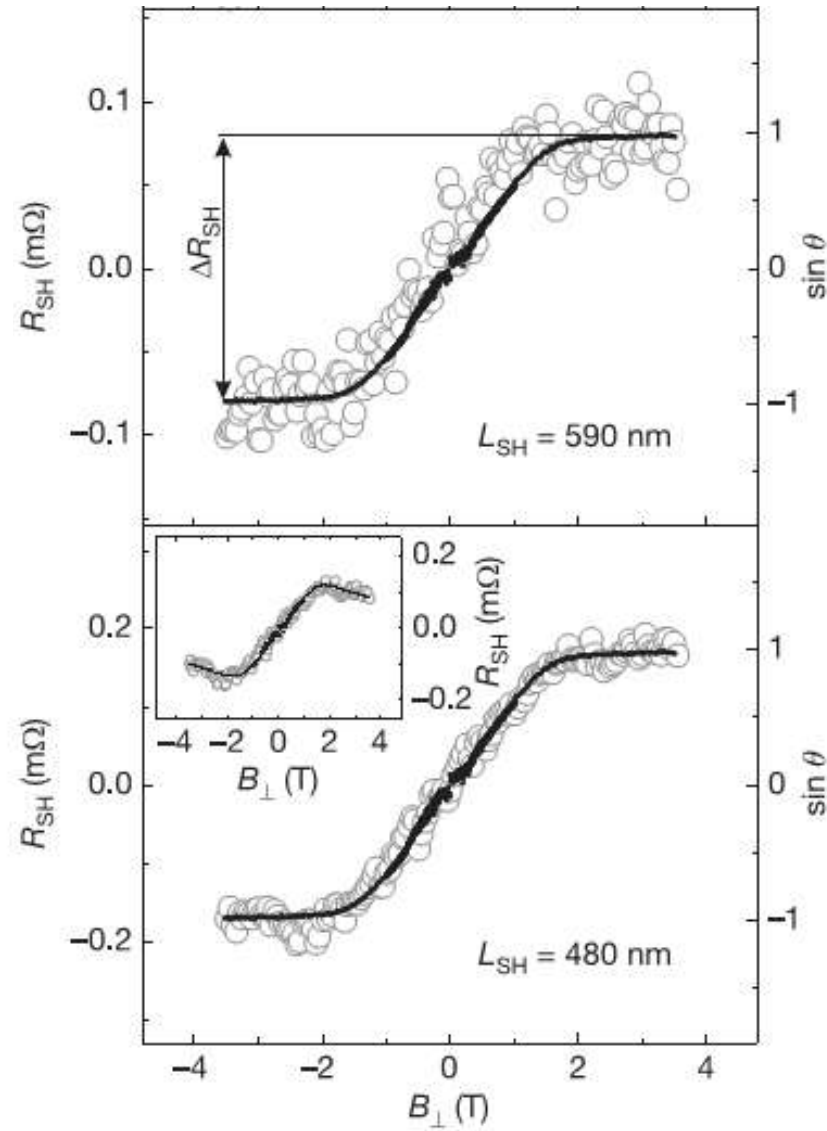
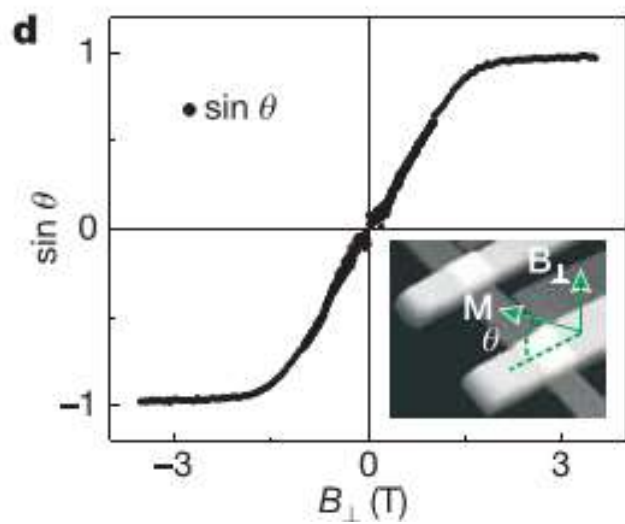
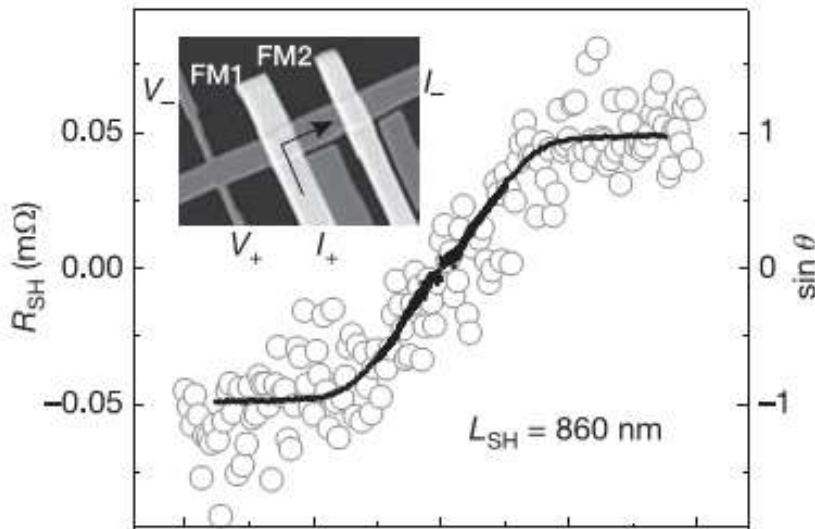


Spin injection and spin Hall

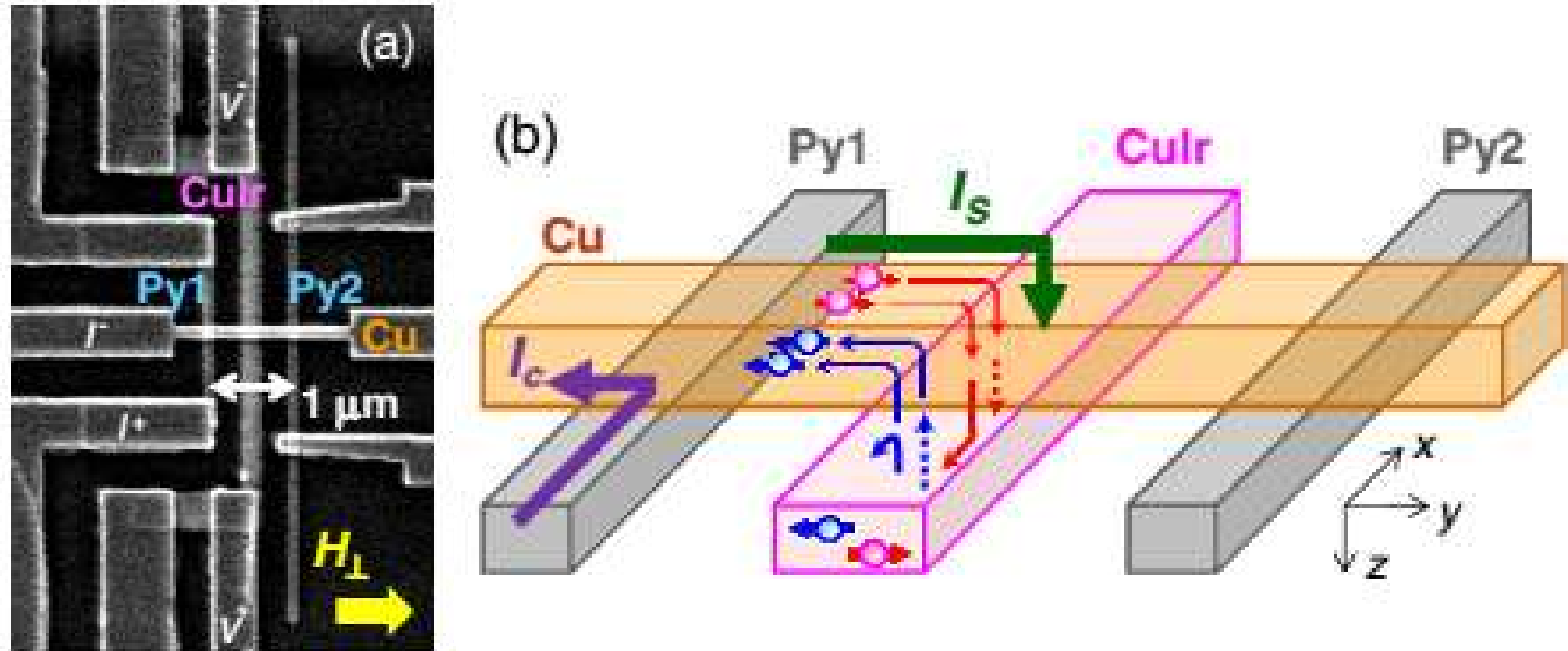


Valenzuela, et al, Nature (2006)

Spin injection and spin Hall

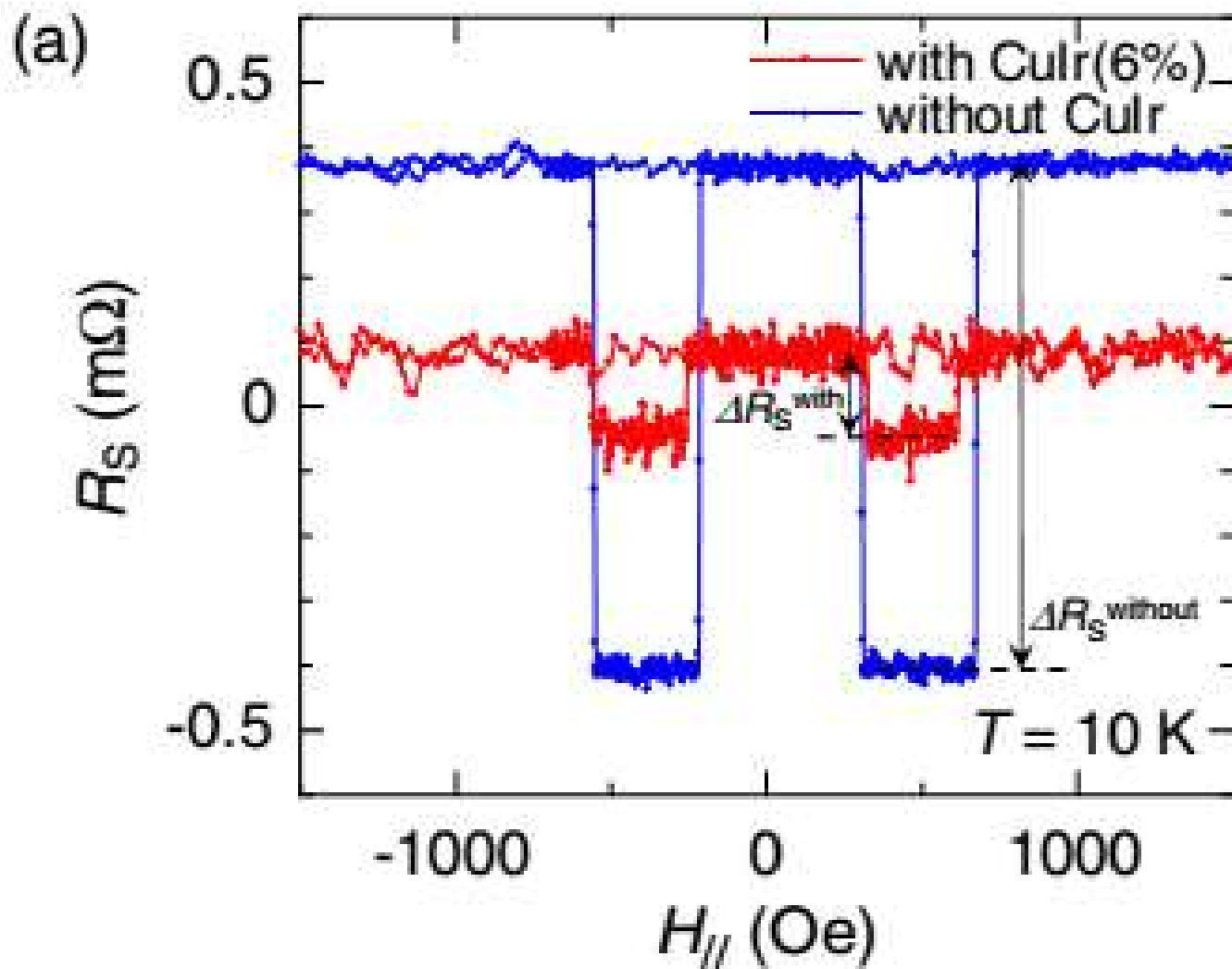


Spin diffusion and absorption

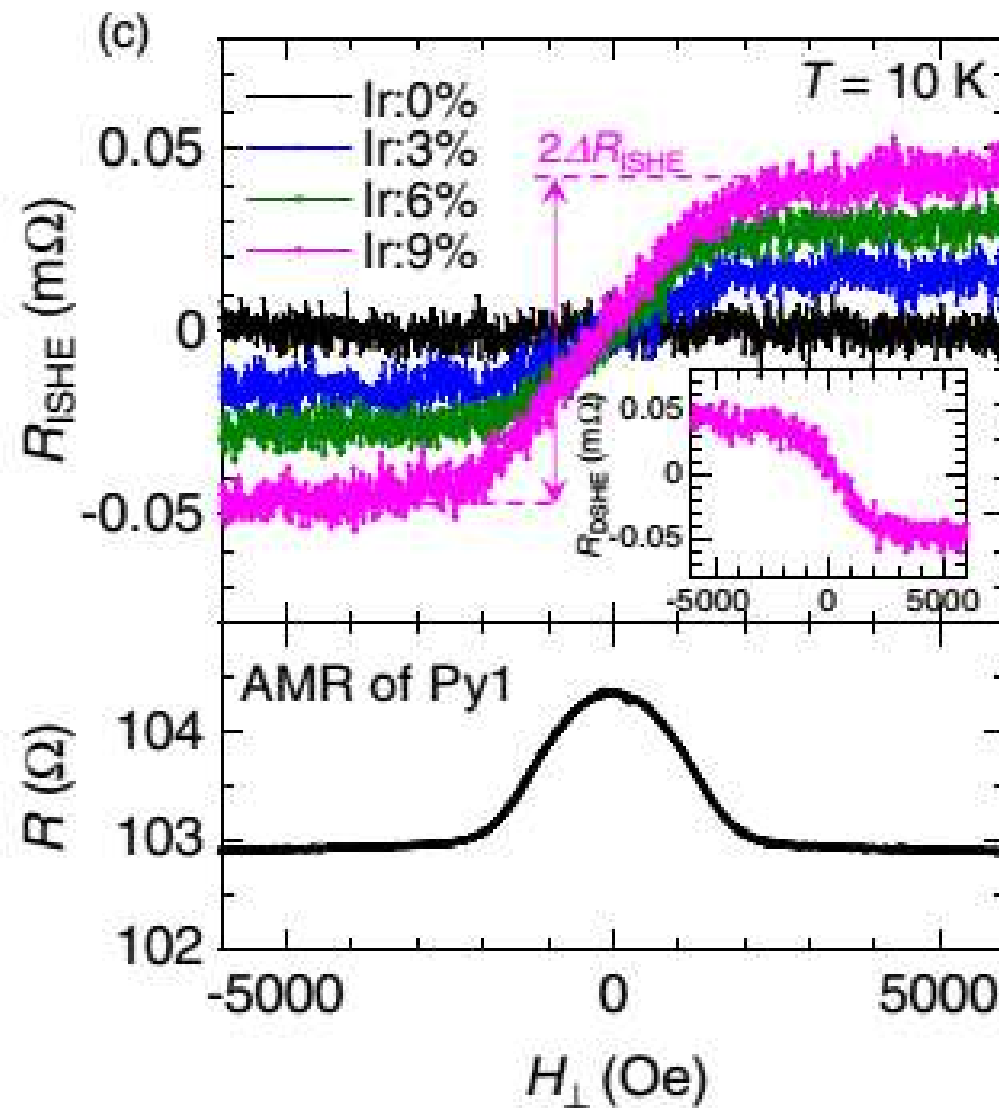


Olejnik, et al, PRL (2012)

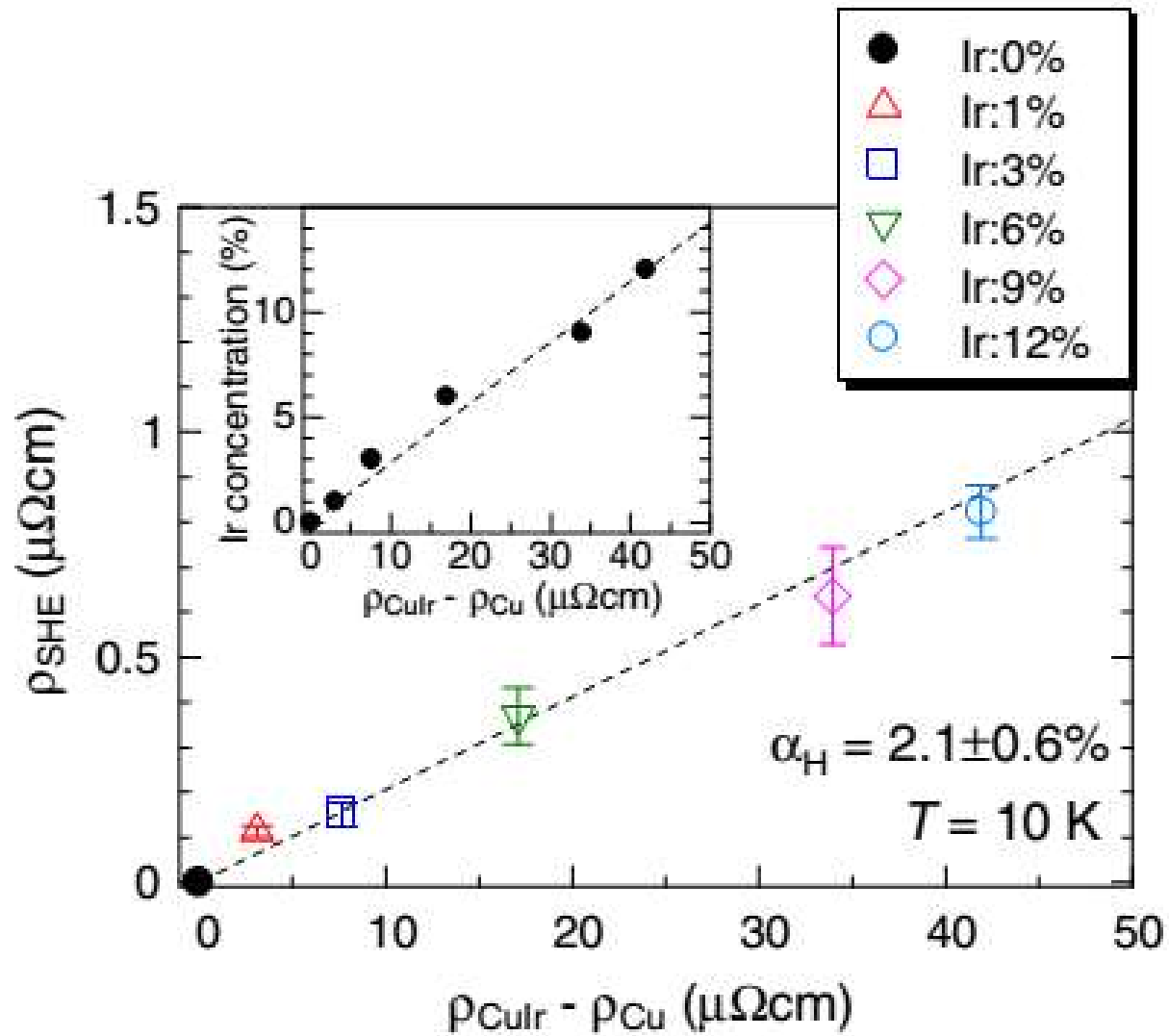
Spin diffusion and absorption



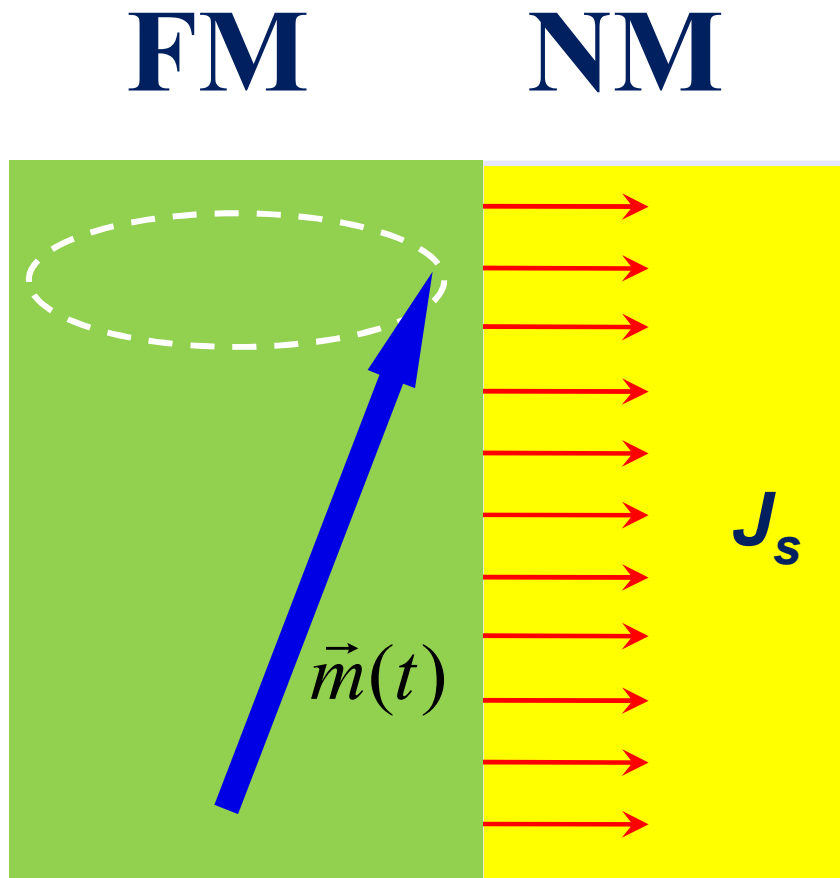
Spin diffusion and absorption



Spin diffusion and absorption



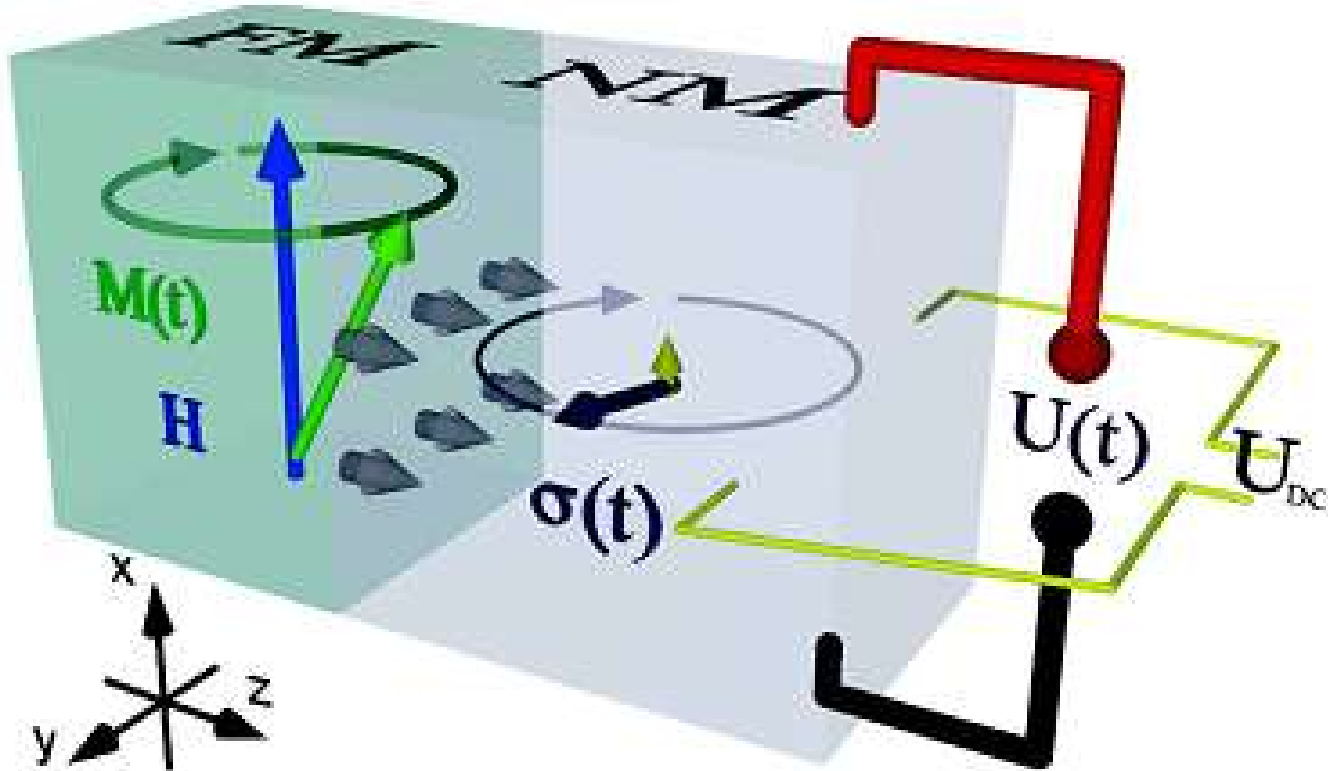
Spin angular momentum



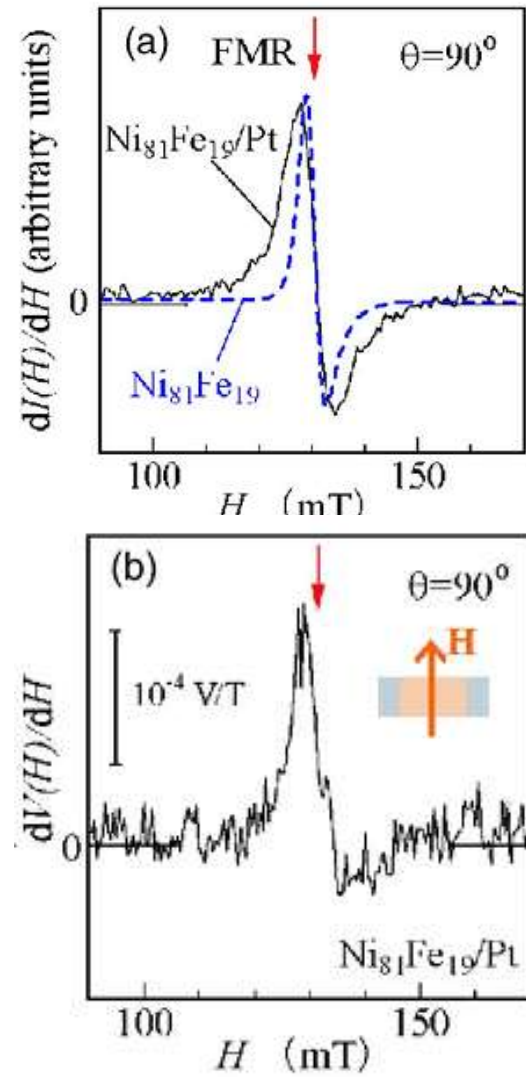
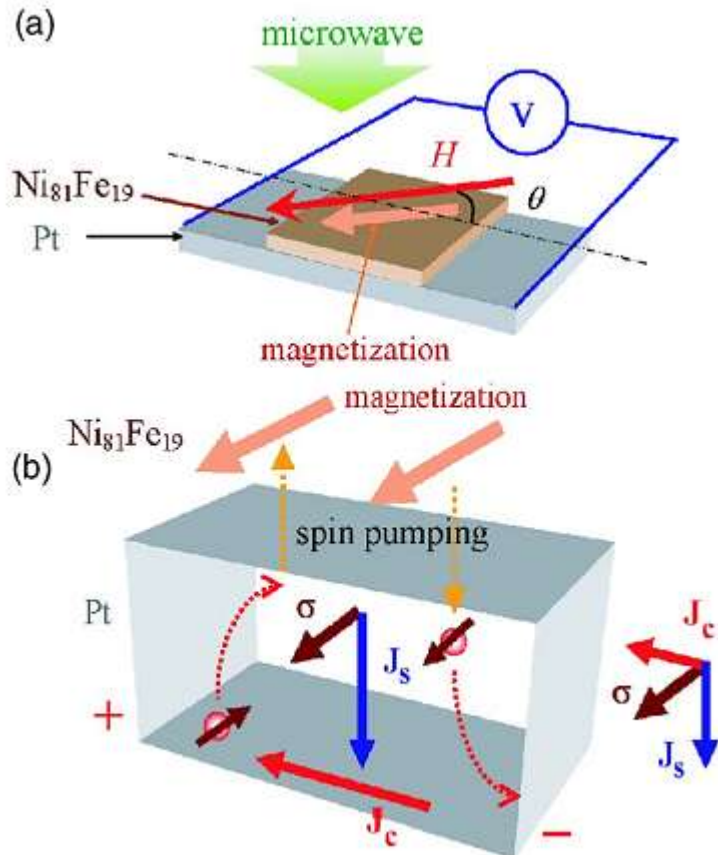
$$\vec{J}_S = \frac{\hbar g_r^{\uparrow\downarrow}}{4\pi M^2} \left(\vec{M} \times \frac{\partial \vec{M}}{\partial t} \right)$$

Precessing **magnetization** in
FM layer pump **spin current**
into NM layer
(Angular momentum
conservation)

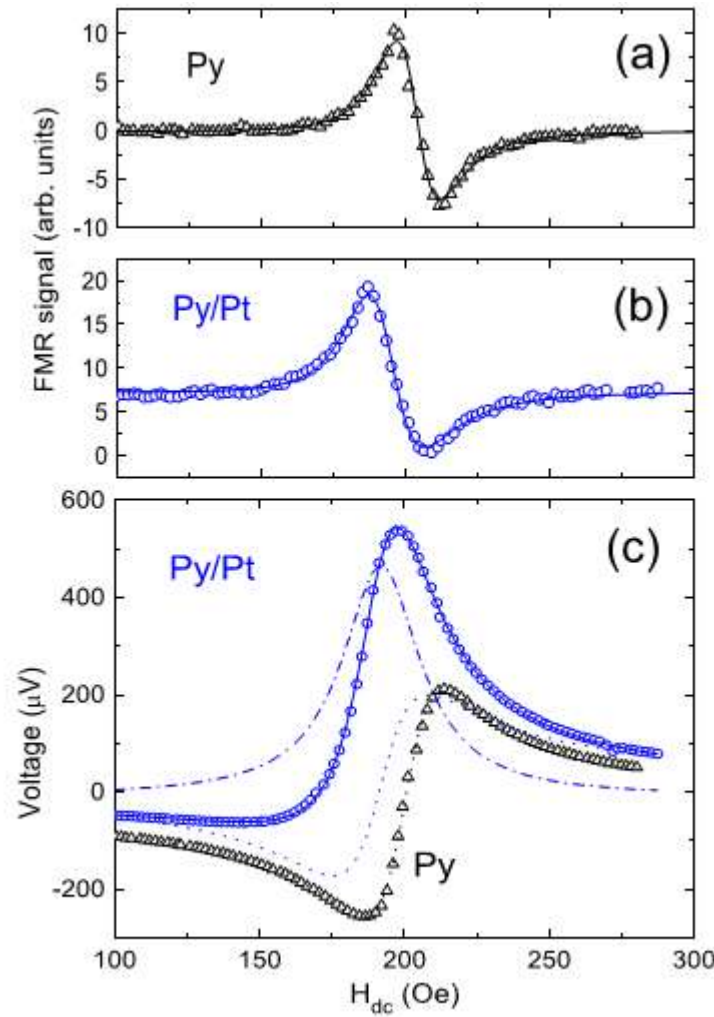
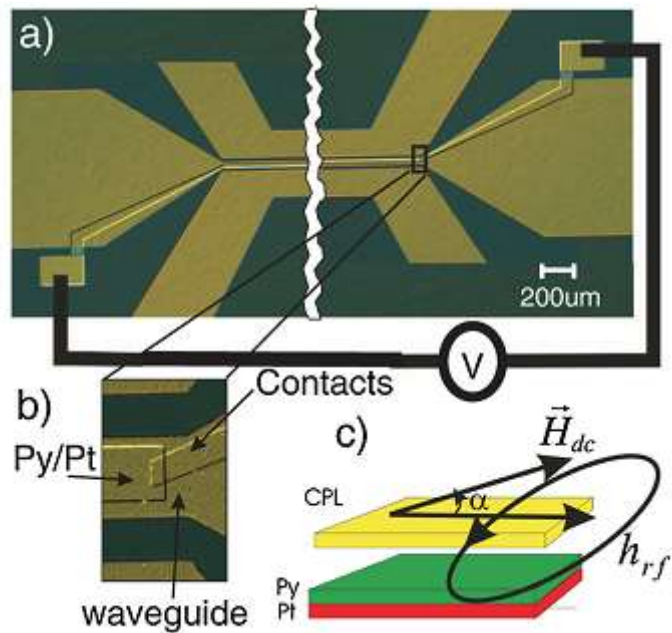
Spin pumping and ISHE



Spin pumping



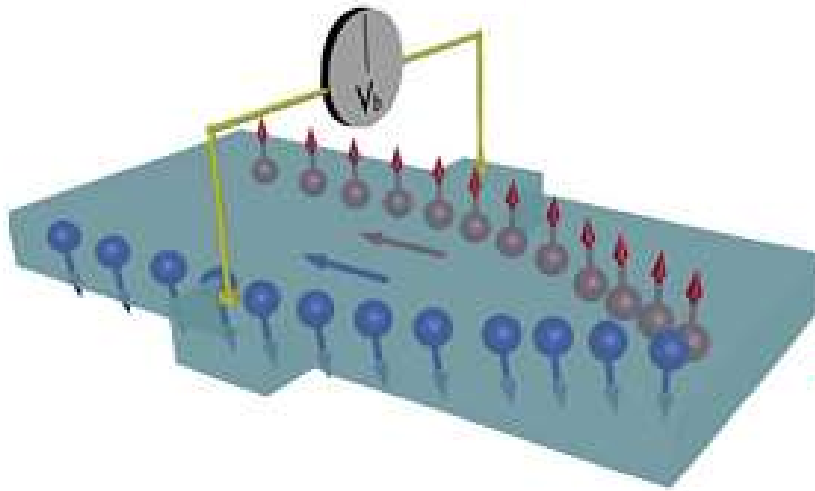
Spin pumping and ISHE



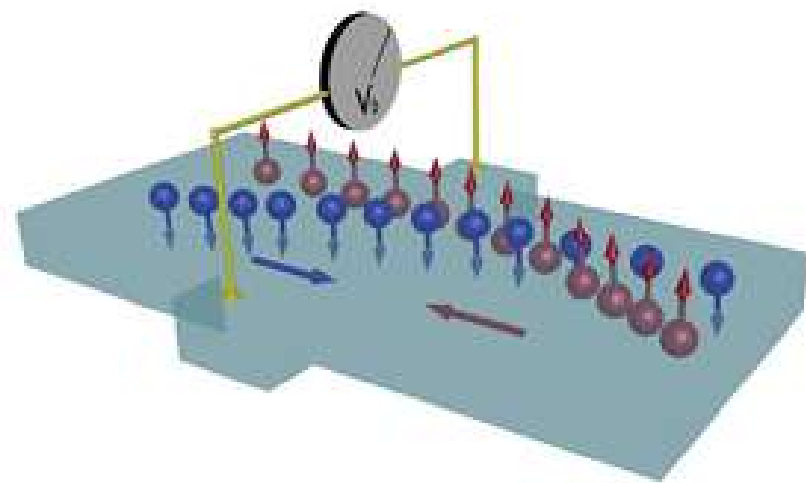
Mosendz, et al, PRL (2010)

SHE vs ISHE

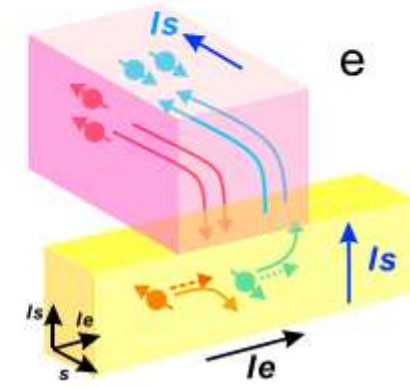
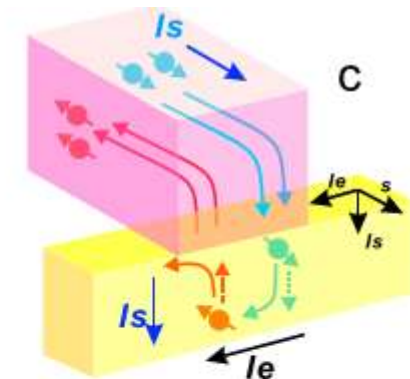
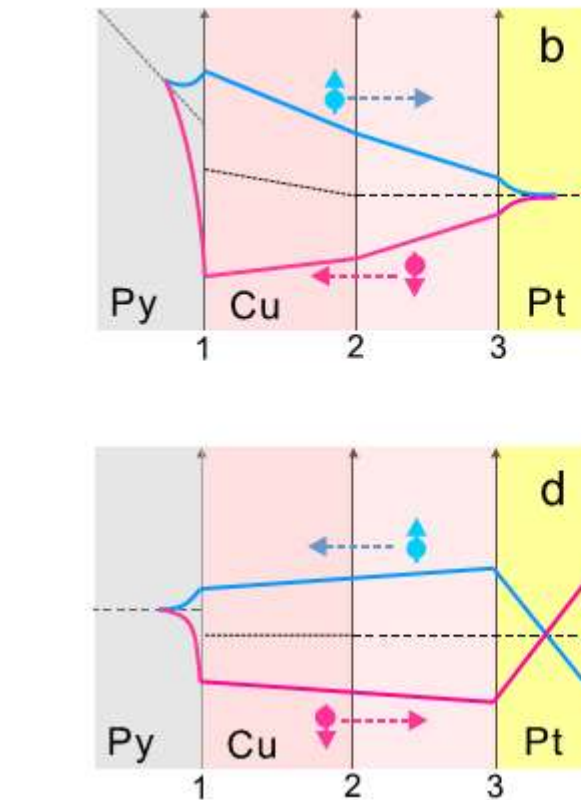
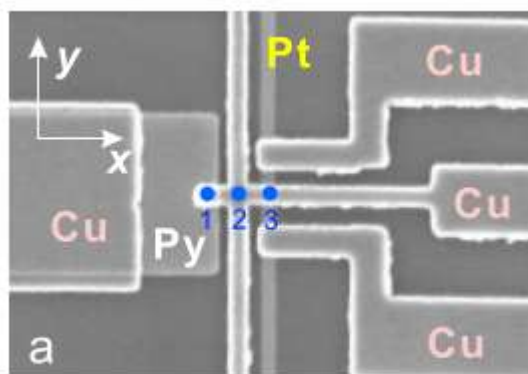
SHE
non-magnetic



ISHE
non-magnetic

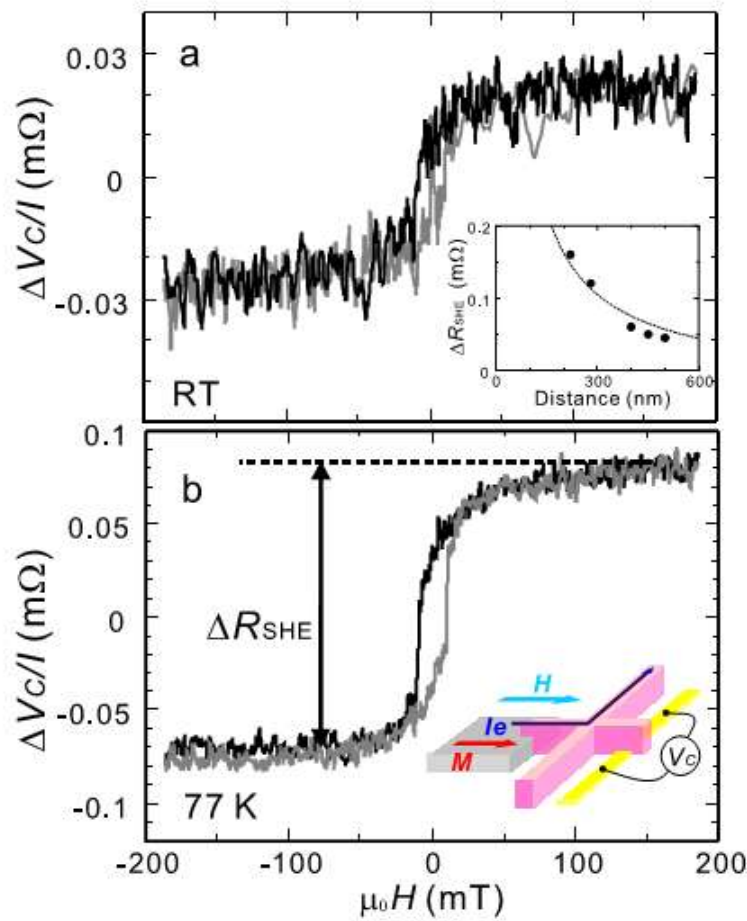


SHE vs. ISHE

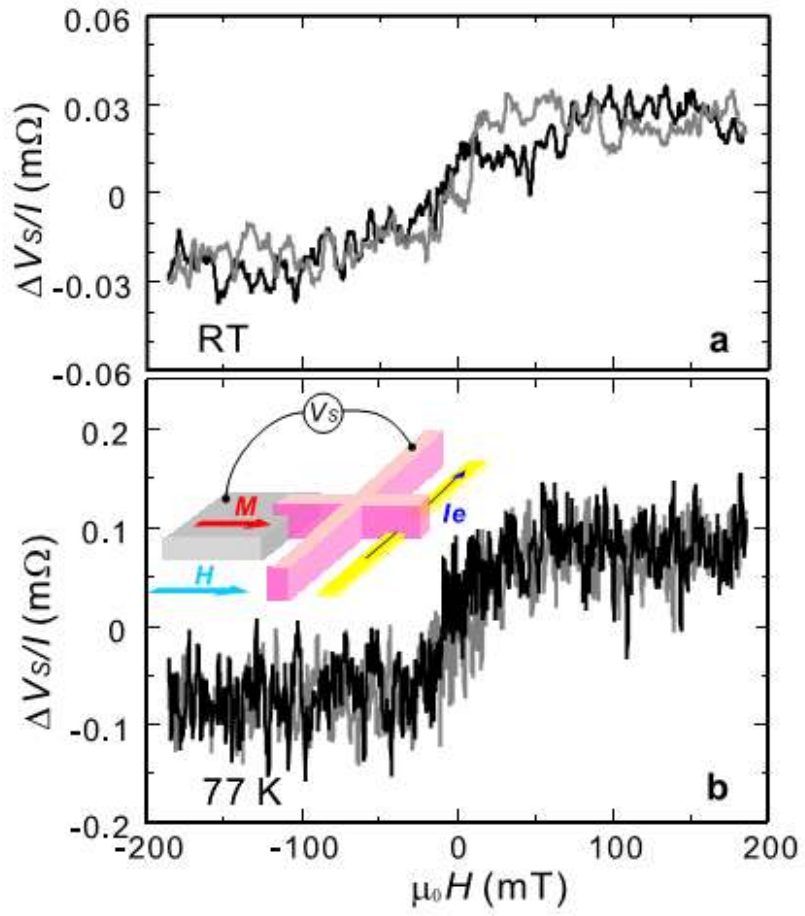


SHE vs. ISHE

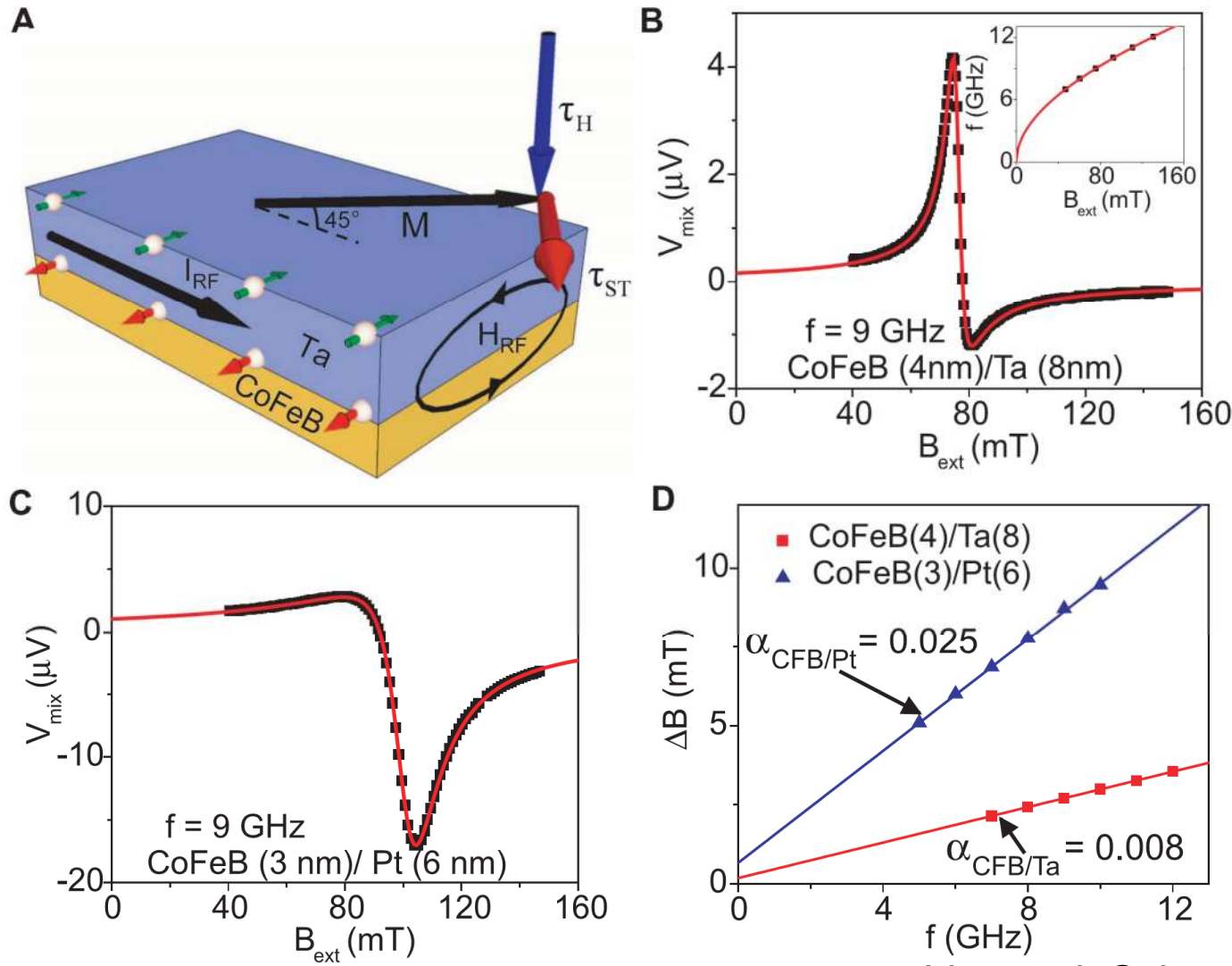
ISHE



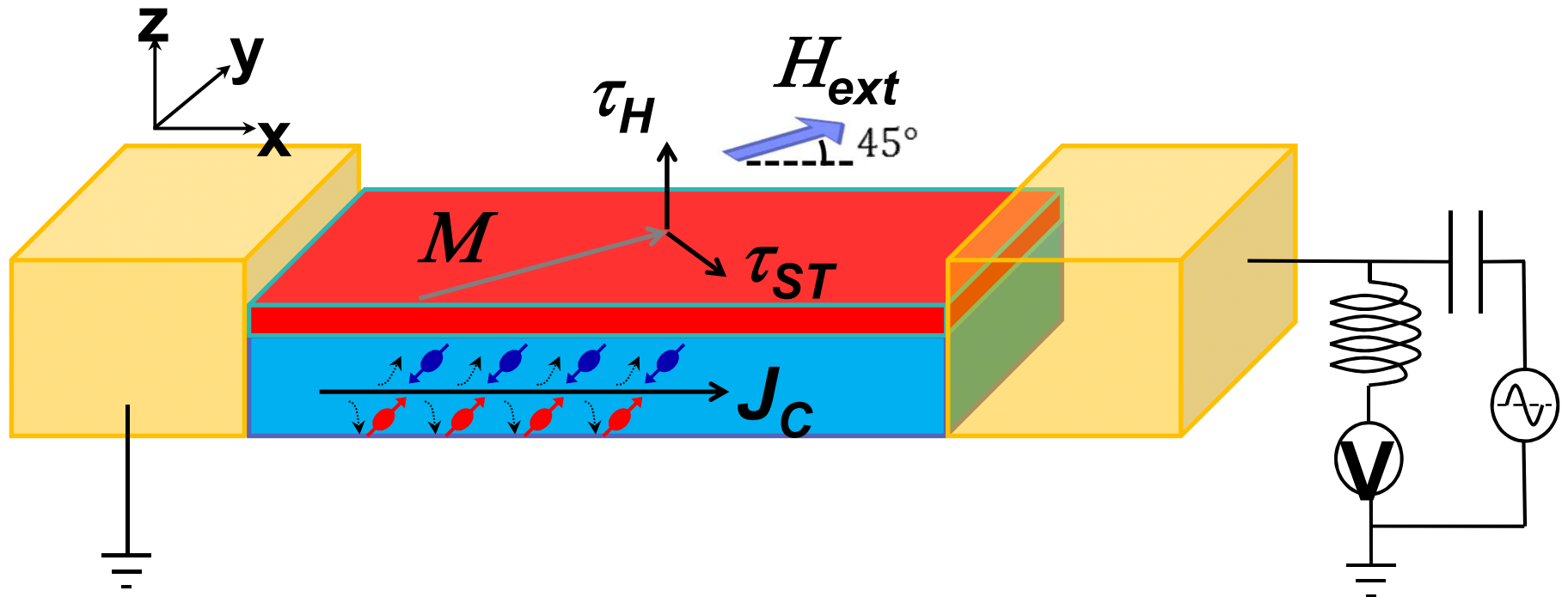
SHE



Spin Hall torque



Spin Hall torque

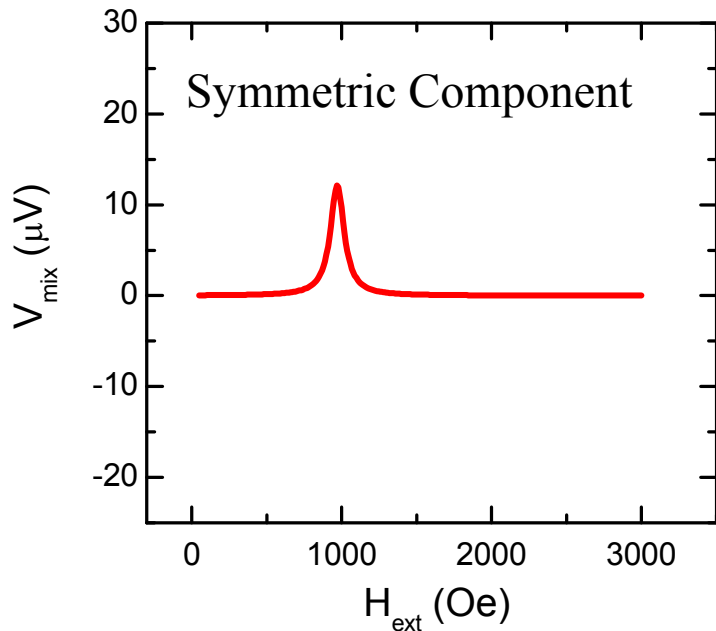
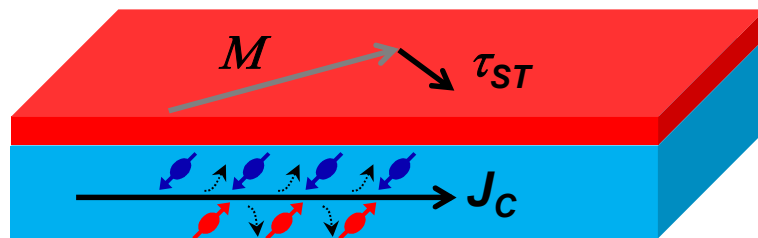


Liu, et al, PRL (2011)

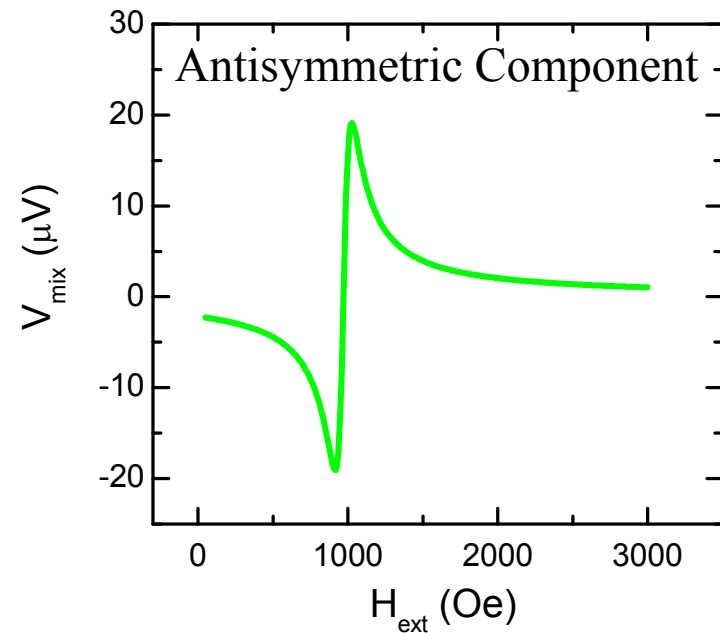
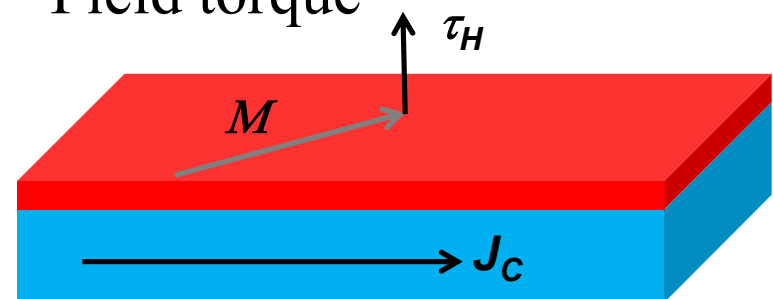
34

Spin Hall torque

Spin Hall torque



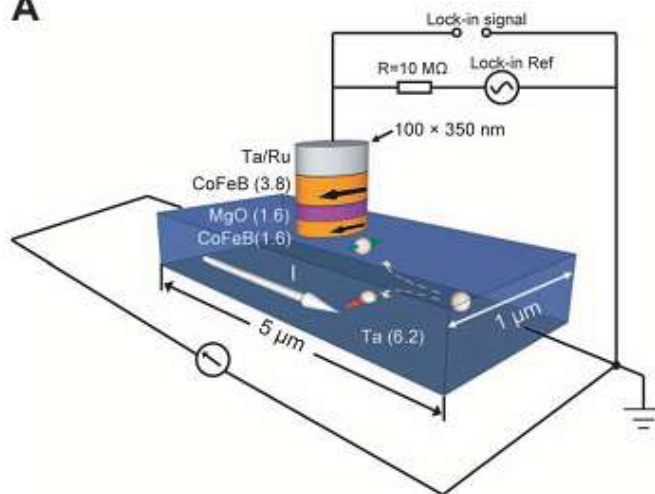
Field torque



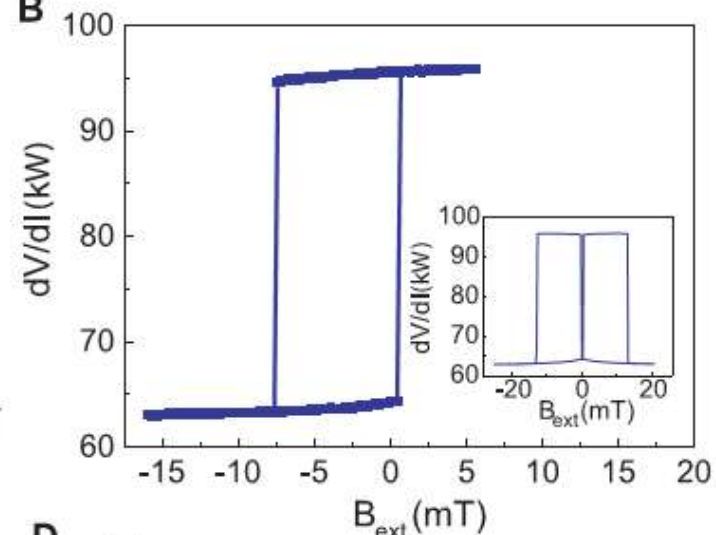
$$SHA = \frac{S}{A} \frac{e\mu_0 M_s t d}{\hbar} [1 + (4\pi M_{eff}/H_{ext})]^{1/2}$$

Spin Hall torque

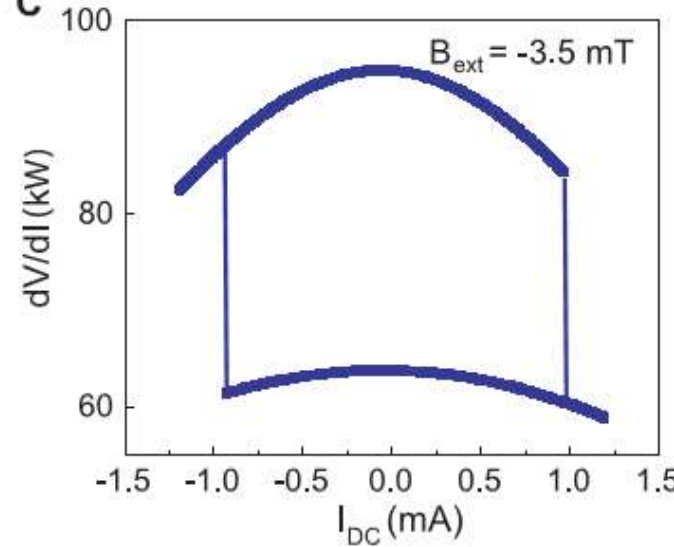
A



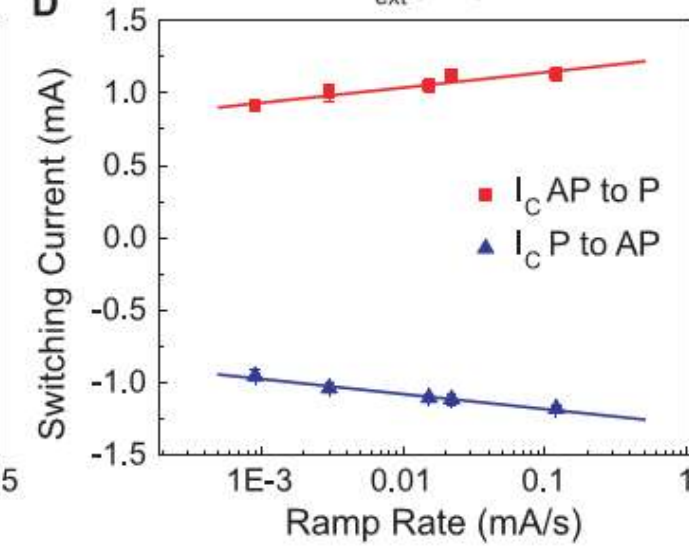
B



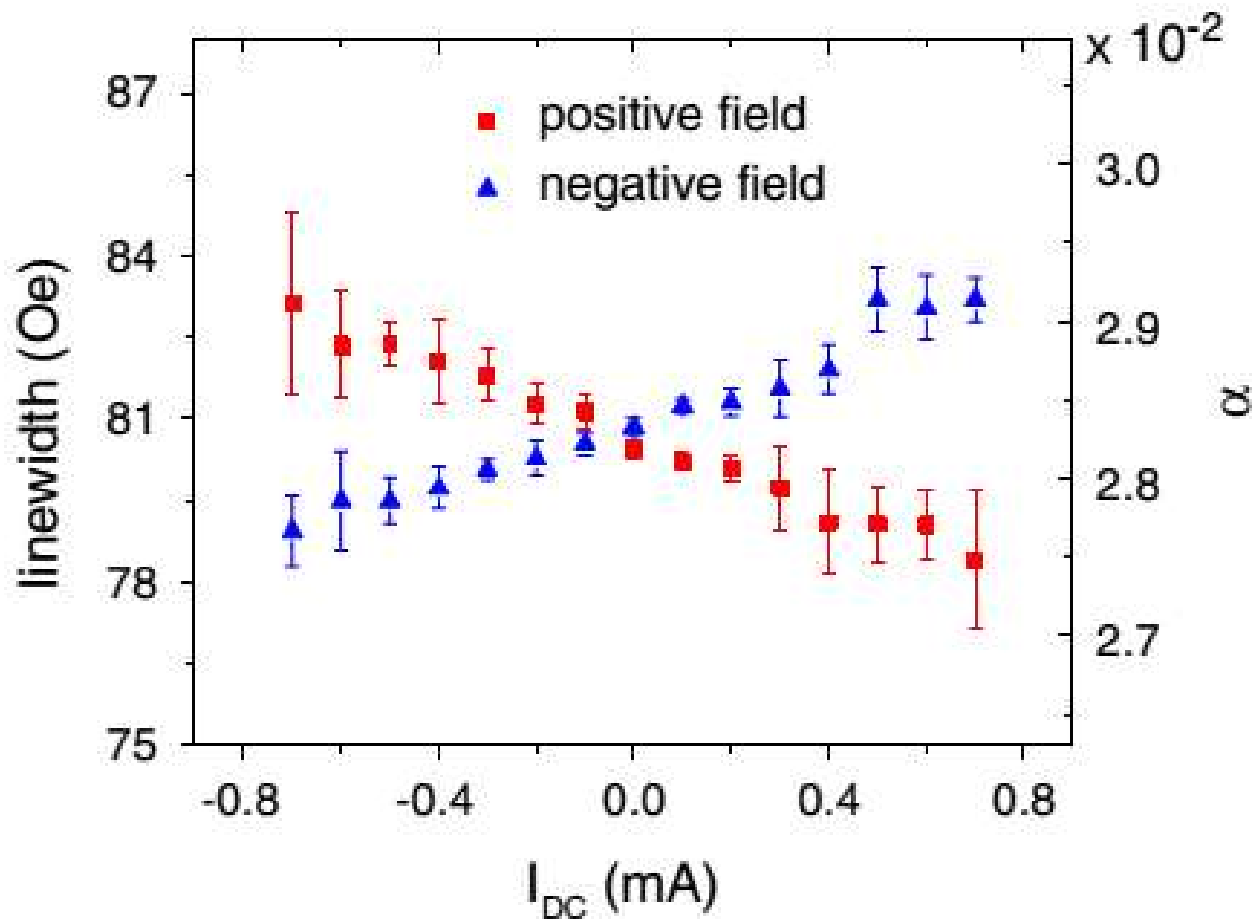
C



D



Spin Hall torque



$$\Delta = \frac{2\pi f}{\gamma} \left(\alpha + \frac{\sin\theta}{(H_{\text{ext}} + 2\pi M_{\text{eff}})\mu_0 M_S t} \frac{\hbar J_S}{2e} \right).$$

1) Large spin Hall in AFM

PRL 112, 017205 (2014)

PHYSICAL REVIEW LETTERS

week ending
10 JANUARY 2014

Anomalous Hall Effect Arising from Noncollinear Antiferromagnetism

Hua Chen, Qian Niu, and A. H. MacDonald

Department of Physics, University of Texas at Austin, Austin, Texas 78712, USA

(Received 3 October 2013; published 10 January 2014)

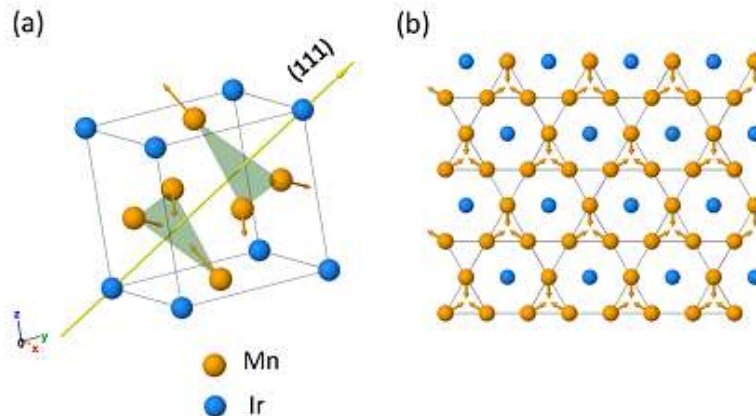


FIG. 1 (color online). Structure of Mn₃Ir. (a) Unit cell of Mn₃Ir with triangular antiferromagnetic order. (b) An individual (111) plane of Mn₃Ir. The Mn atoms form a kagome lattice.

- **Large spin orbit coupling of Ir transfer to Mn.**
- **Non-collinear antiferromagnetism**

1) Large spin Hall in AFM

PRL 113, 196602 (2014)

PHYSICAL REVIEW LETTERS

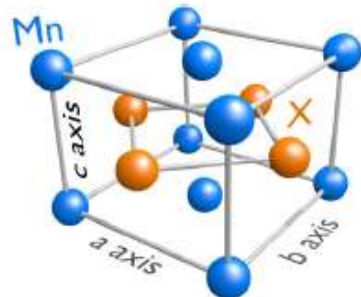
week ending
7 NOVEMBER 2014

Spin Hall Effects in Metallic Antiferromagnets

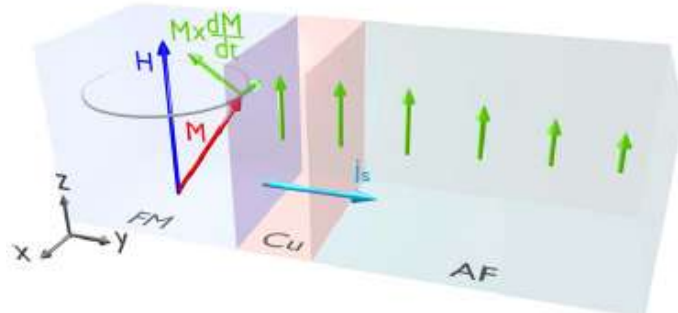
Wei Zhang, Matthias B. Jungfleisch, Wanjun Jiang, John E. Pearson, and Axel Hoffmann
Materials Science Division, Argonne National Laboratory, Argonne, Illinois 60439, USA

Frank Freimuth and Yuriy Mokrousov

Peter Grünberg Institut and Institute for Advanced Simulation, Forschungszentrum Jülich and JARA, D-52425 Jülich, Germany
(Received 12 August 2014; published 4 November 2014)



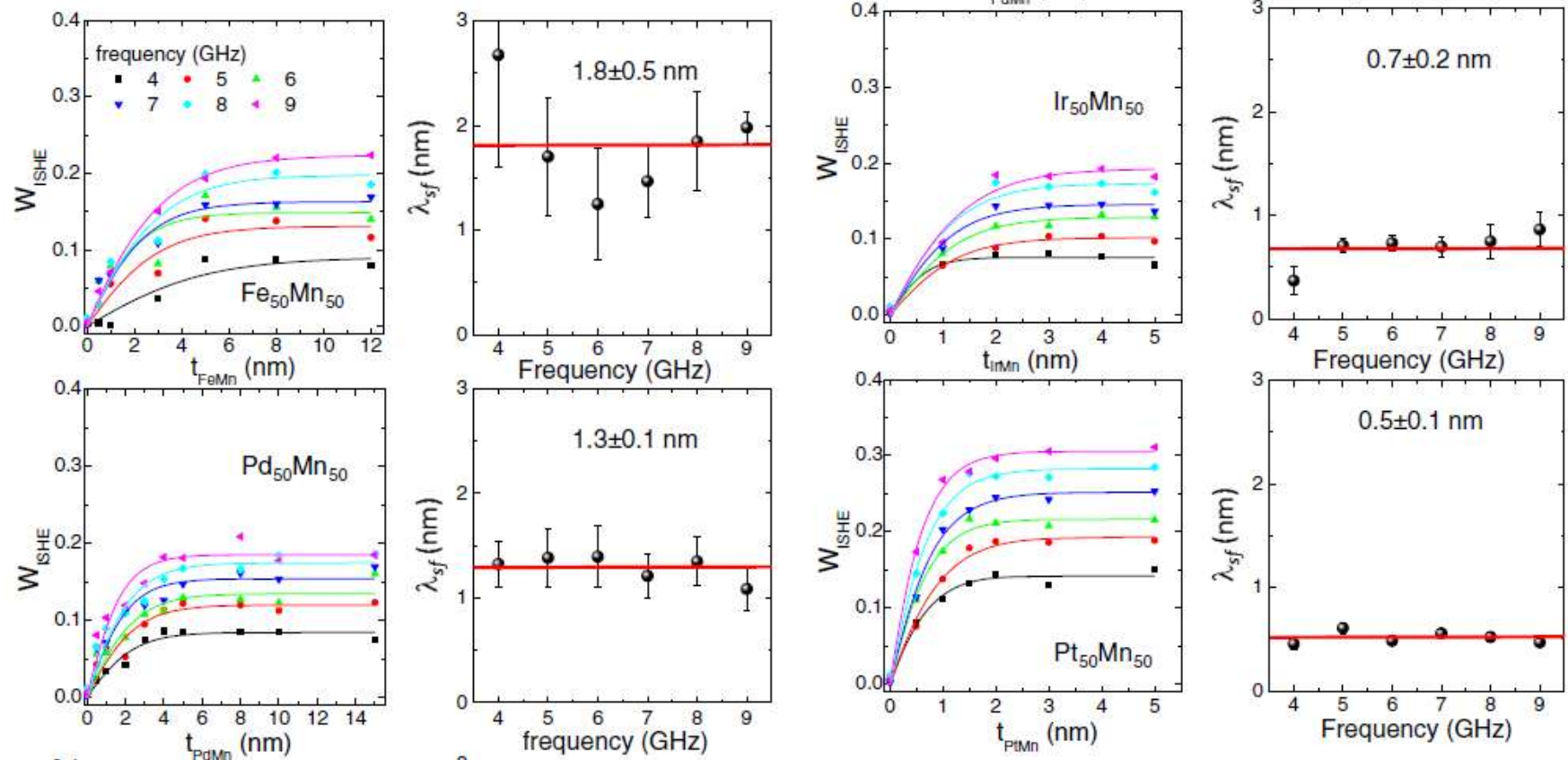
Crystal structure of CuAu-I -type Afs



Schematic of spin pumping and spin Hall effect

Zhang, et al, PRL (2014) 39

1) Large spin Hall in AFM



Thickness dependence shows
spin diffusion length to be short
 $\sim 1\text{nm}$

$\text{Fe}_{50}\text{Mn}_{50}$
 $\text{Pd}_{50}\text{Mn}_{50}$

$\text{Ir}_{50}\text{Mn}_{50}$
 $\text{Pt}_{50}\text{Mn}_{50}$

1) Large spin Hall in AFM

Spin Hall angle

0.008 ± 0.002 for FeMn

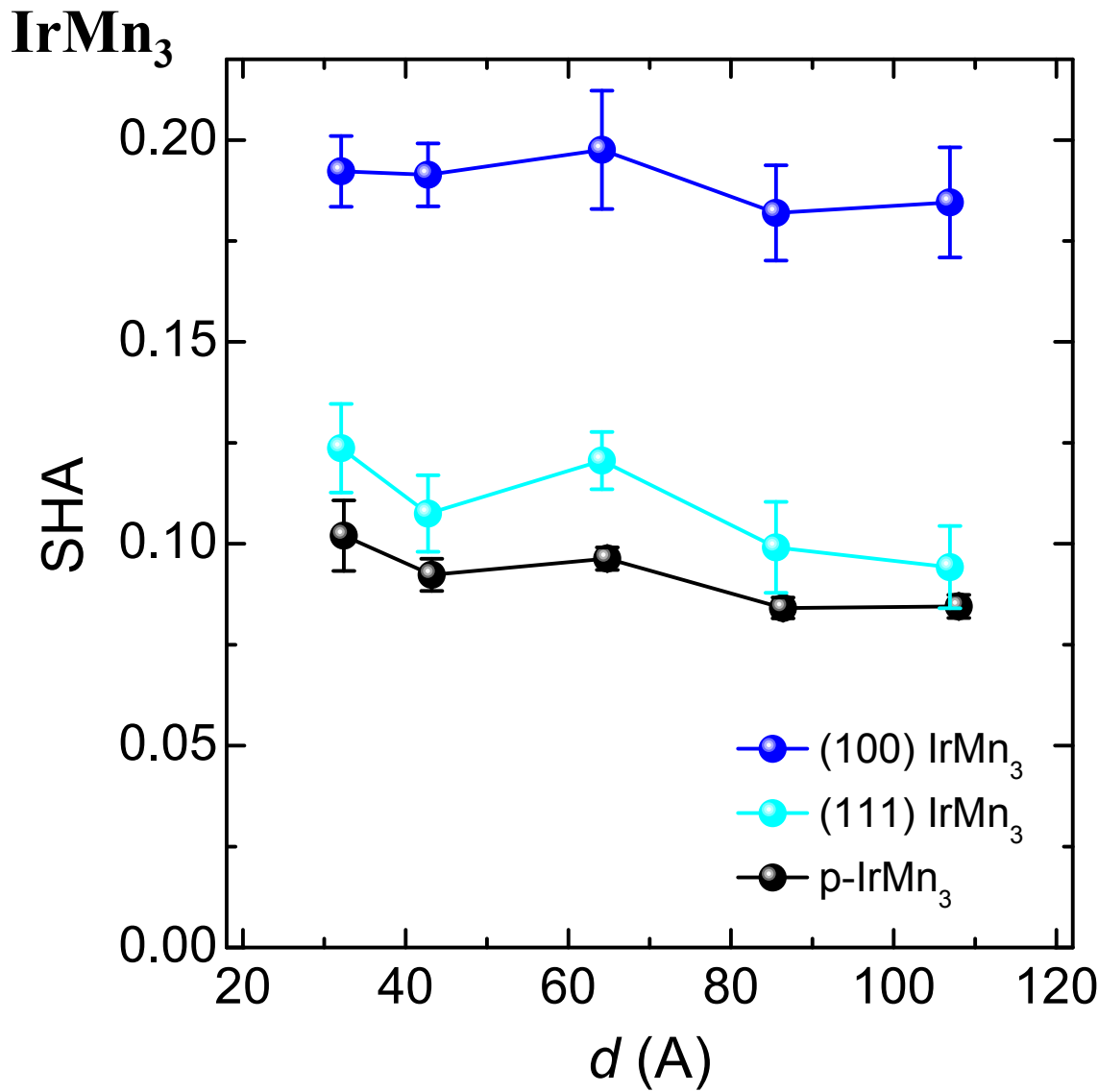
0.015 ± 0.005 for PdMn

0.022 ± 0.005 for IrMn

0.060 ± 0.010 for PtMn Large value, comparable to Pt

		σ_{yz}^x	σ_{zy}^x	σ_{zx}^y	σ_{xz}^y	σ_{xy}^z	σ_{yx}^z	$\bar{\sigma}$	σ_{av}	σ_{exp}
PtMn	c axis	303.9	-219.9	219.9	-303.9	60.3	-60.3	194.7	125.2	182.9
	a axis	30.4	-10.5	52.3	-260.9	92.5	-96.5	90.5		
IrMn	c axis	372.8	-59.7	59.7	-372.8	40.9	-40.9	157.8	41.6	40.8
	\bar{a} axis	-21.3	-94.6	126.3	-351.6	-325.1	325.1	-16.5		
PdMn	c axis	69.5	-17.0	17.0	-69.5	17.8	-17.8	34.8	3.9	33.6
	\bar{a} axis	0.0	3.5	7.4	-66.8	-70.8	69.8	-11.6		
FeMn	c axis	51.9	48.4	-47.6	50.9	-100.3	96.5	-48.6	-59.0	23.9
	a axis	-82.6	85.9	-47.8	47.5	-121.6	0.0	-64.2		

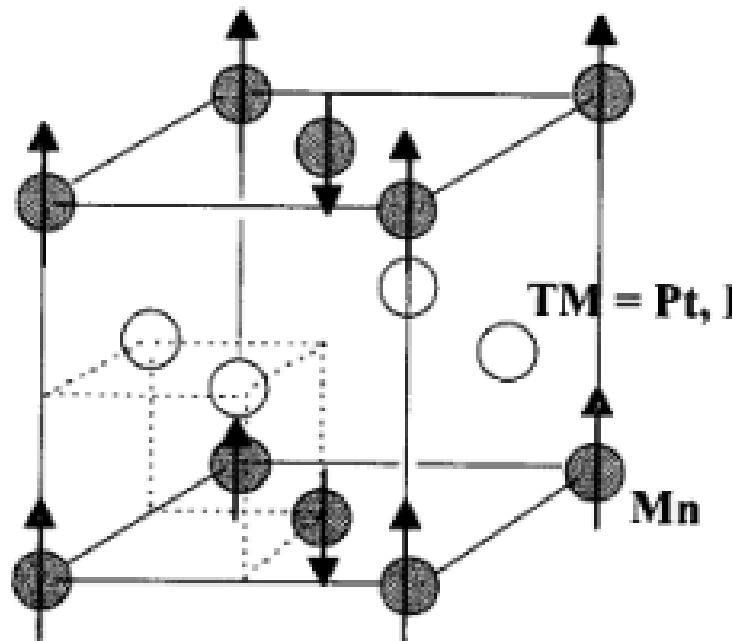
1) Large spin Hall in AFM



- The effective SHA is the largest for (100) IrMn₃
- (111) and polycrystalline IrMn₃ show similar SHA.

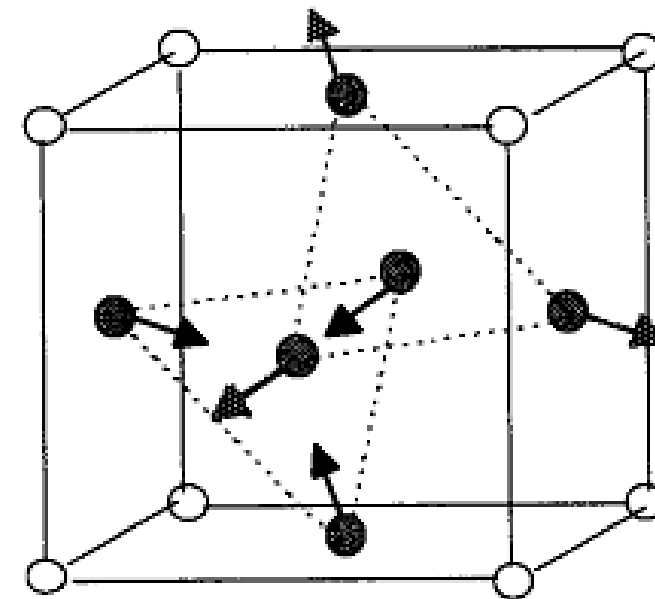
1) Large spin Hall in AFM

IrMn



➤ Collinear AFM

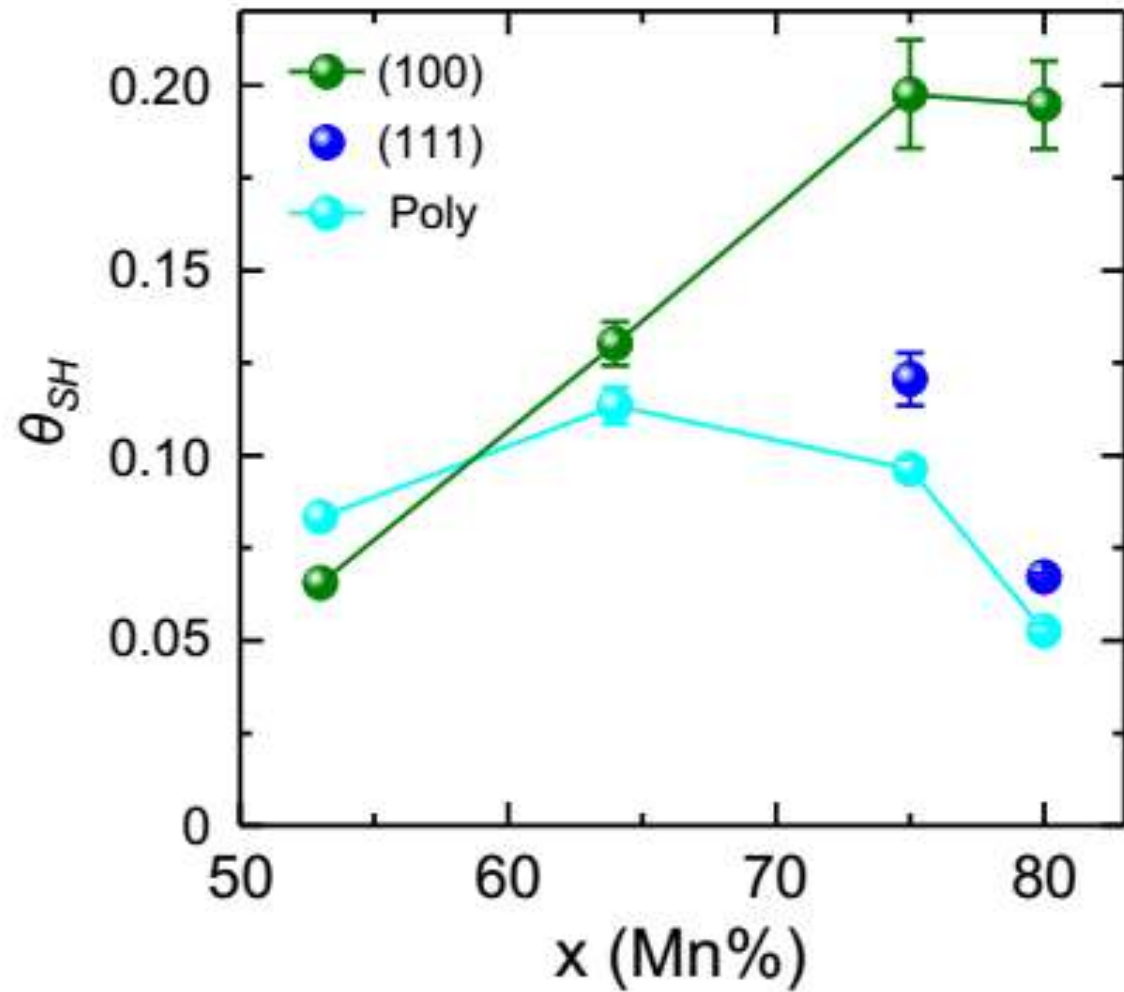
IrMn₃



➤ Non-Collinear AFM

Non-collinear AFM spin structure

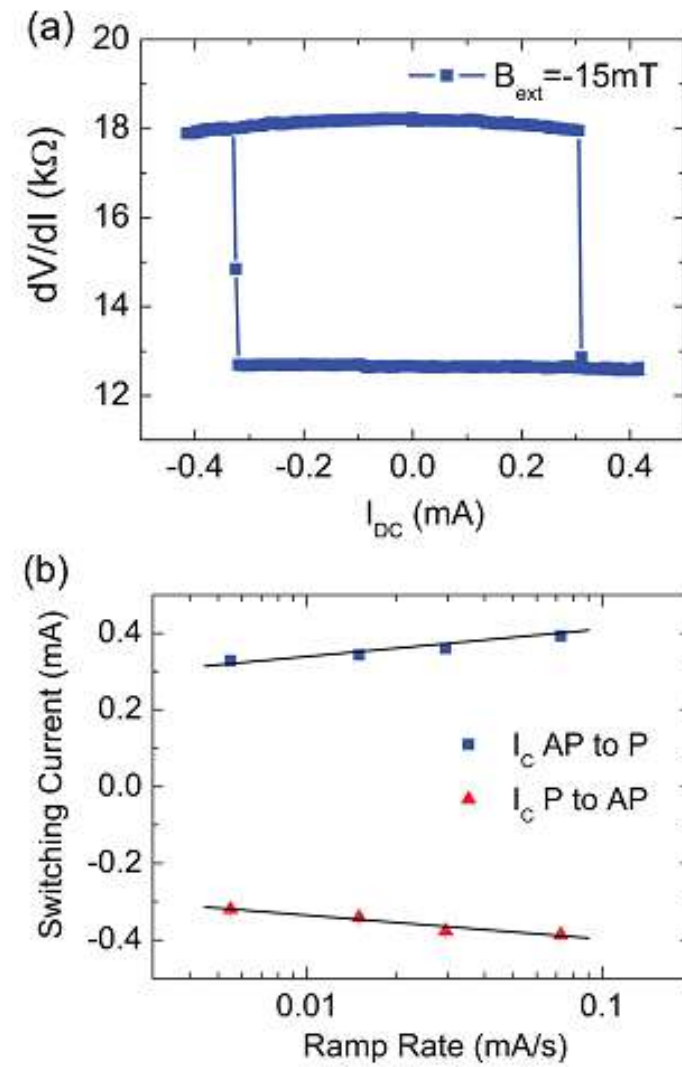
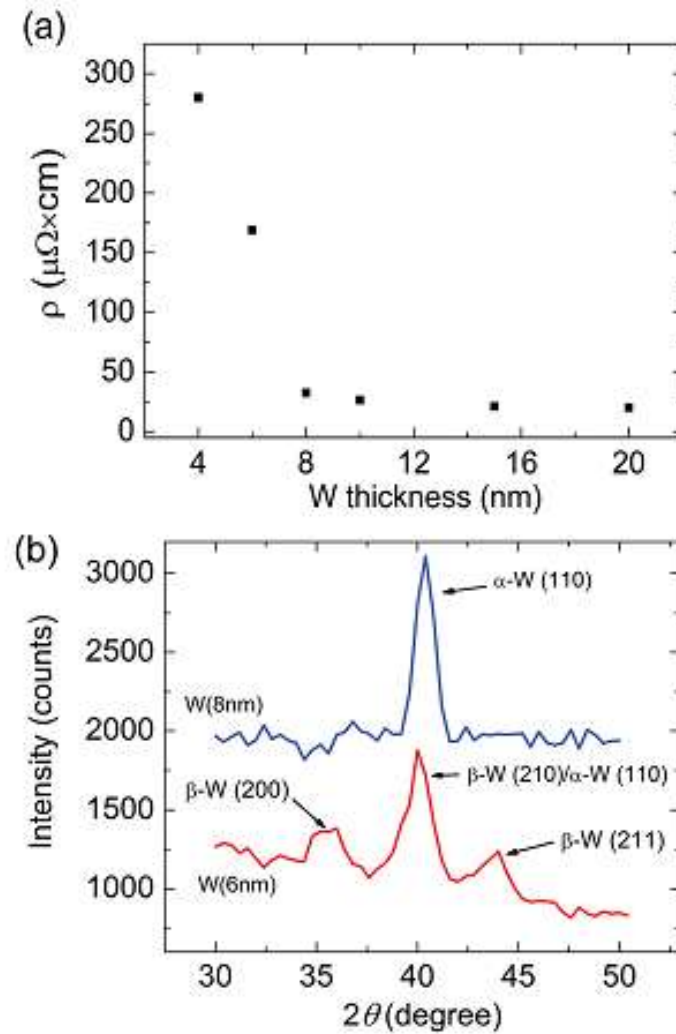
1) Large spin Hall in AFM



➤ Little facet dependence in **collinear AFM**

➤ Strong Facet dependence in **non-collinear AFM**

2) Large spin Hall in Beta-W, Ta



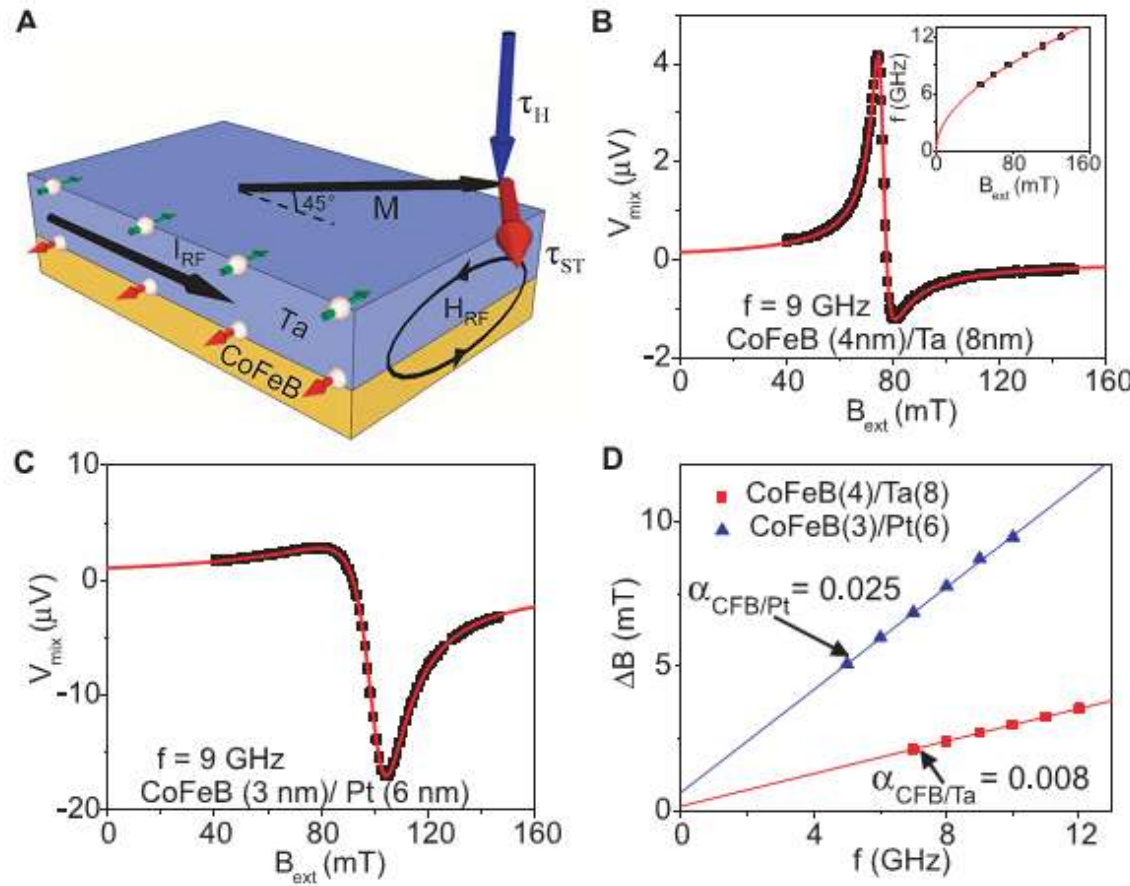
Spin Hall angle: 0.38 ± 0.06

Pai, et al, ARL (2012)

45

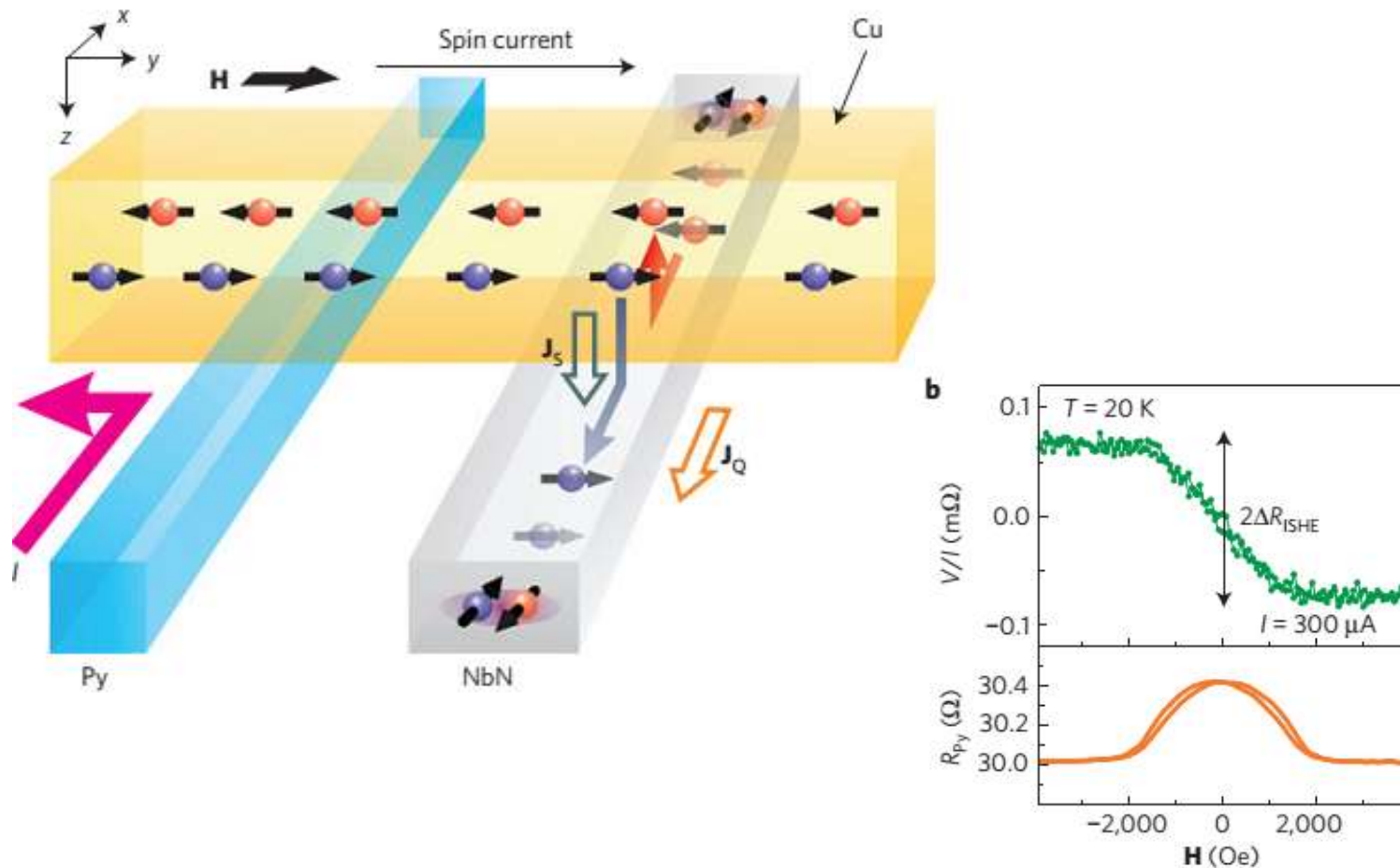
2) Large spin Hall in Beta-W, Ta

Beta-Ta



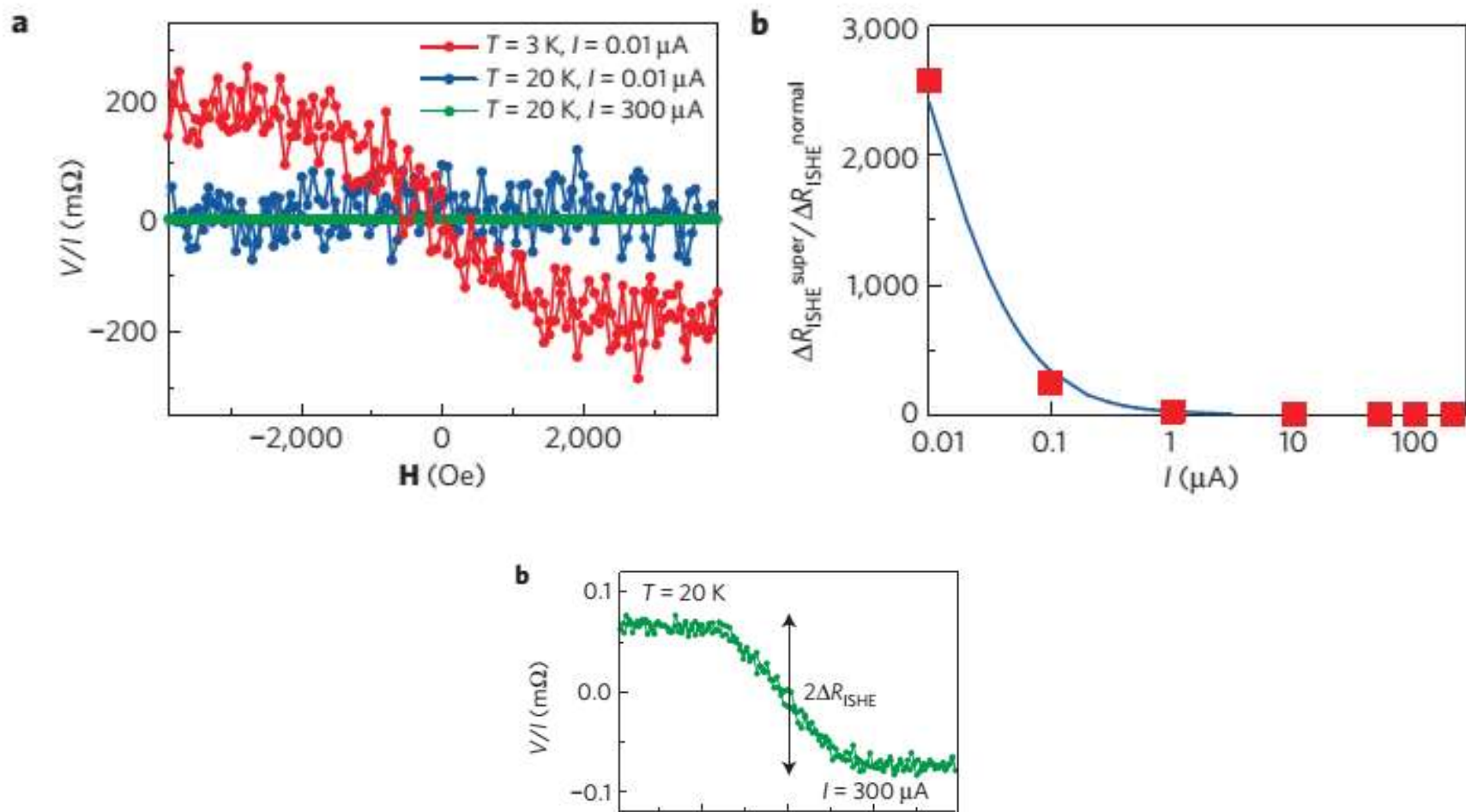
Liu, et al, Science (2012)

3) Large spin Hall in S. C.

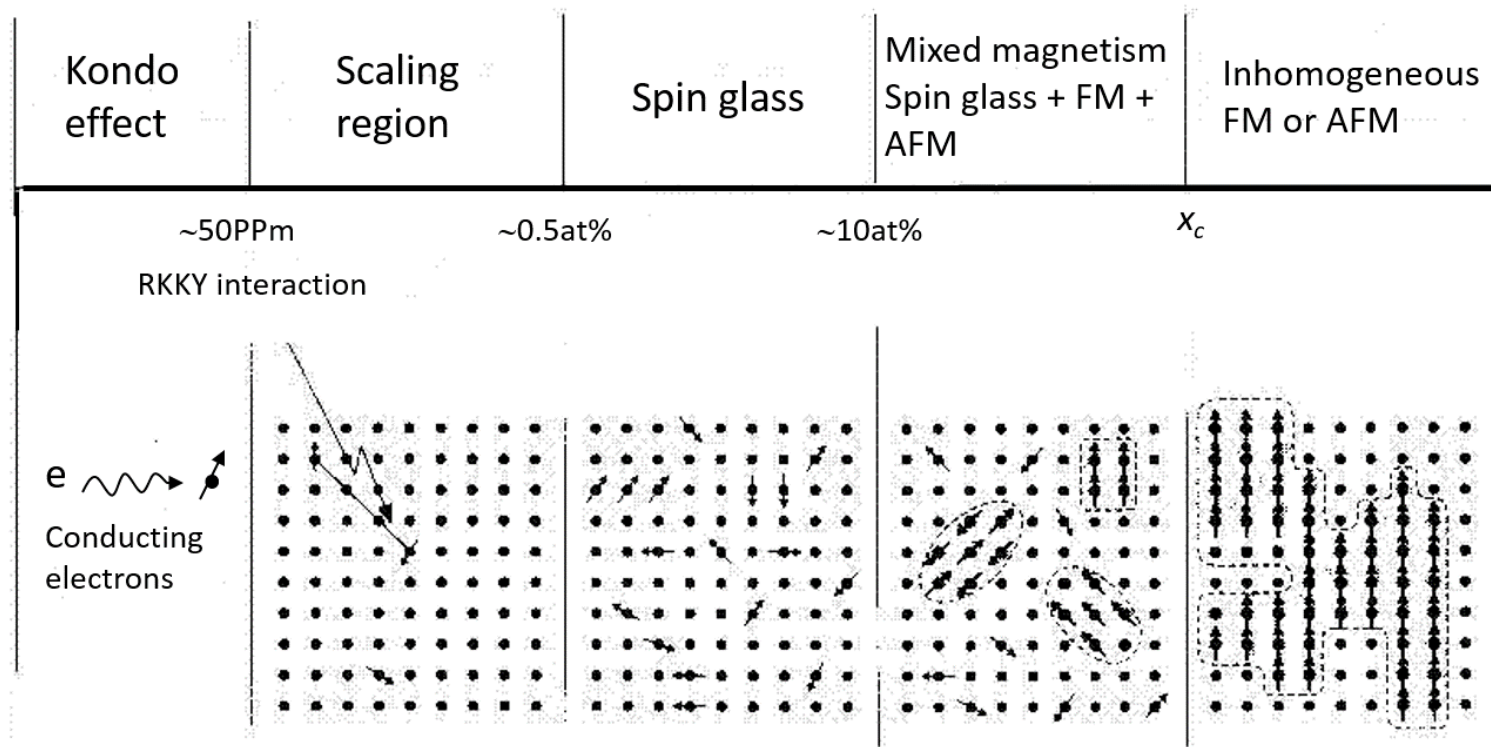


Wakamura, et al, Nature Materials (2015)

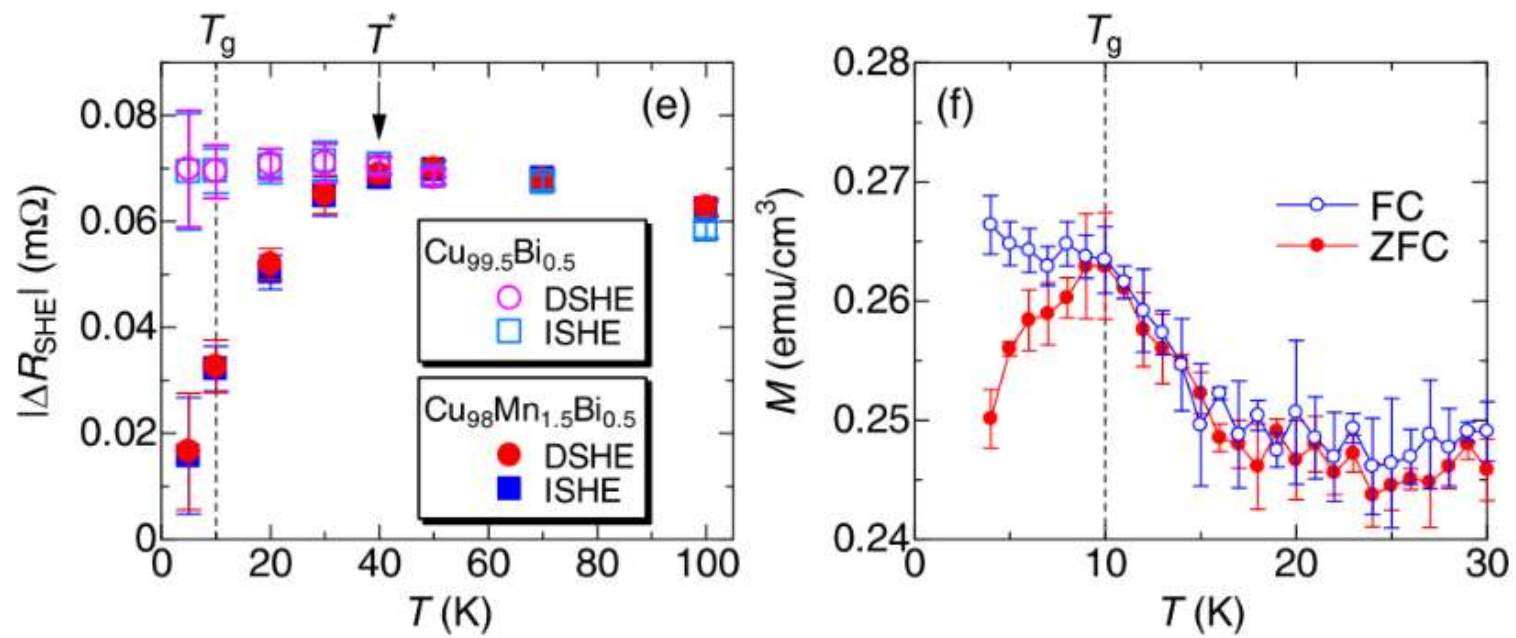
3) Large spin Hall in S. C.



4) Suppression of SHE in spin Glass



4) Suppression of SHE in spin Glass

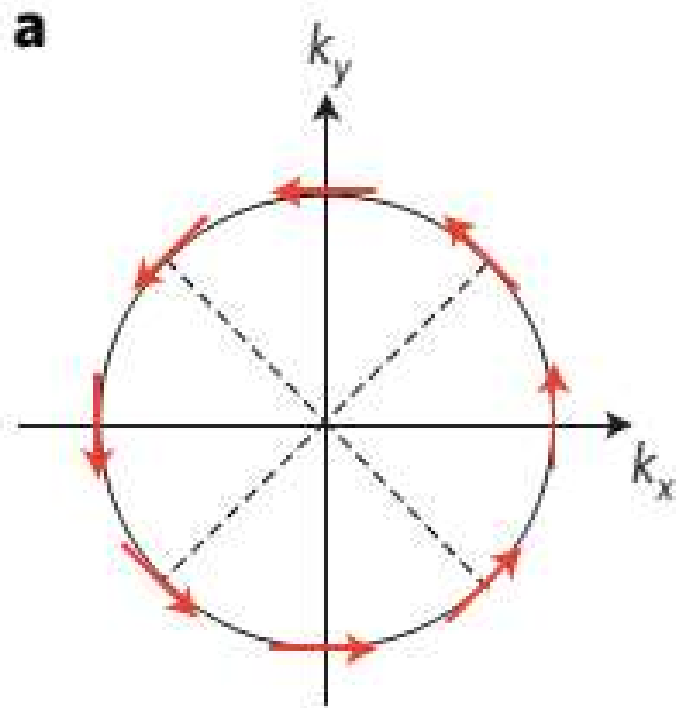


休息10分钟

Outline

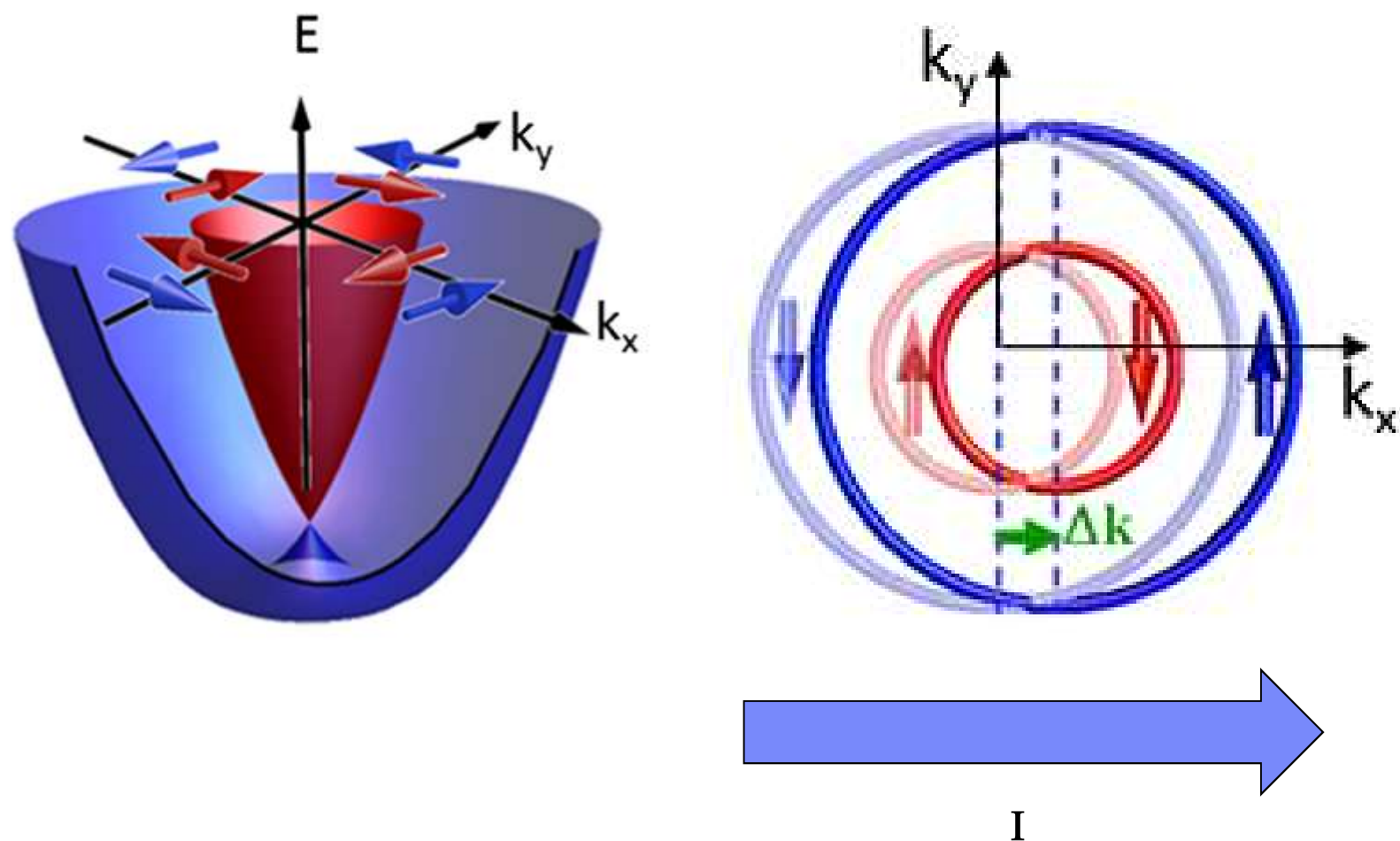
3. Rashba-Edelstein effect

Rashba effect



$$\hat{H}_R = (\alpha_R/\hbar) (\mathbf{z} \times \mathbf{p}) \cdot \boldsymbol{\sigma}$$

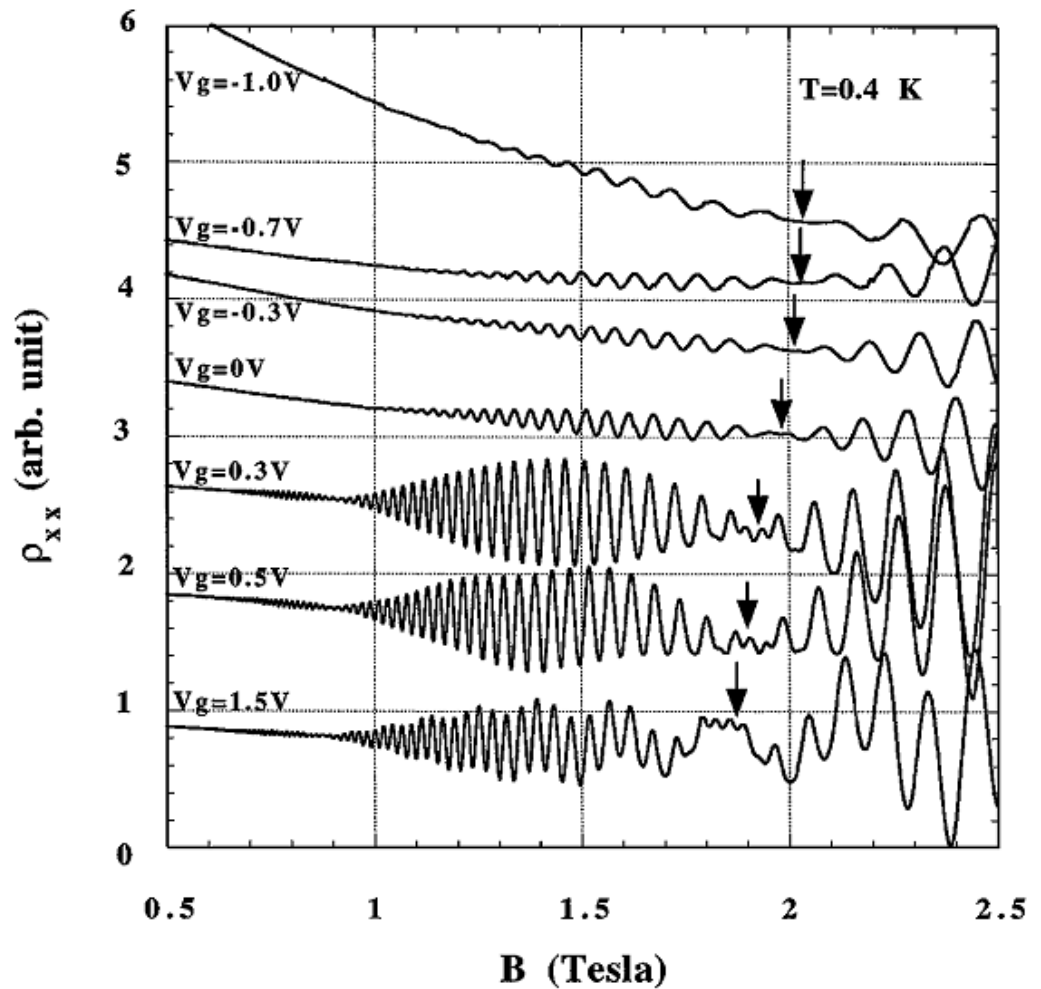
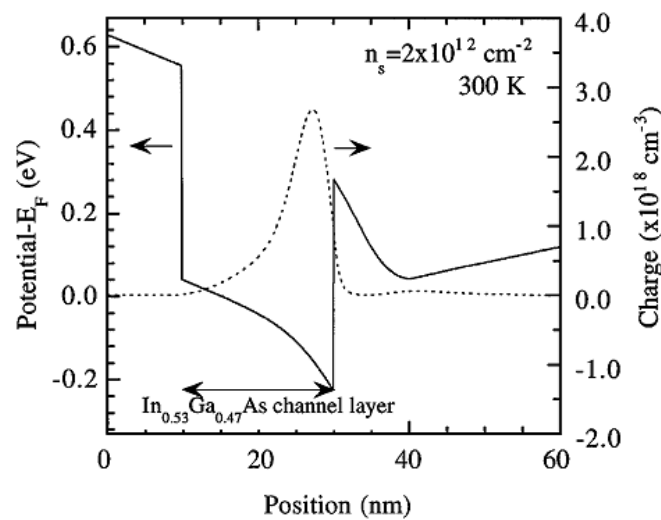
Edelstein effect



V. M. Edelstein, Solid State Commun. 73, 233 (1990)

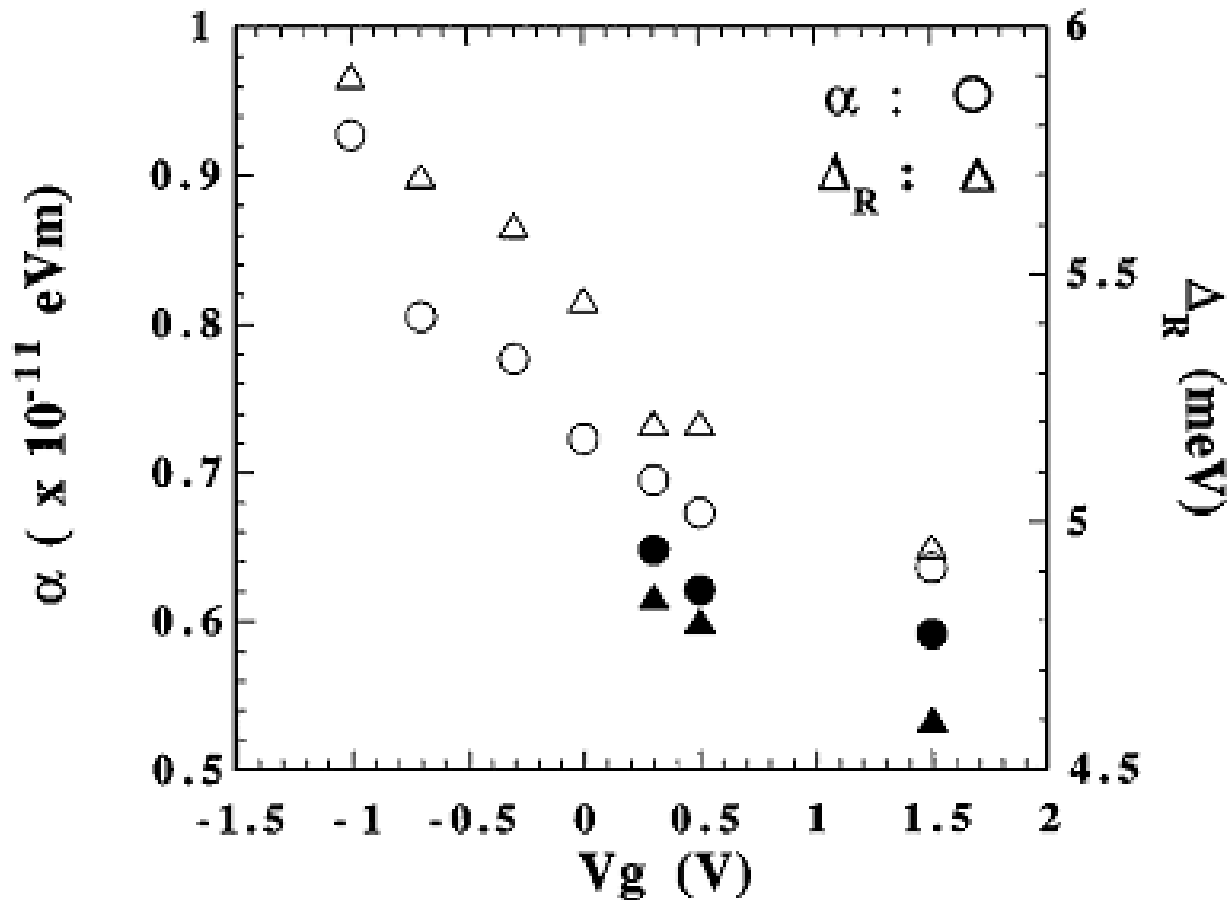
Experimental of Rashba effect

InGaAs



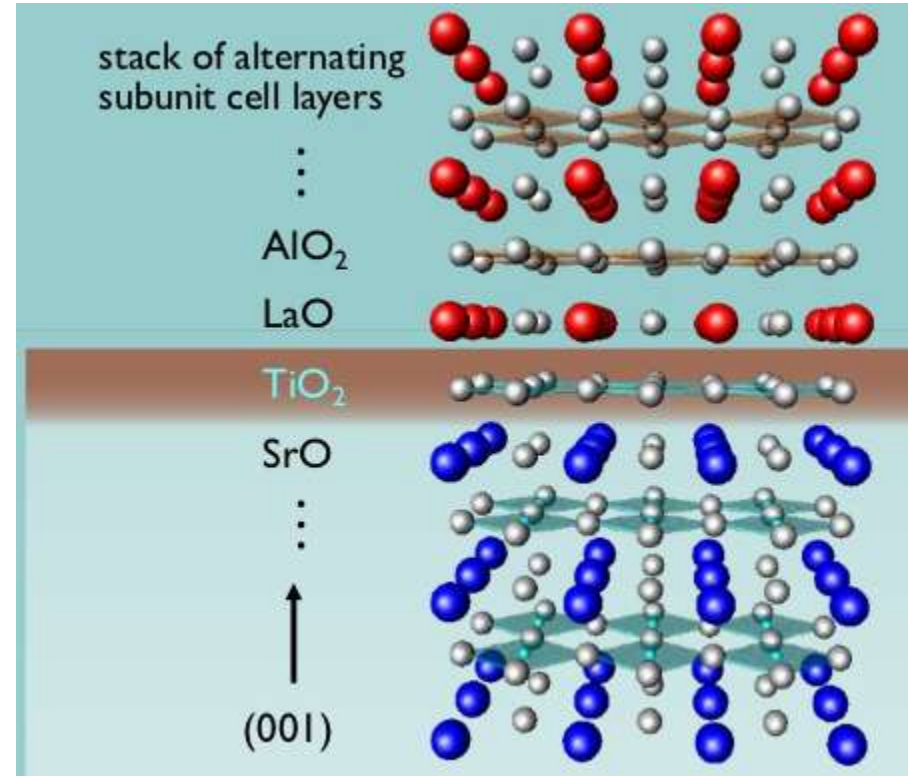
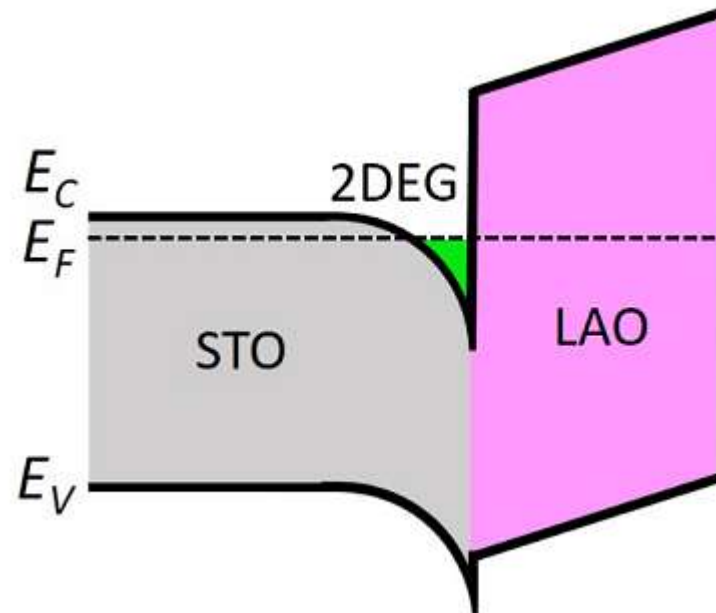
Experimental of Rashba effect

$$E_n^{\pm} = \hbar\omega_c \left[n \pm \frac{1}{2} \sqrt{(1 - gm^*/2)^2 + n \frac{\Delta_R^2}{E_F \hbar\omega_c}} \right]$$



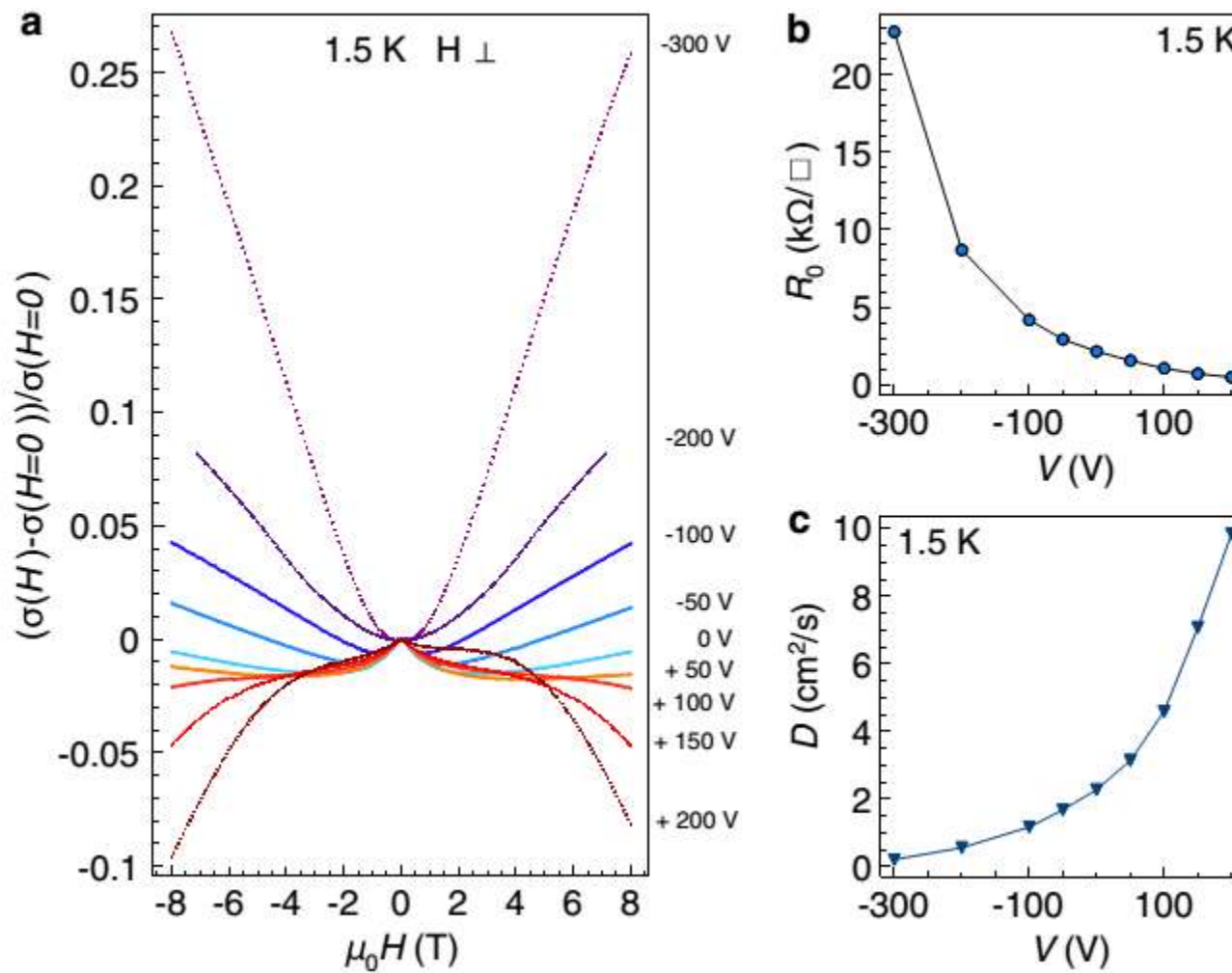
Experimental of Rashba effect

STO-LAO



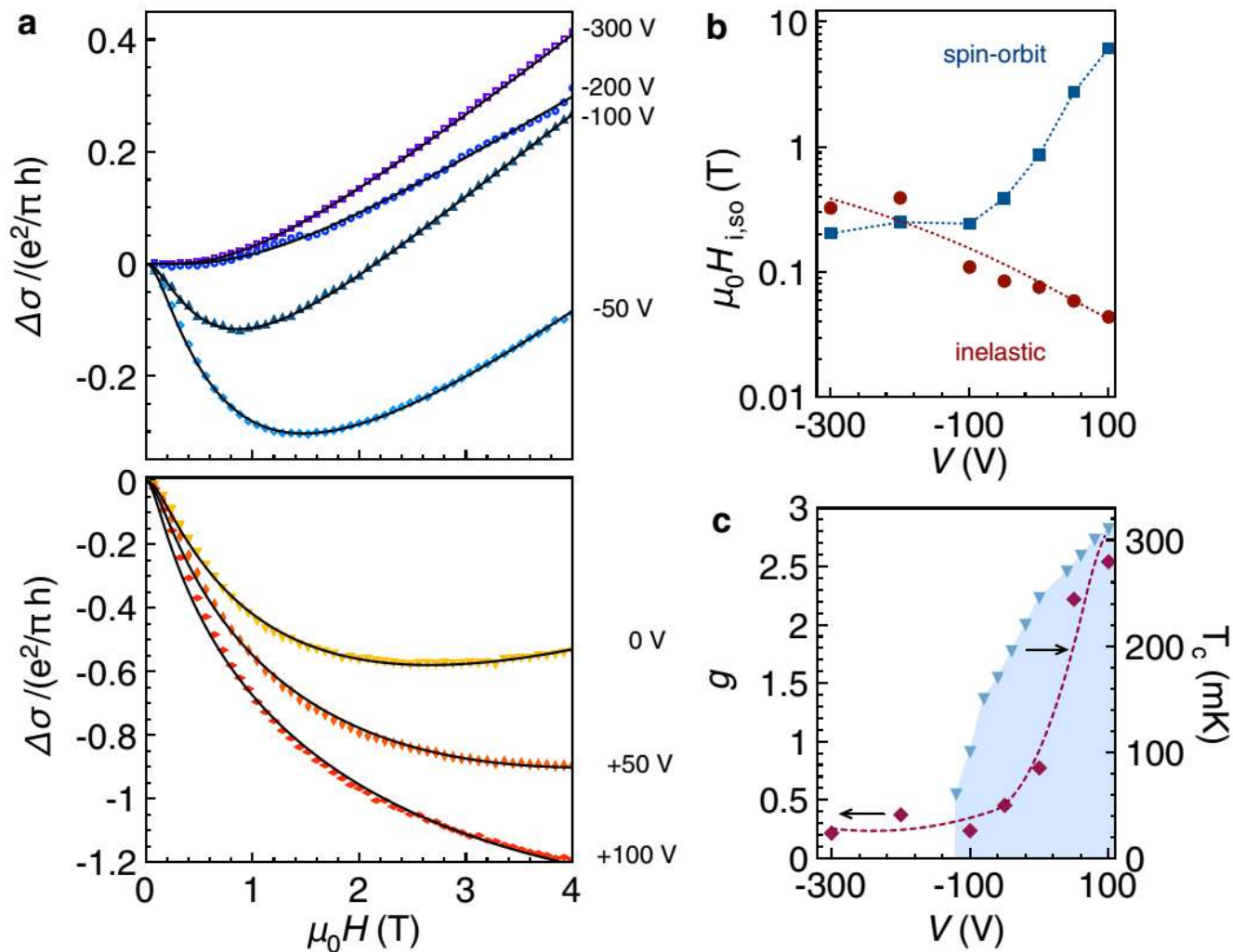
Hwang, et al. Nat. Mater. (2012)

Experimental of Rashba effect

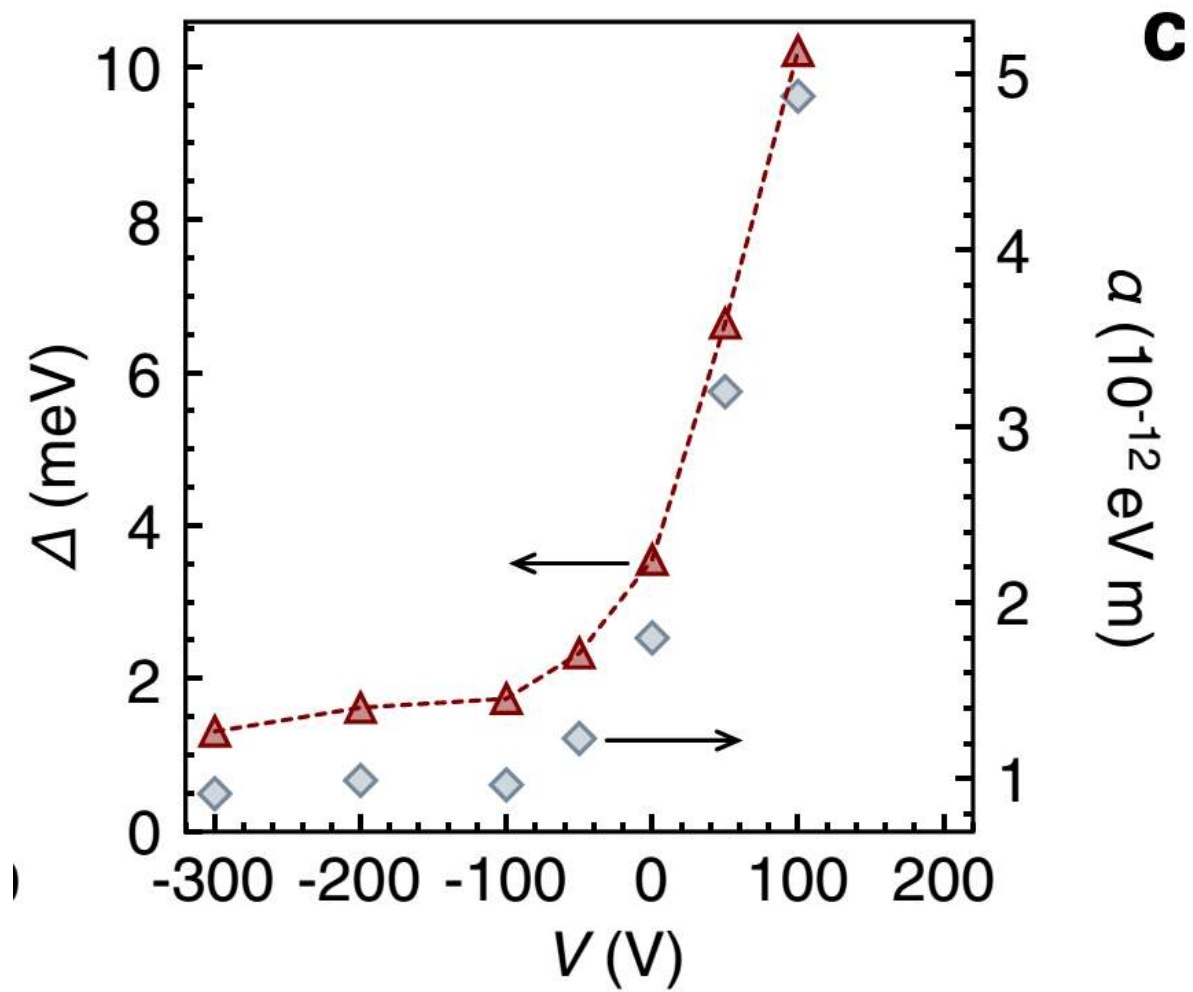


Caviglia, et al. PRL (2010)

Experimental of Rashba effect



Experimental of Rashba effect



Rashba effect

Spin-ARPES of Bi/Ag

$$\hat{H}_{\text{SO}} = \alpha_R \boldsymbol{\sigma} \cdot (\mathbf{k}_{\parallel} \times \mathbf{e}_z),$$

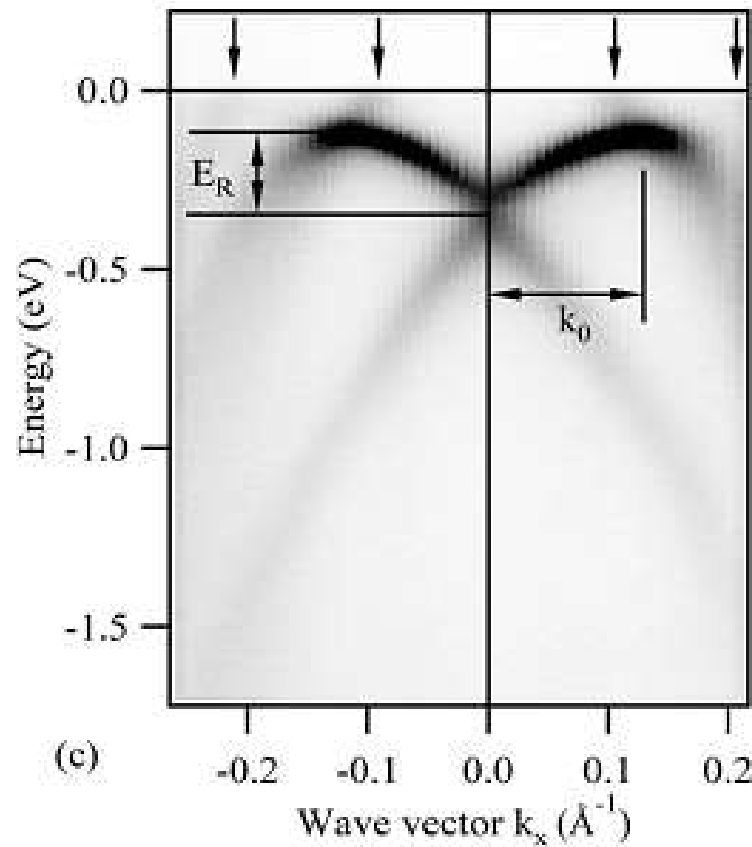
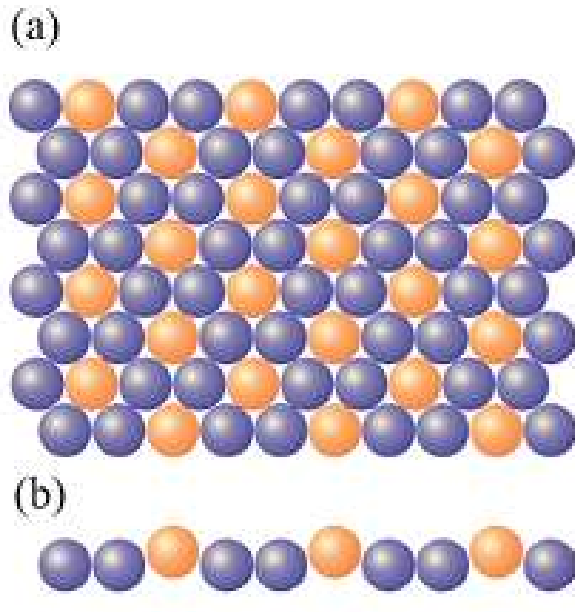
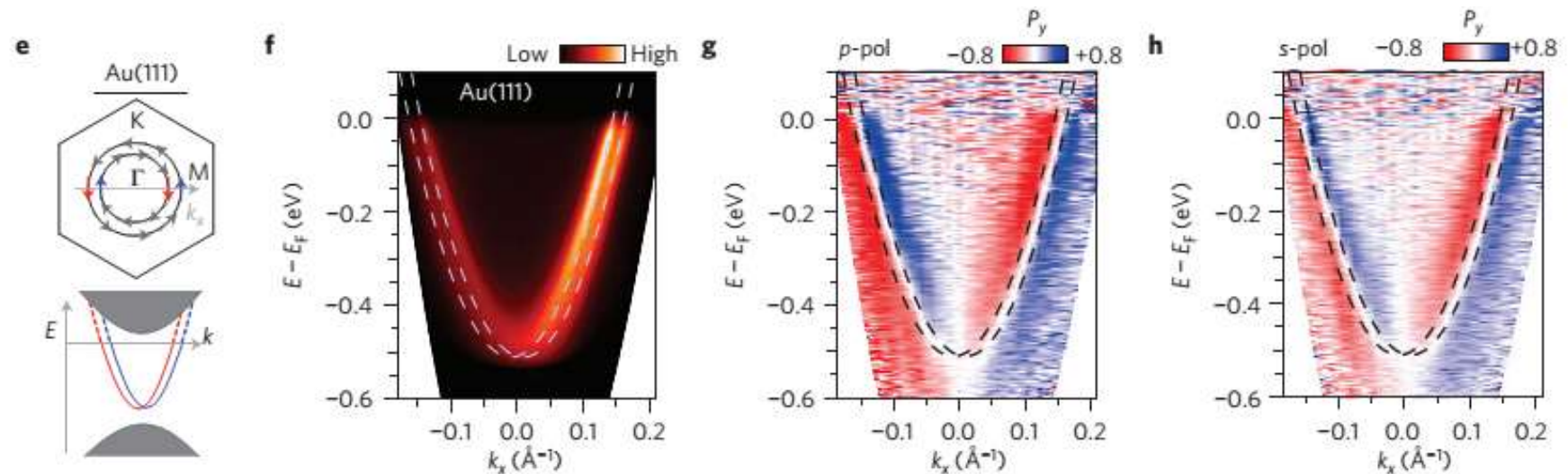


FIG. 1 (color online). (a) Schematic top view of the $(\sqrt{3} \times \sqrt{3})R30^\circ$ Bi/Ag(111) surface alloy [Bi, light gray (orange); Ag, dark gray (blue)]. (b) Side view of the schematic, illustrating the

Ast, et al. PRL (2007)

Rashba effect

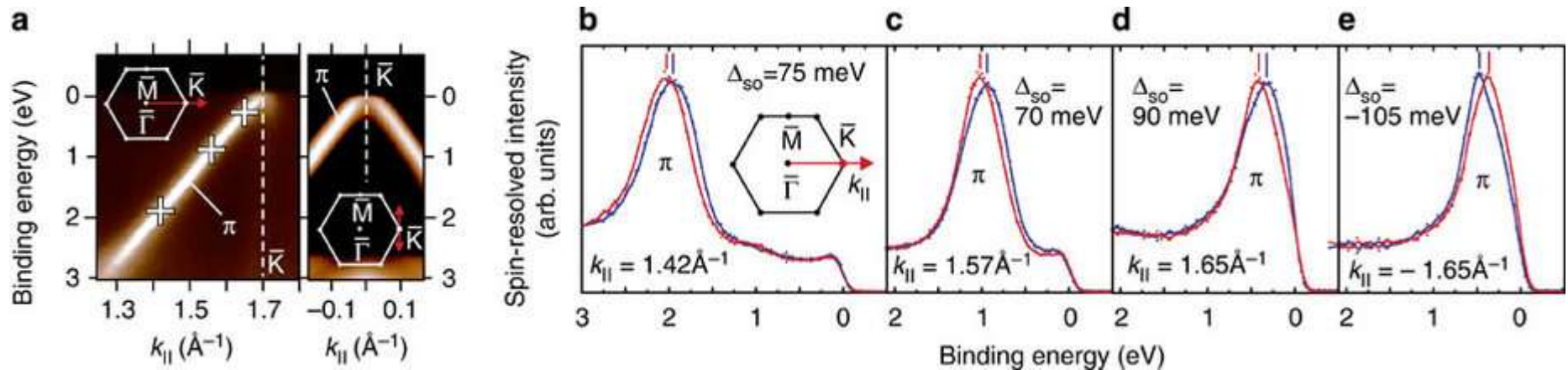
Spin-ARPES of Au (111)



Jozwiak, et al. Nature Physics (2013)

Rashba effect

Spin-ARPES of Graphene/Au (111)

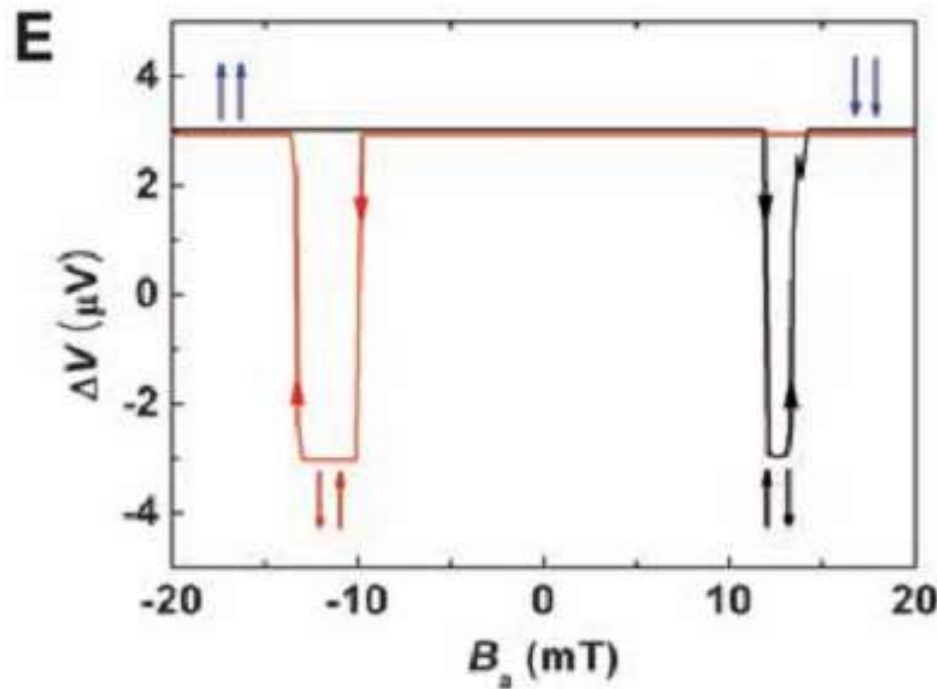
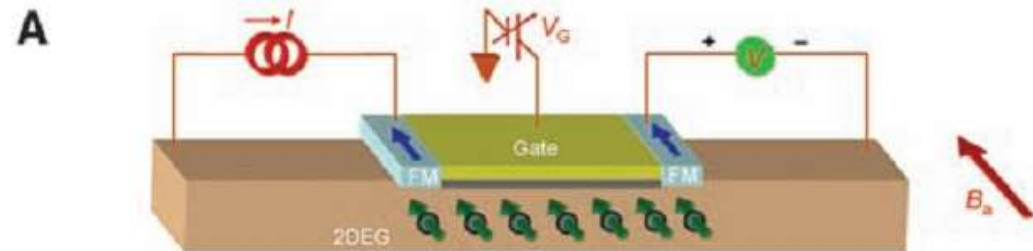
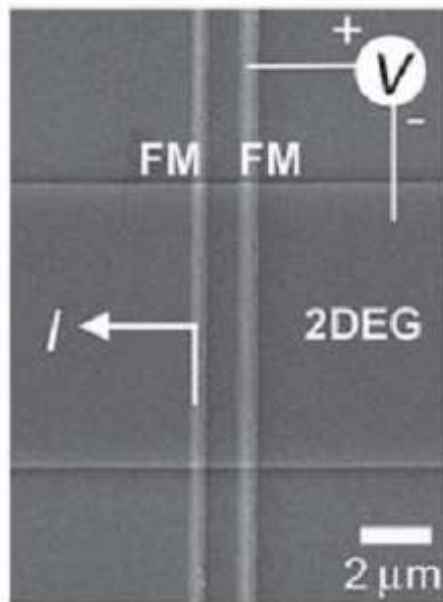


Marchenko, et al. Nature Commun. (2012)

Rashba effect for Spin-FET

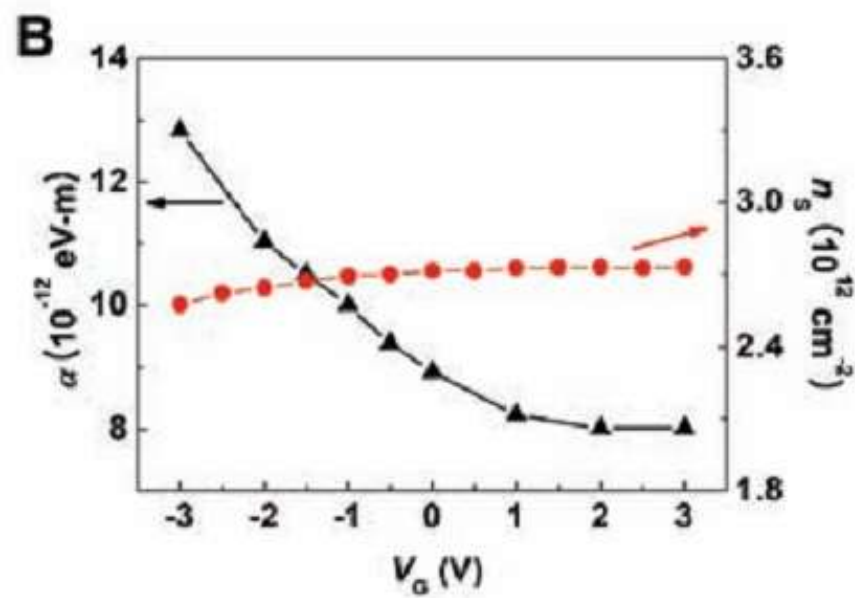
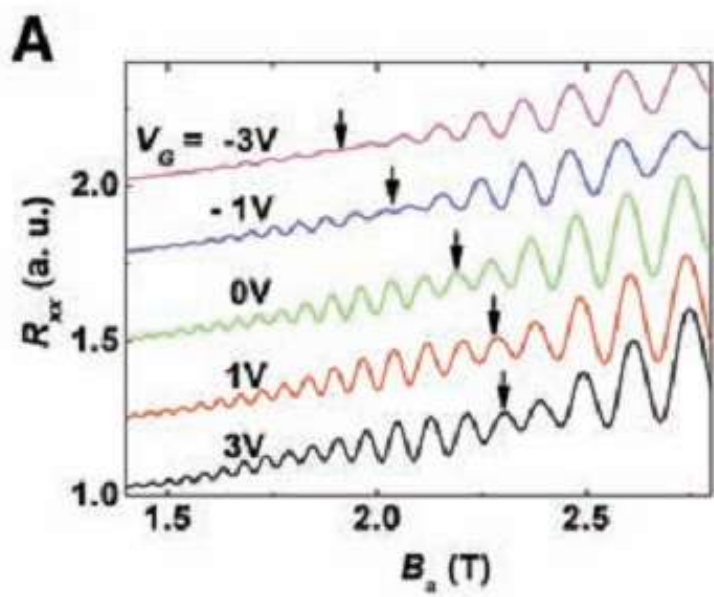
InAs channel

C

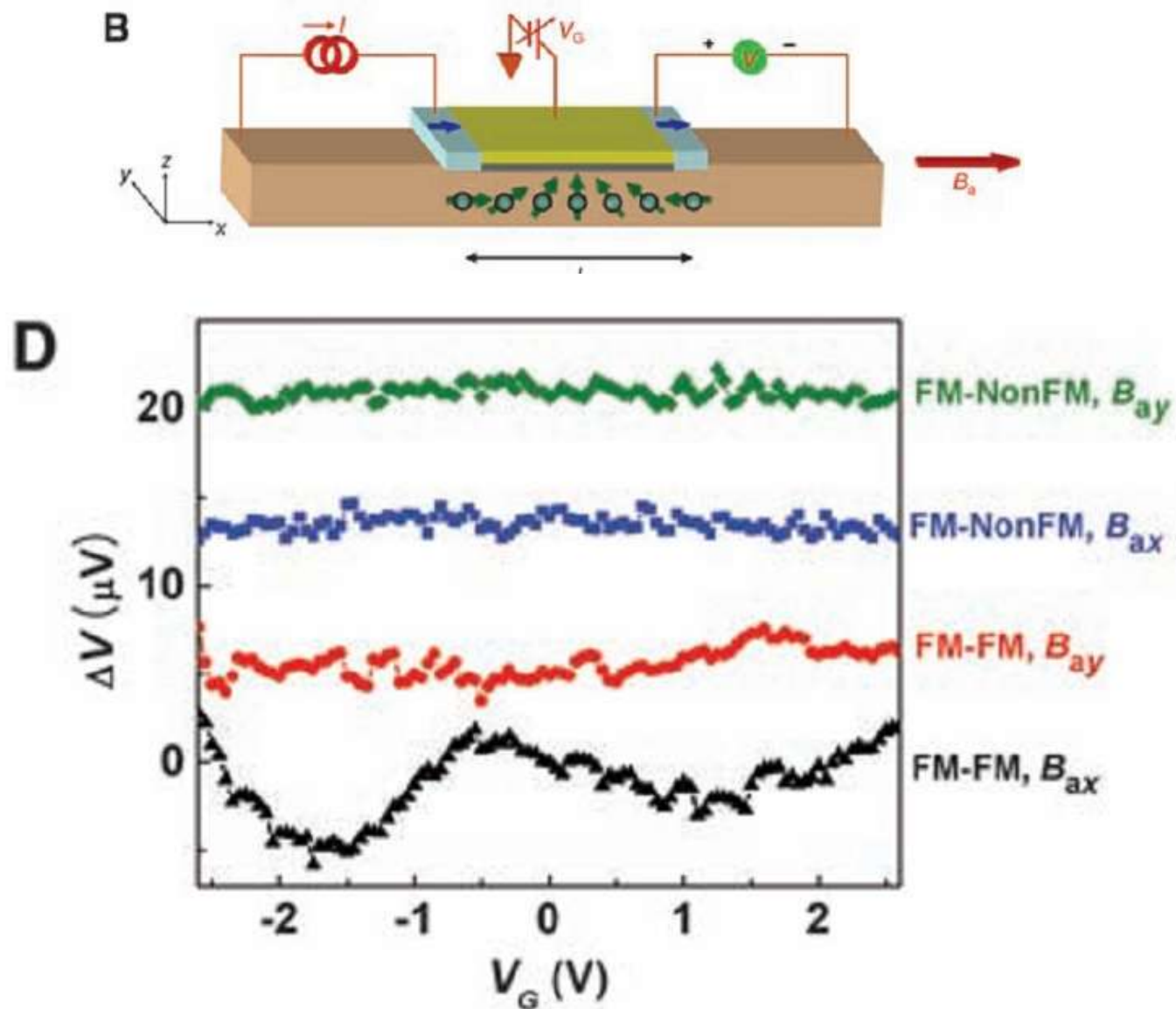


Koo, et al, Science (2009)

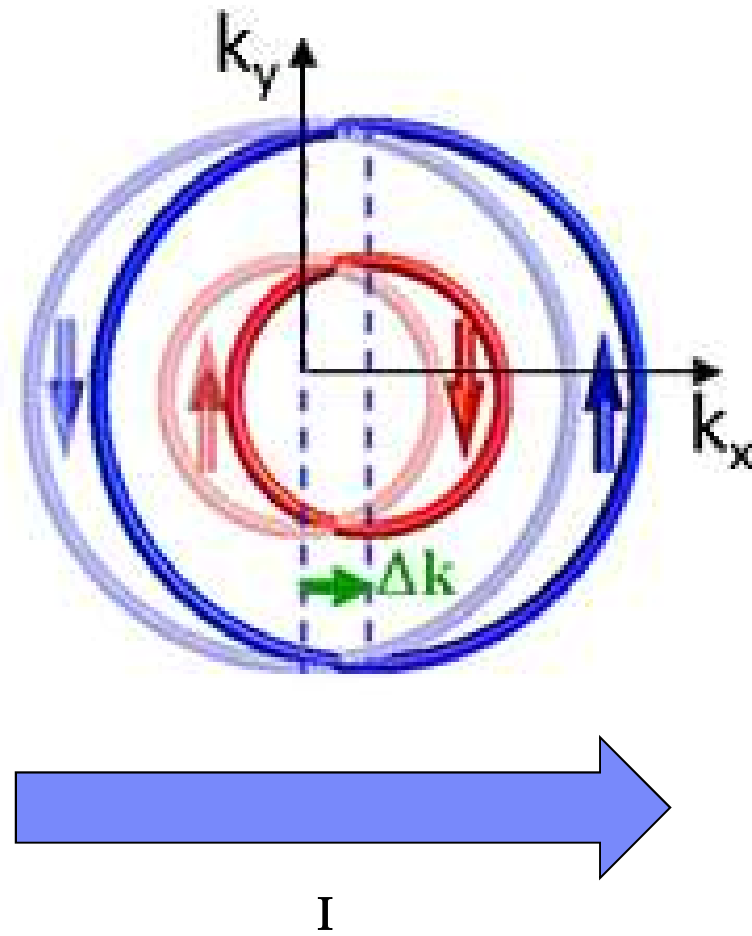
Rashba effect for Spin-FET



Rashba effect for Spin-FET



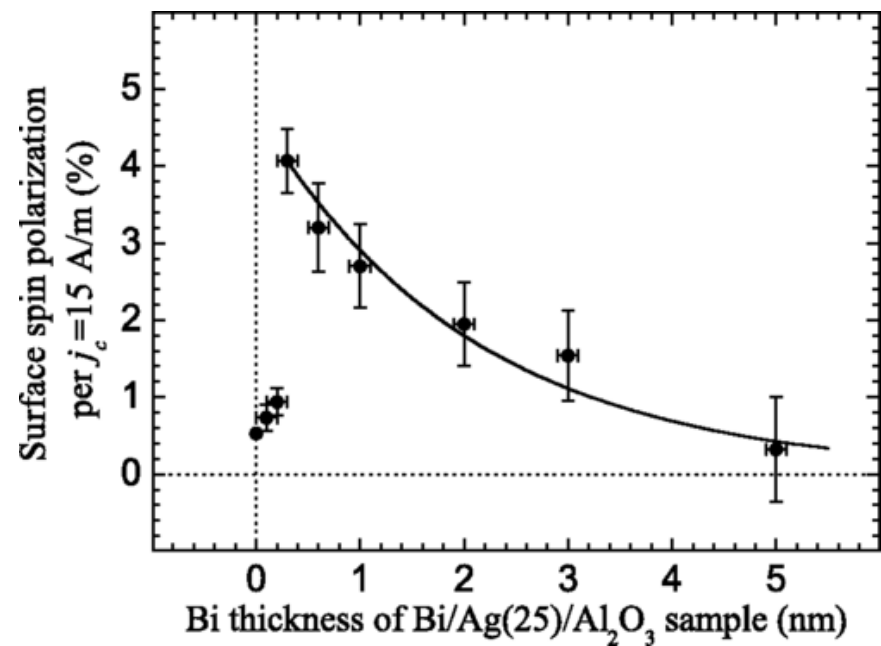
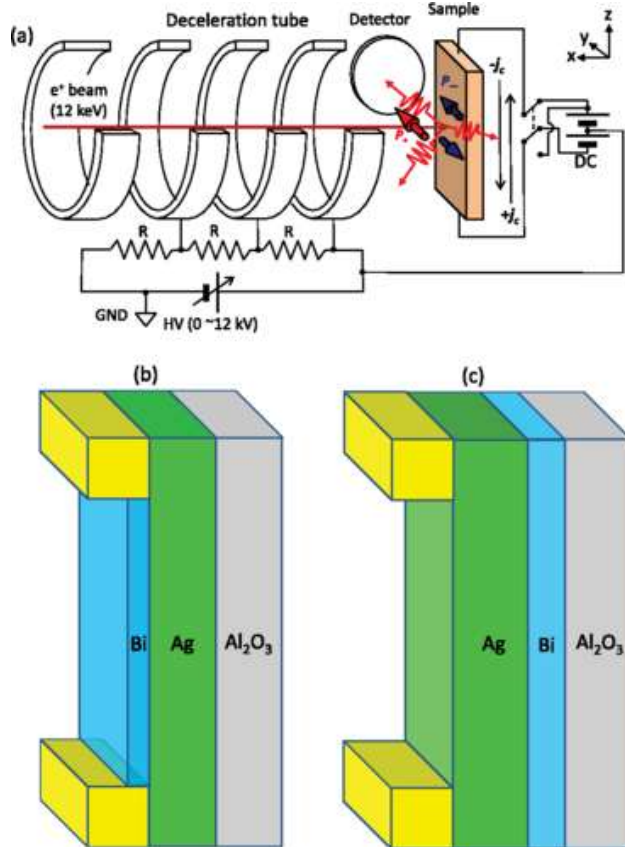
Edelstein effect



Edelstein effect

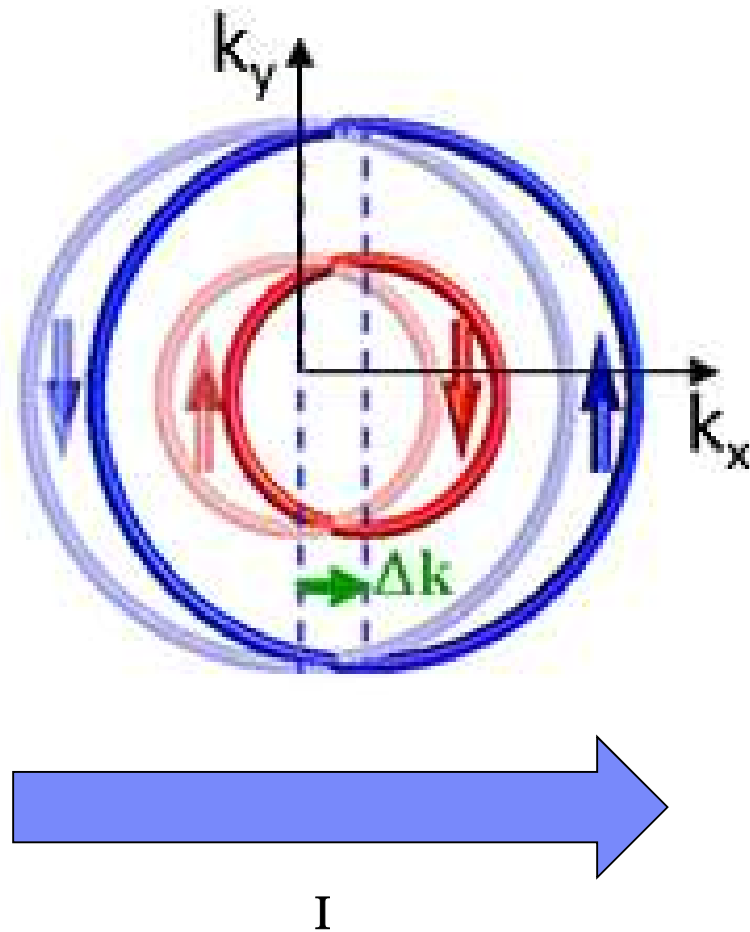
Bi/Ag

The spin polarized positron beam

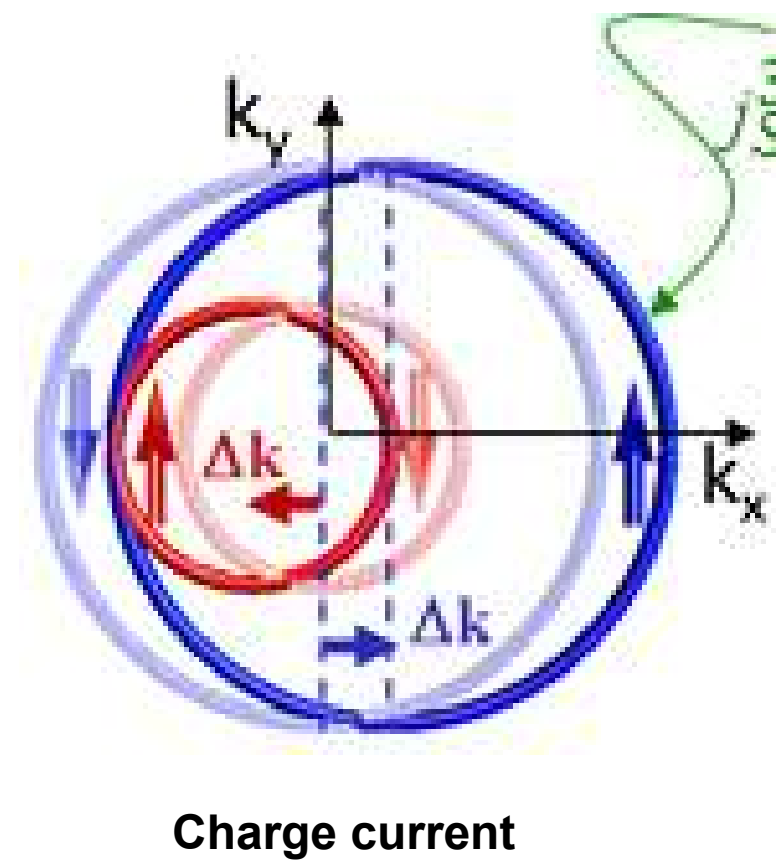


Zhang, et al. PRL (2015)

Edelstein effect



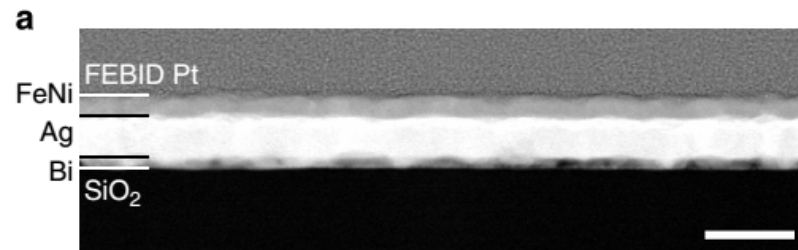
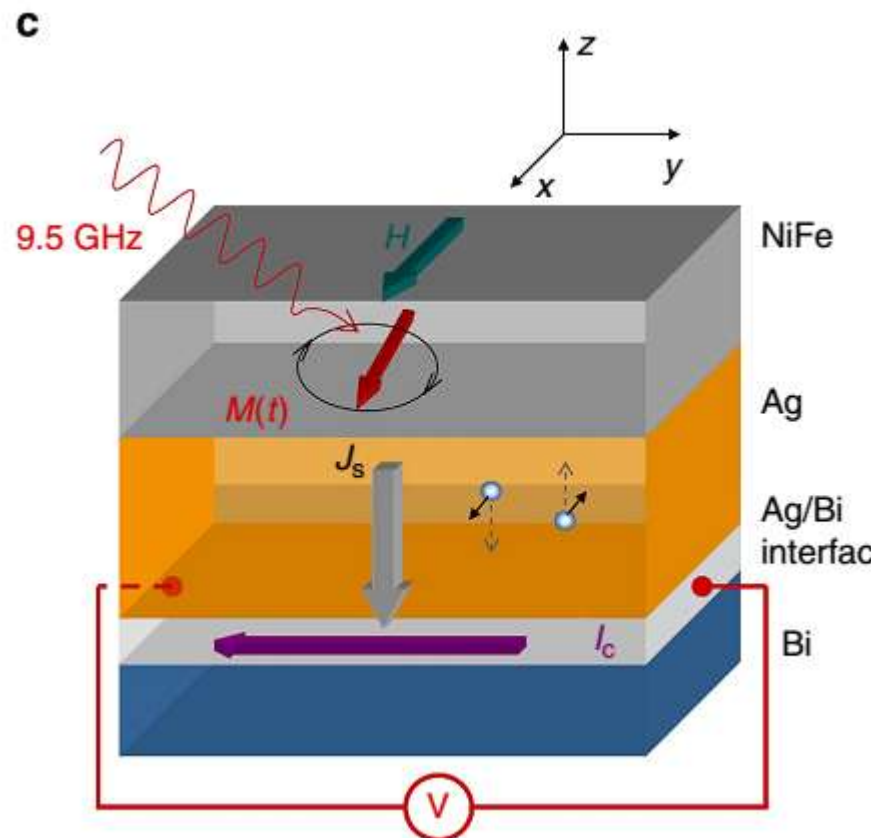
Spin injection



Charge current

Inverse Edelstein effect

Bi/Ag



Sanchez, et al. Nature Comm. (2013)

Inverse Edelstein effect

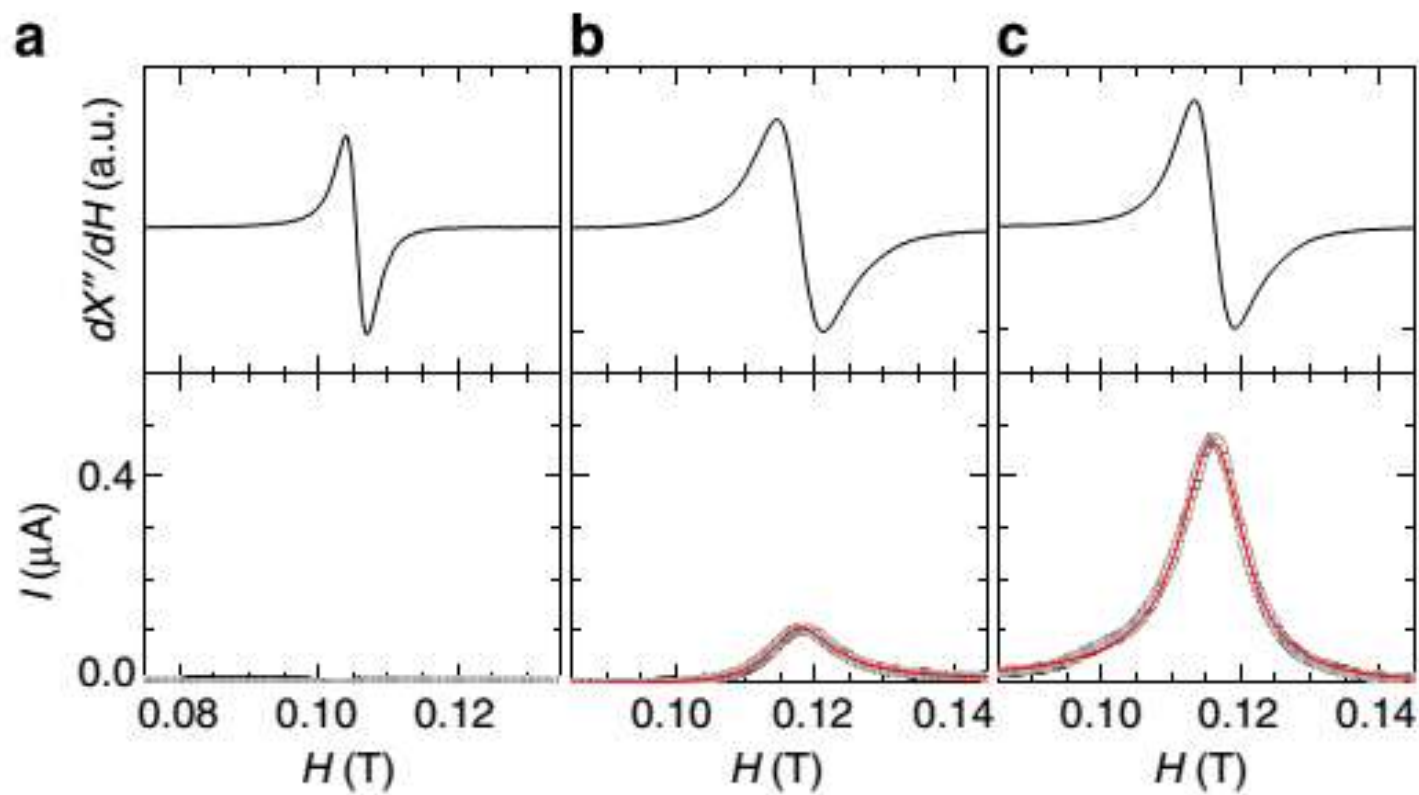


Figure 2 | Spin pumping results. FMR spectrum (top) and corresponding field dependence of the current I_C derived from the DC voltage V (bottom) for NiFe(15)/Ag(10) **(a)**, NiFe(15)/ Bi(8) **(b)** and NiFe(15)/Ag(5)/Bi(8) **(c)** samples. Red lines are Lorentzian fits. The narrow FMR line and

Inverse Edelstein effect

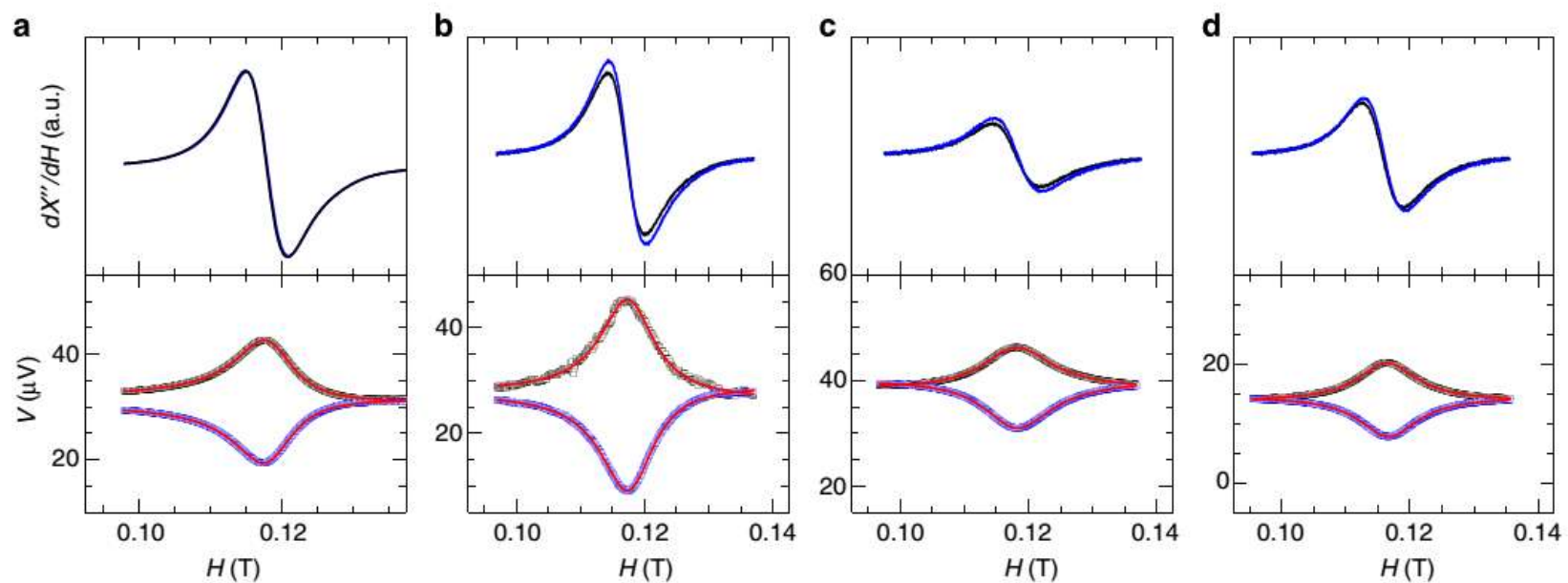
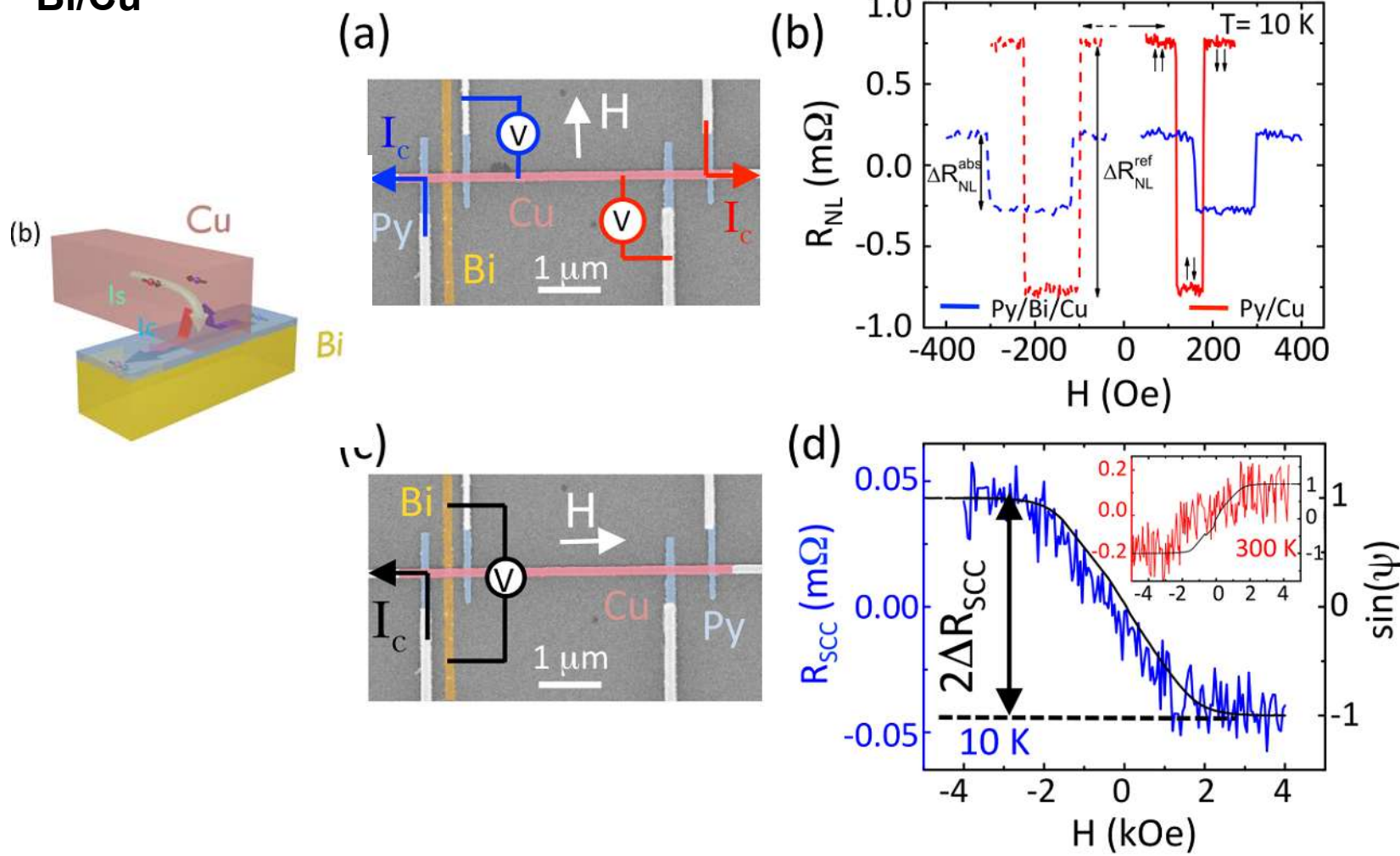


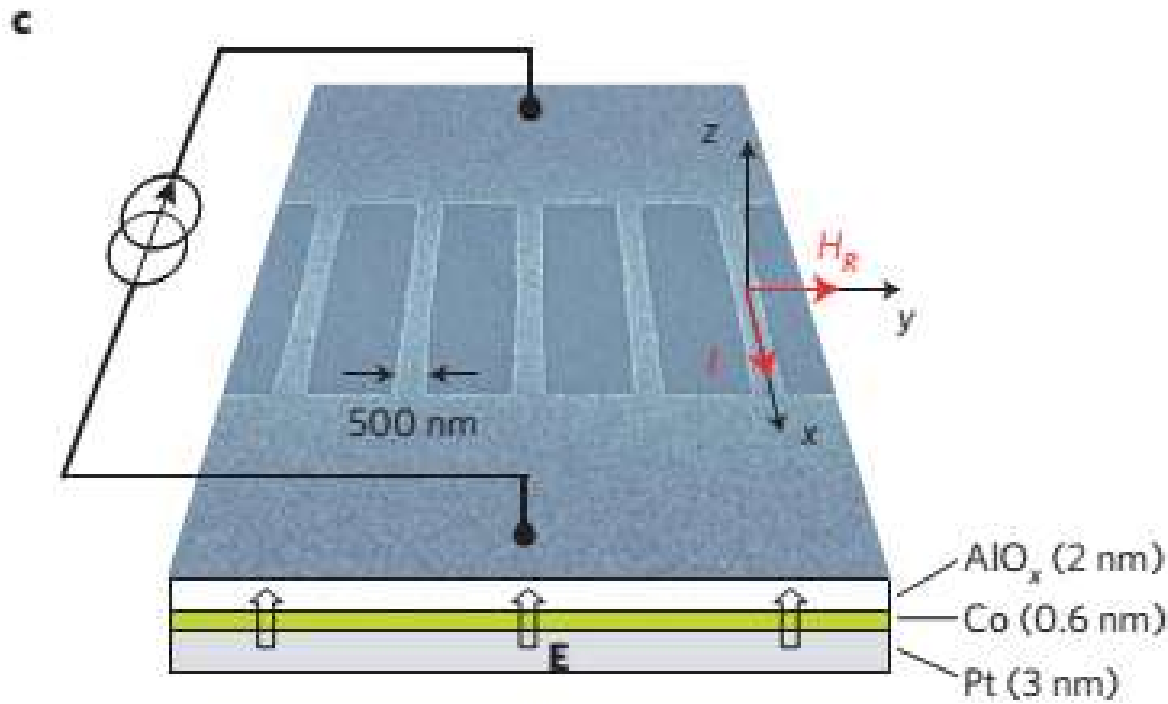
Figure 8 | FMR and measured voltage. Raw data of FMR-V curves on NiFe(15)/Ag(t)/Bi(8), in the series with length of 1.0 mm. (a) 0 nm of Ag. (b) 5 nm of Ag. (c) 10 nm of Ag. (d) 20 nm of Ag. The two voltage curves correspond to the parallel and antiparallel cases. Black and blue experimental data stand

Inverse Edelstein effect

Bi/Cu



Edelstein spin torque



Miron, et al, Nature Materials (2010)

Miron, et al, Nature (2011)

Miron, et al, Nature Materials (2011)

Edelstein spin torque

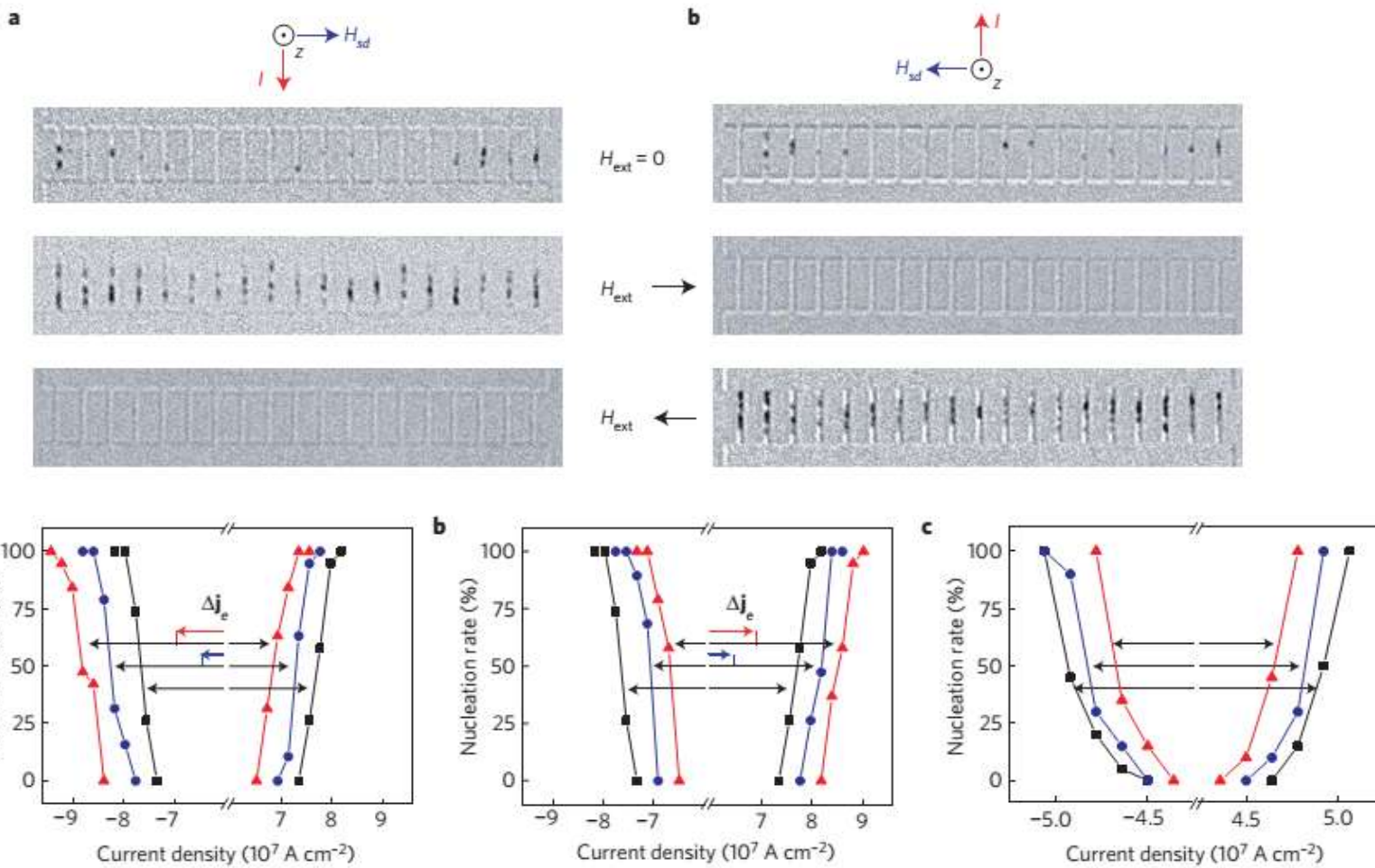
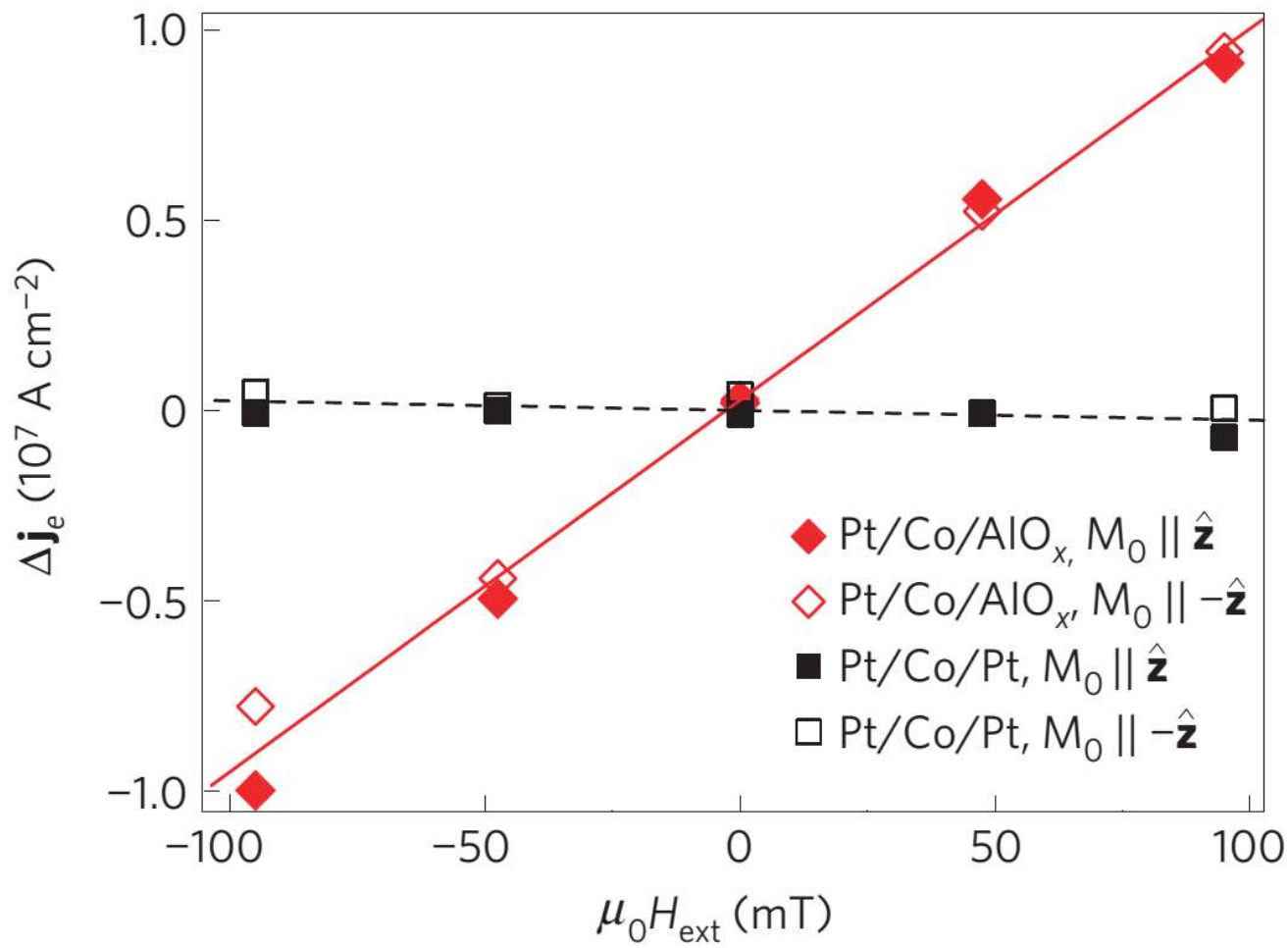
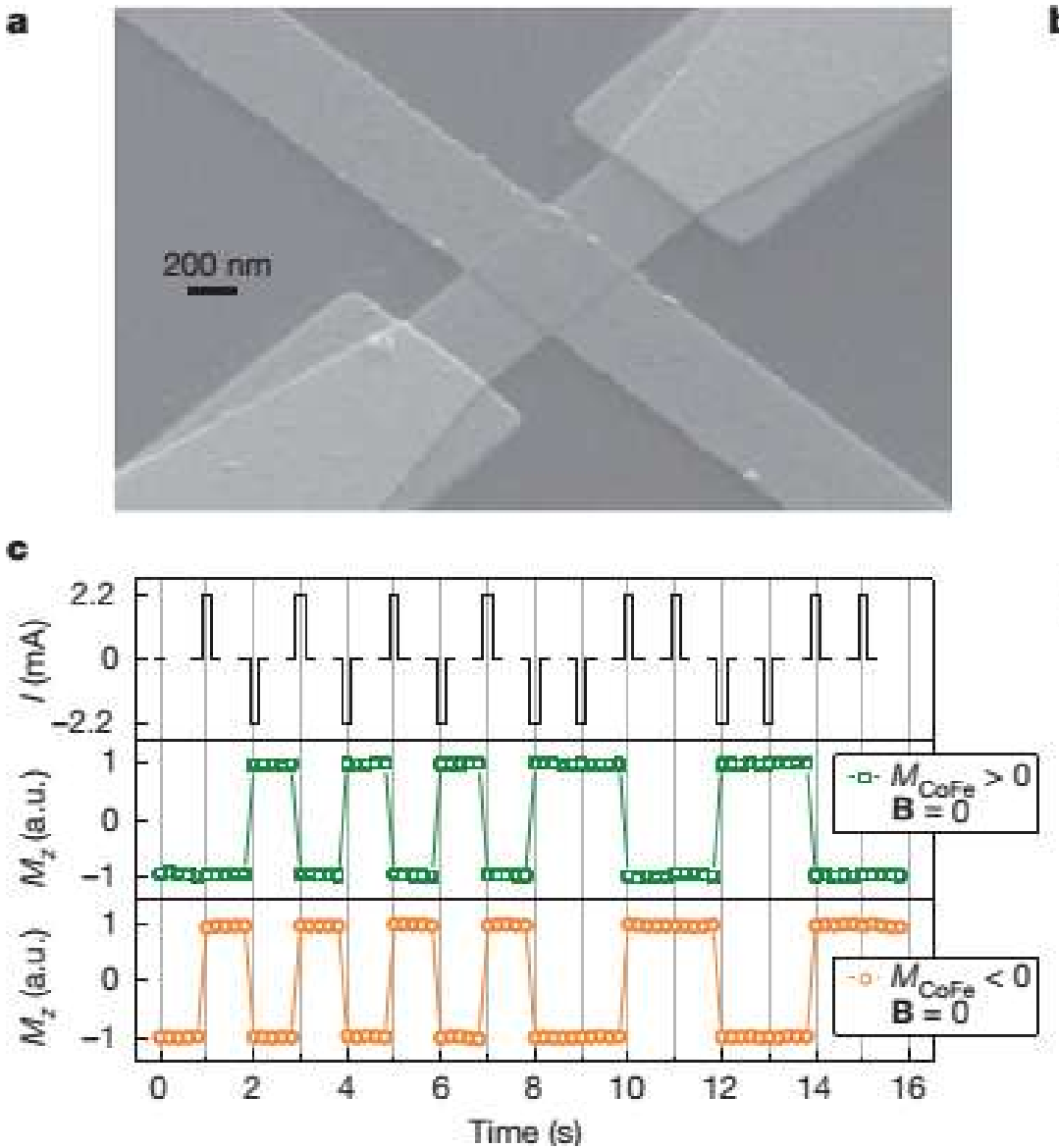


Figure 3 | Percentage of wires that present reversed magnetic domains after the injection of a current pulse as a function of current density and external field. **a,b**, Pt/Co/AlO_x wire array for $H_{ext} \parallel \hat{\mathbf{y}}$ (a) and $H_{ext} \parallel -\hat{\mathbf{y}}$ (b). **c**, Pt/Co/Pt wire array, $H_{ext} \parallel \hat{\mathbf{y}}$. The nucleation rate curves shift by an amount Δj_e proportional to H_{ext} , as indicated by red and blue arrows, reflecting the direction and magnitude of H_{sd} . Values of $\mu_0 H_{ext}$ are 0 mT (black squares), ± 47.5 mT (blue dots), ± 95 mT (red triangles).

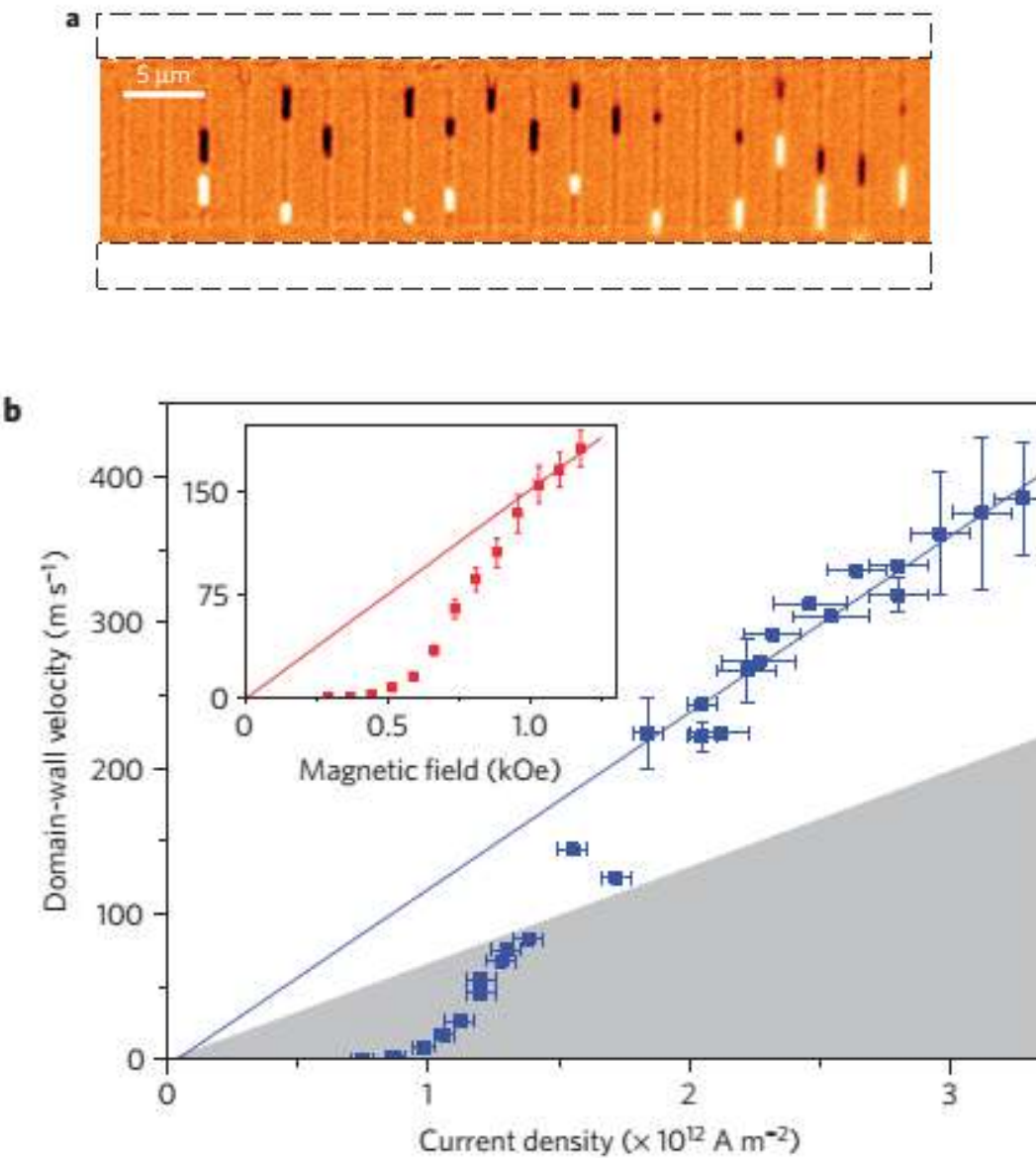
Edelstein spin torque



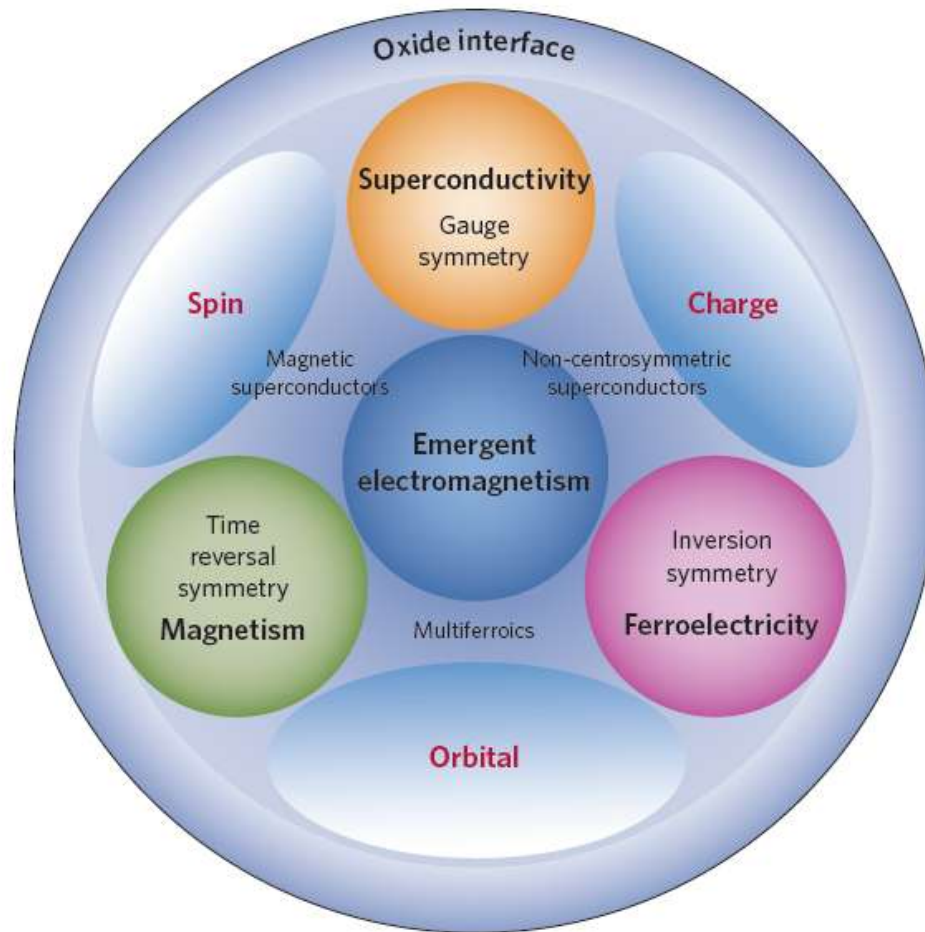
Edelstein spin torque



Edelstein spin torque

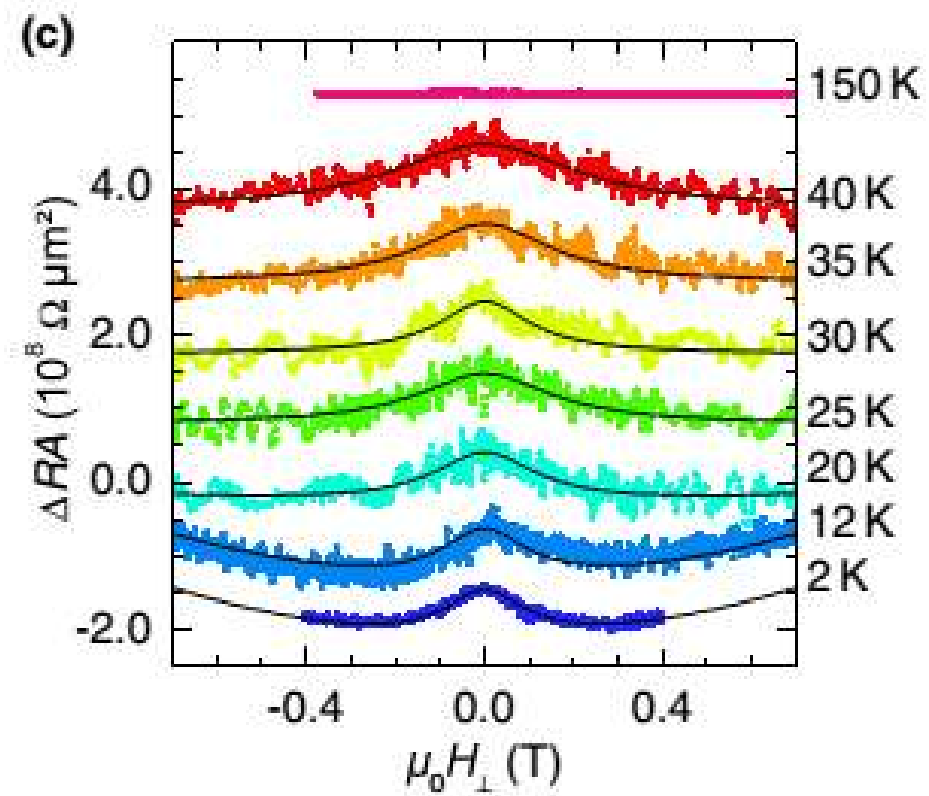
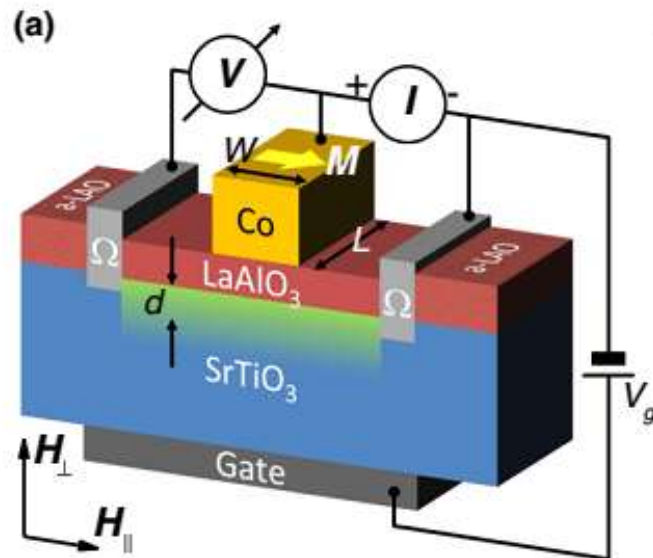


Inverse Edelstein in Oxide interface



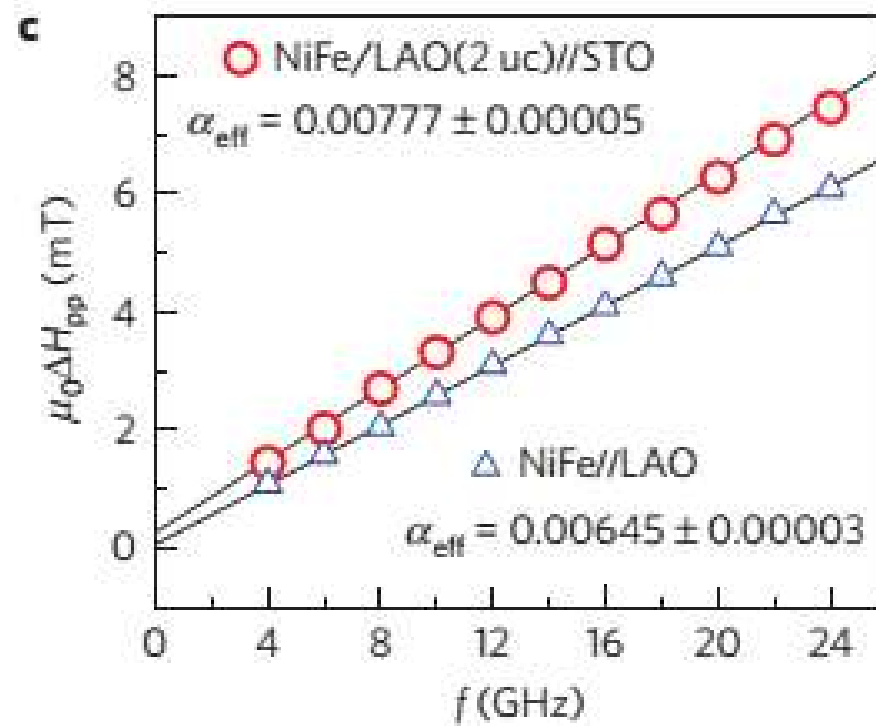
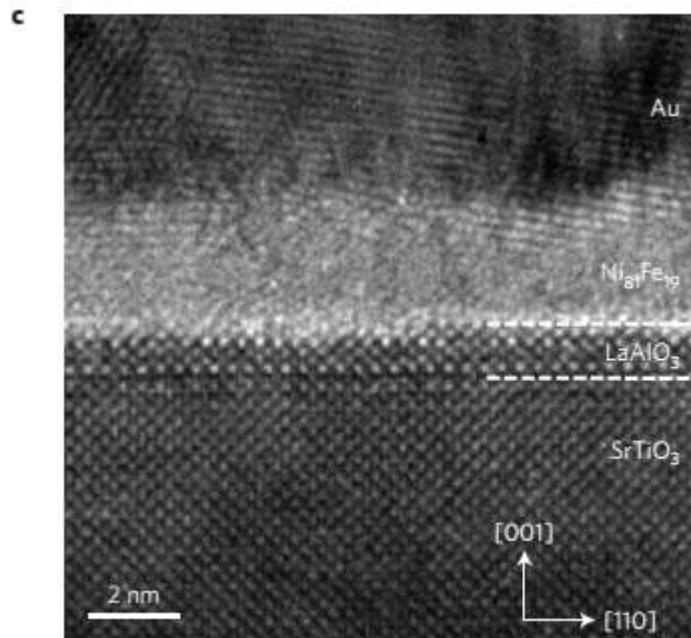
Hwang, et al. Nat. Mater. (2012)

Inverse Edelstein in Oxide interface



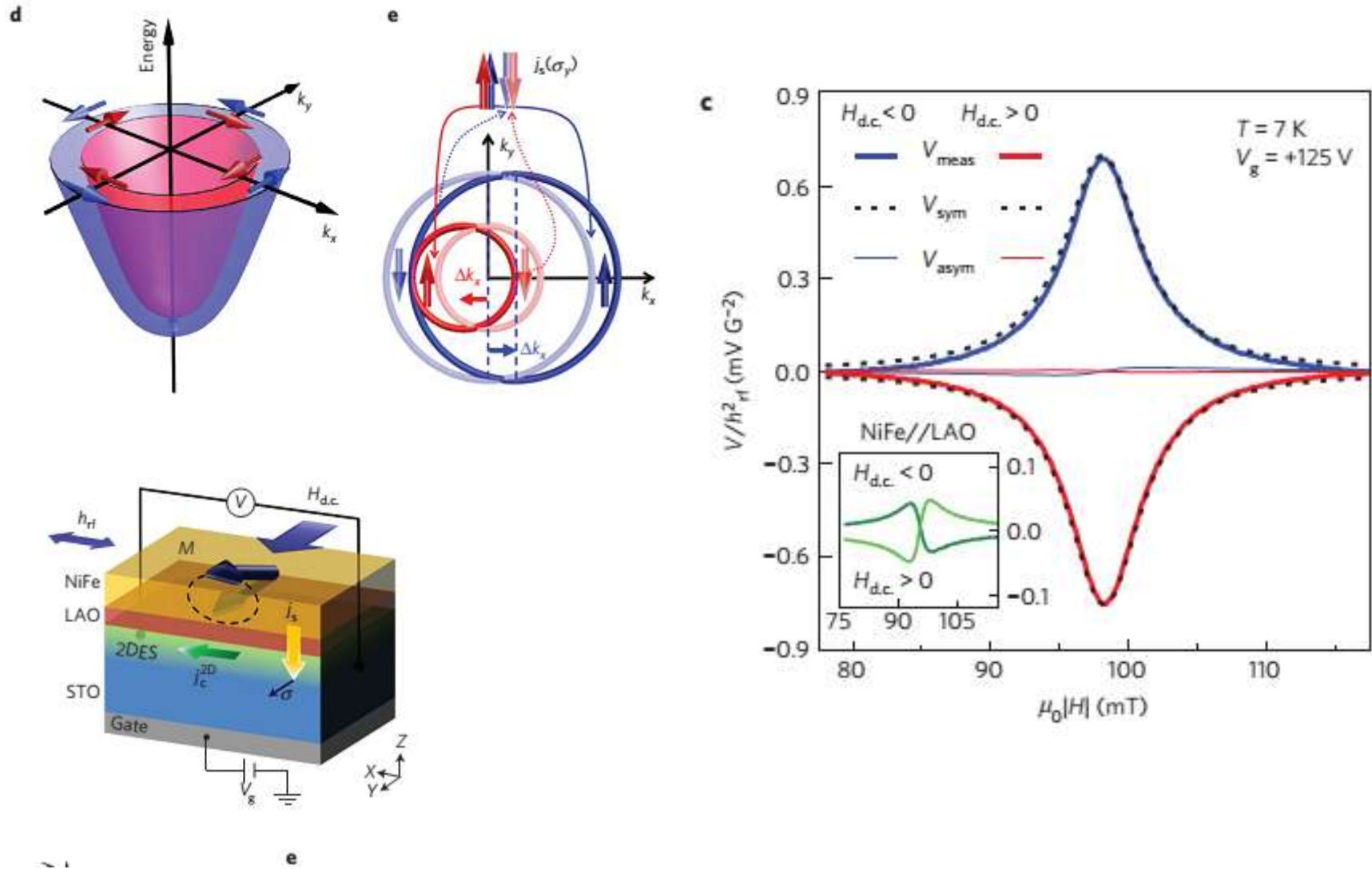
Reyren, et al, PRL (2012)

Inverse Edelstein in Oxide interface

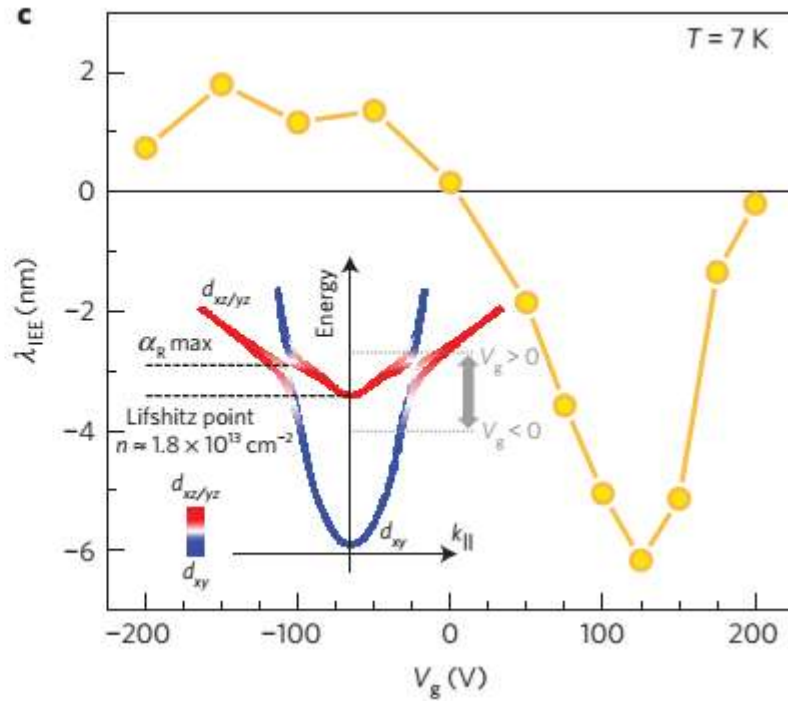
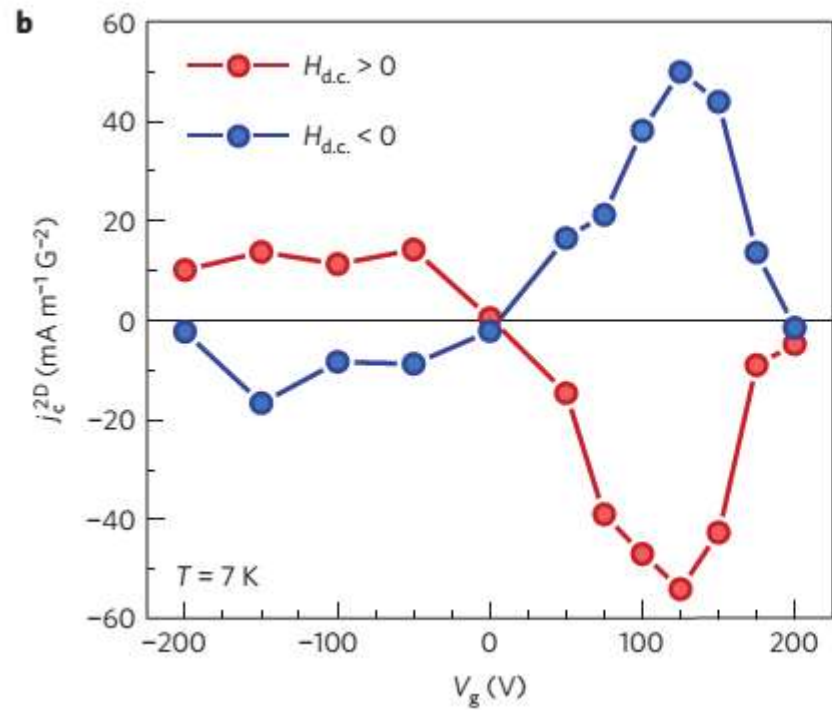


Lesne, et al, Nature Materials (2016)

Inverse Edelstein in Oxide interface

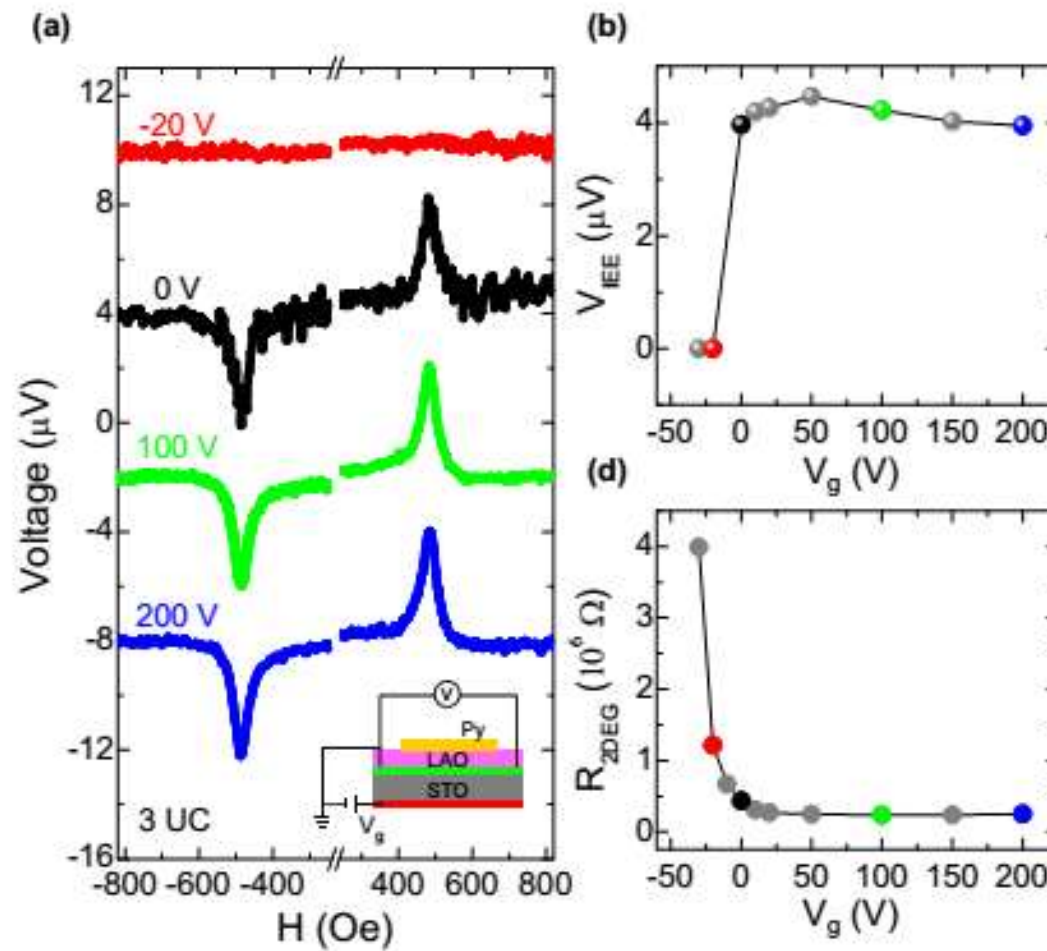
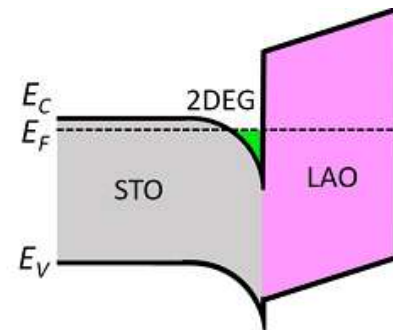


Inverse Edelstein in Oxide interface



Inverse Edelstein in Oxide interface

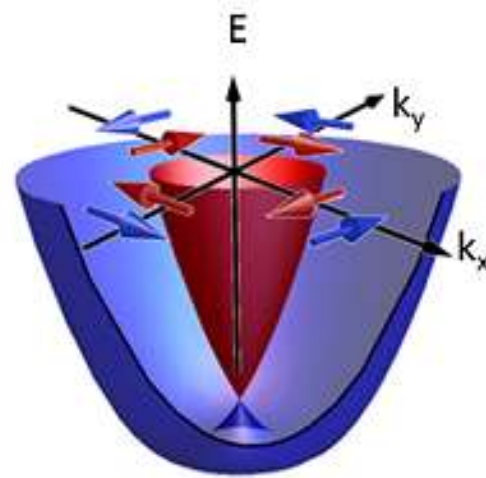
Room temperature



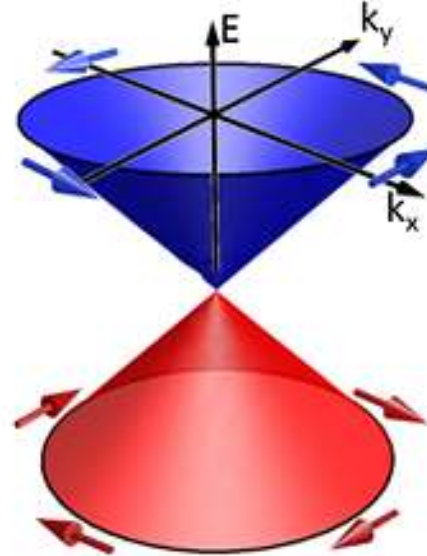
Song, et al, arXiv (2016)

Inverse Edelstein in TI

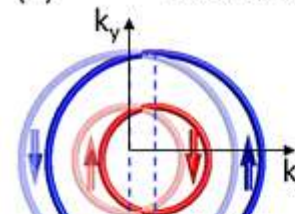
(a) Rashba Interface



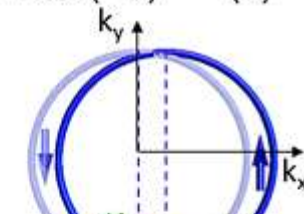
(b) TI Interface



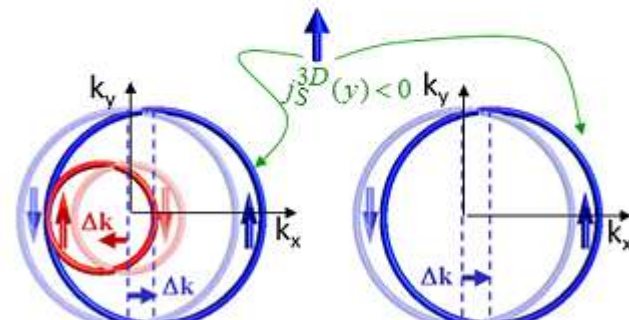
(c) Edelstein Effect (EE)



(d)



(e) Inverse Edelstein Effect (IEE) (f)



$$j_C^{2D} = \lambda_{IEE} j_S^{3D}$$

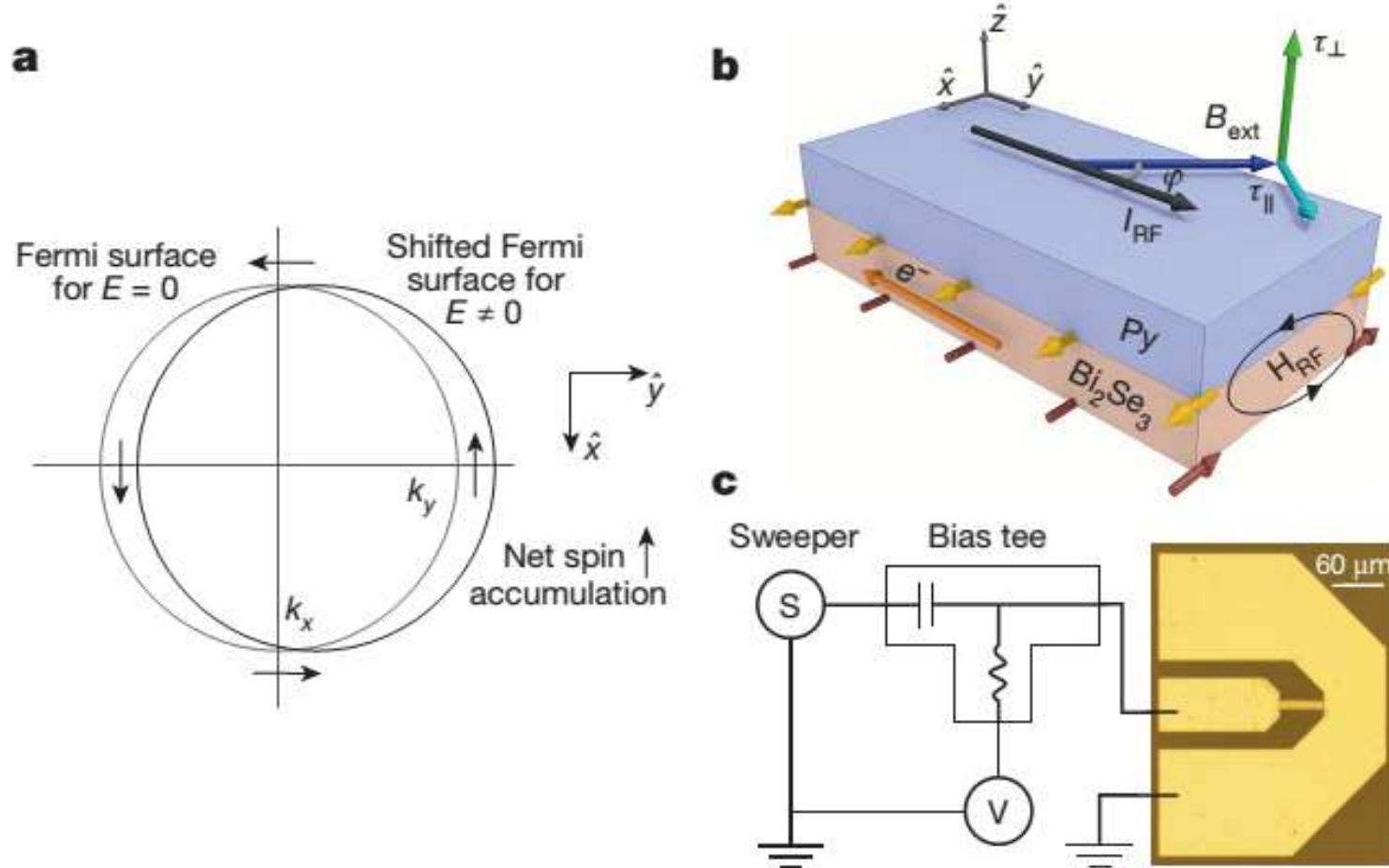
$$\lambda_{IEE} = \frac{\alpha_R \tau}{\hbar}$$

$$j_C^{2D} = \lambda_{IEE} j_S^{3D}$$

$$\lambda_{IEE} = v_F \tau$$

Sanchez, et al. PRL (2016)

Inverse Edelstein in TI



Inverse Edelstein in TI

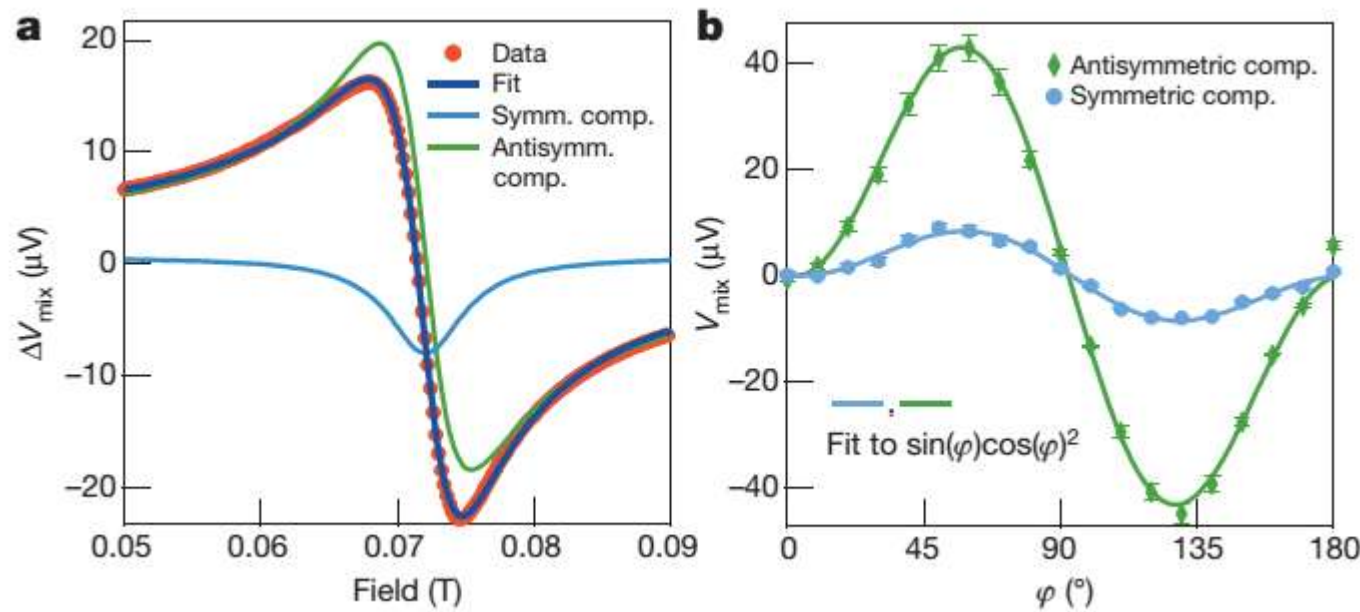
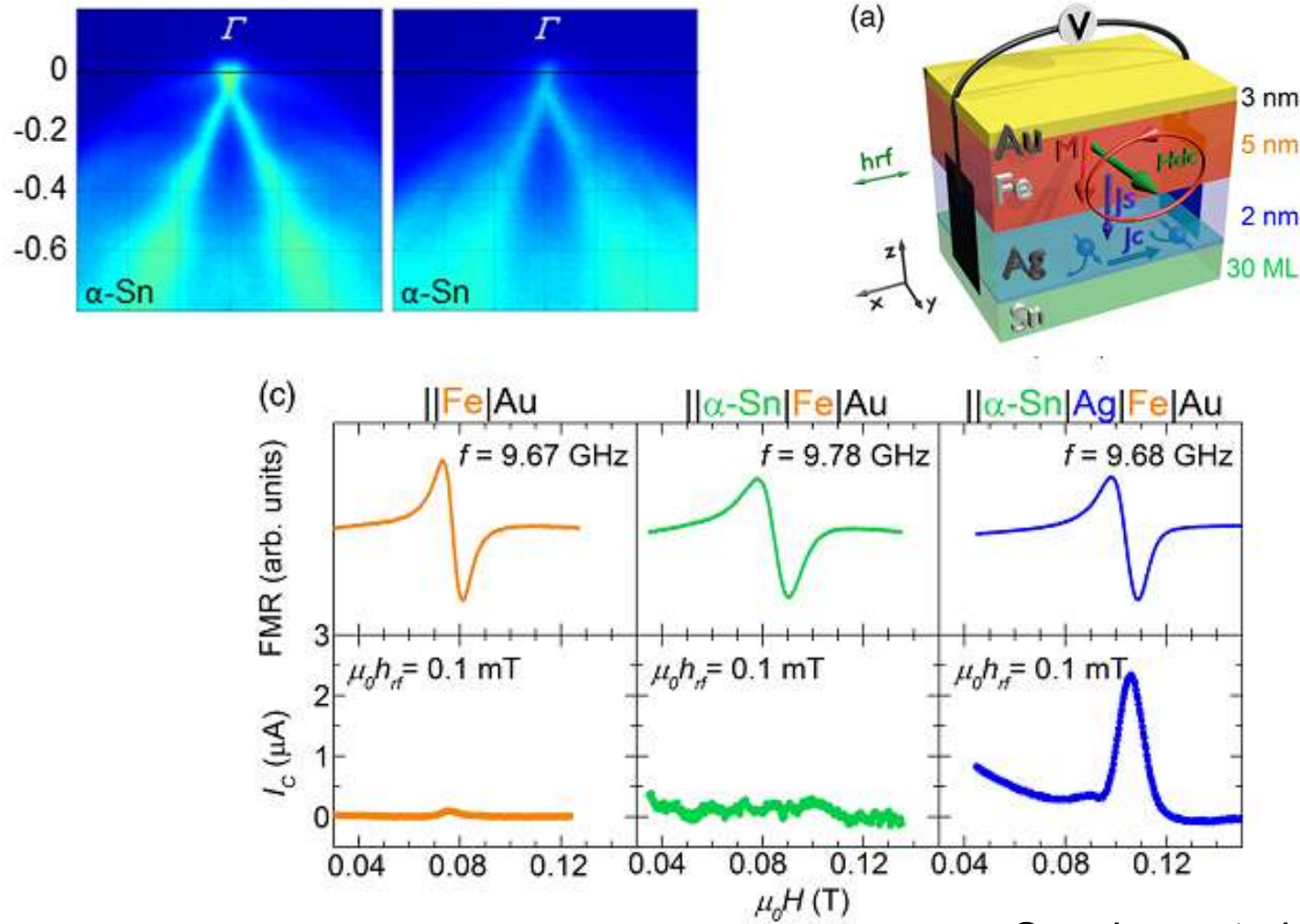


Table 1 | Comparison of room-temperature $\sigma_{s,\parallel}$ and $\theta_{s,\parallel}$ for Bi_2Se_3 with other materials

Parameter	Bi_2Se_3 (this work)	Pt (ref. 4)	$\beta\text{-Ta}$ (ref. 6)	Cu(Bi) (ref. 23)	$\beta\text{-W}$ (ref. 24)
θ_{\parallel}	2.0–3.5	0.08	0.15	0.24	0.3
$\sigma_{s,\parallel}$	1.1–2.0	3.4	0.8	—	1.8

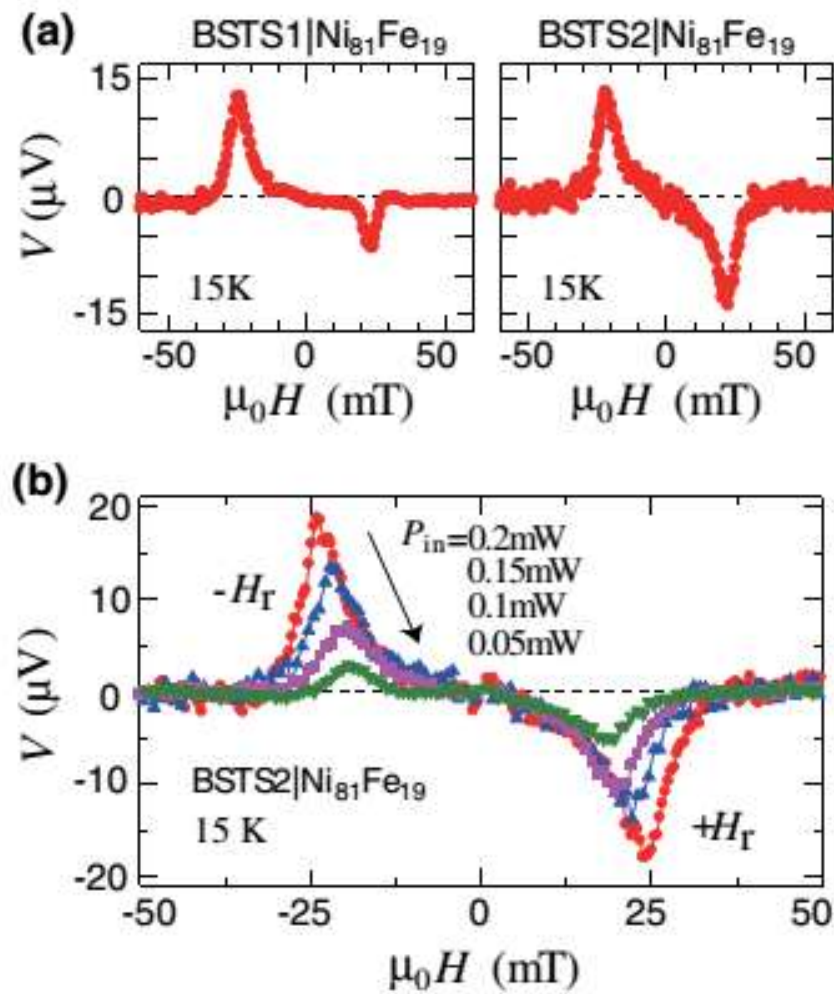
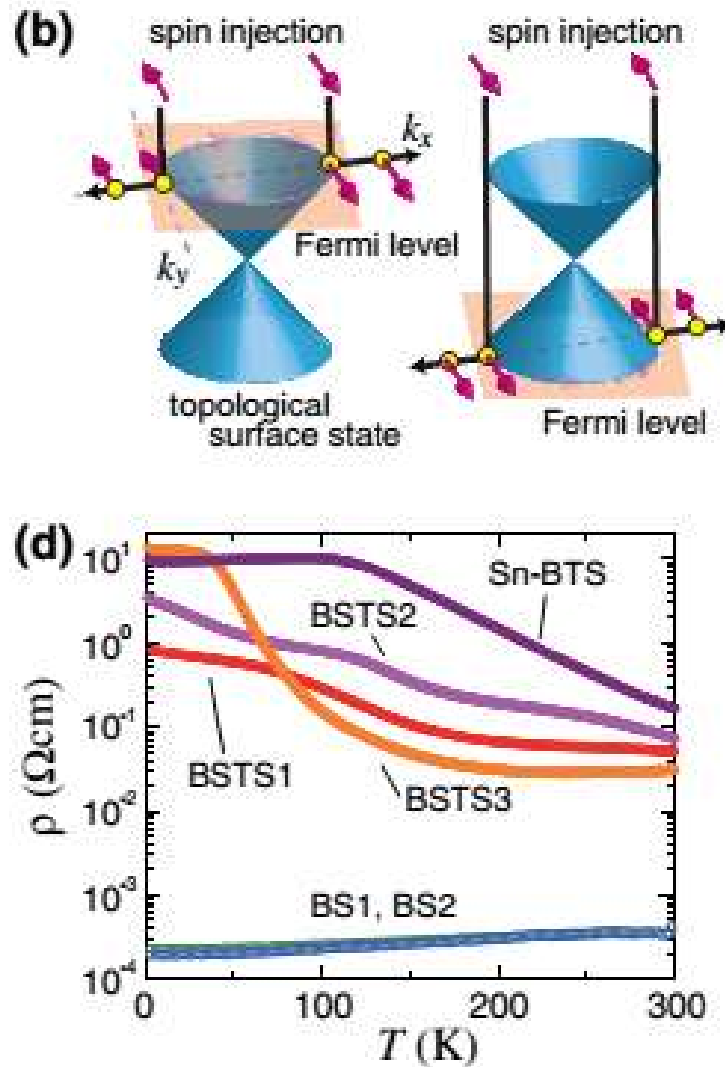
θ_{\parallel} is dimensionless and the units for $\sigma_{s,\parallel}$ are $10^5 \hbar/2e \Omega^{-1} \text{m}^{-1}$.

Inverse Edelstein in TI



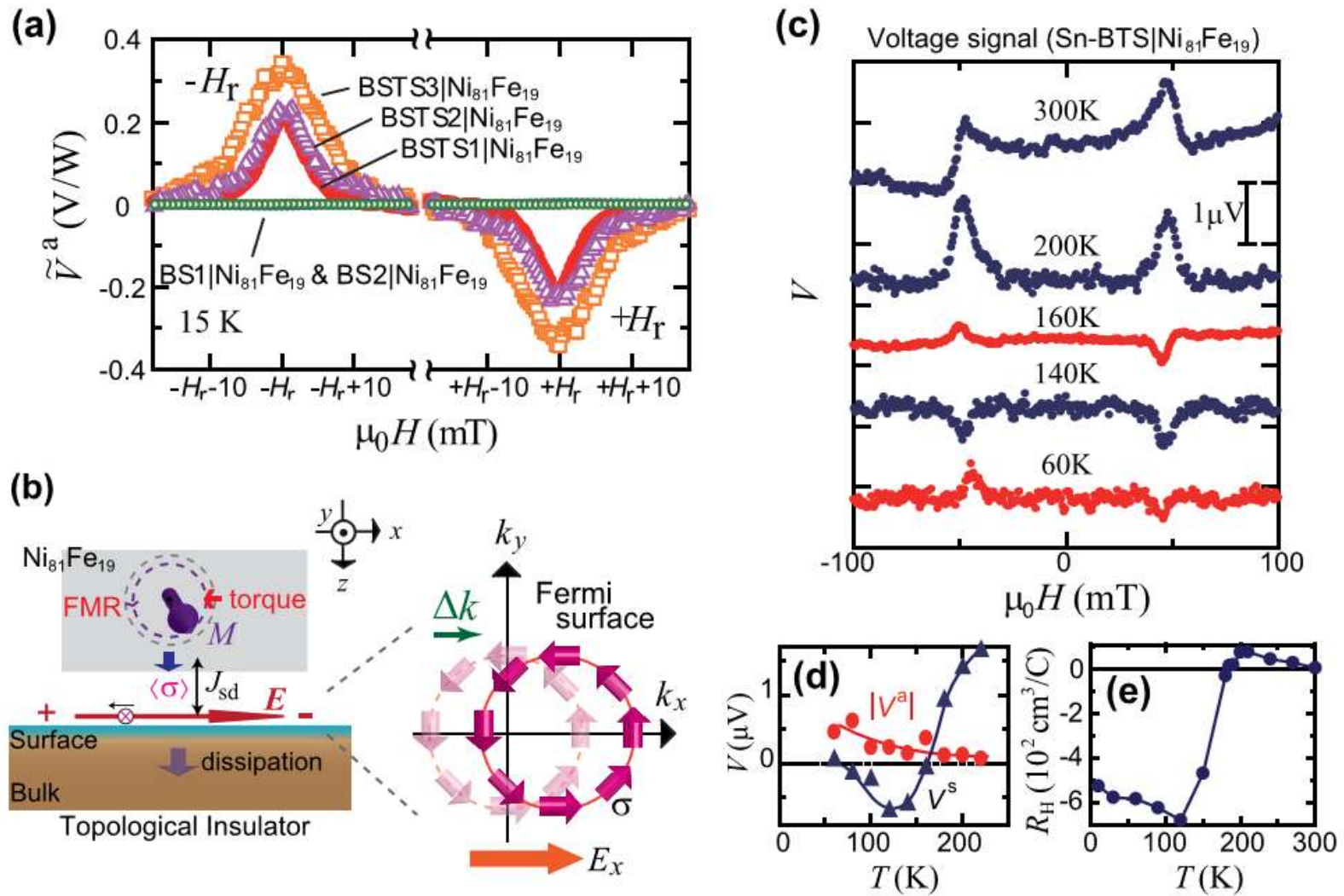
Sanchez, et al. PRL (2016)

Inverse Edelstein in TI



Shiomi, et al. PRL (2016)

Inverse Edelstein in TI



Inverse Edelstein in TI

PRL 113, 196601 (2014)

PHYSICAL RE

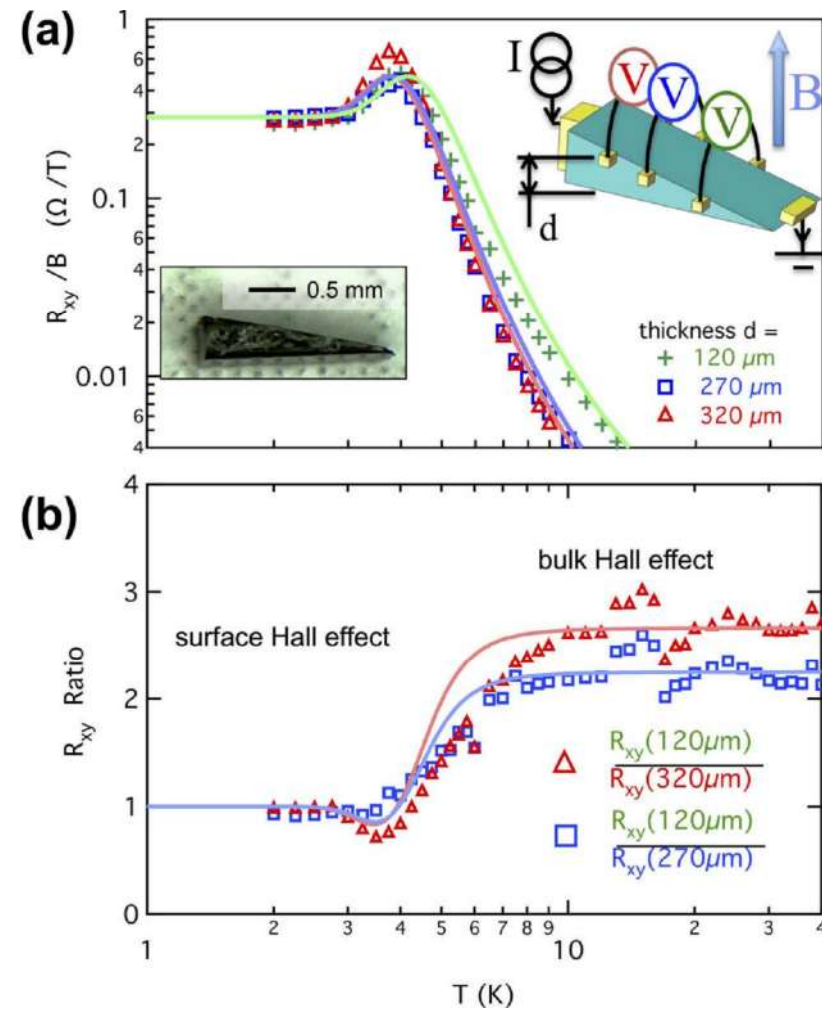
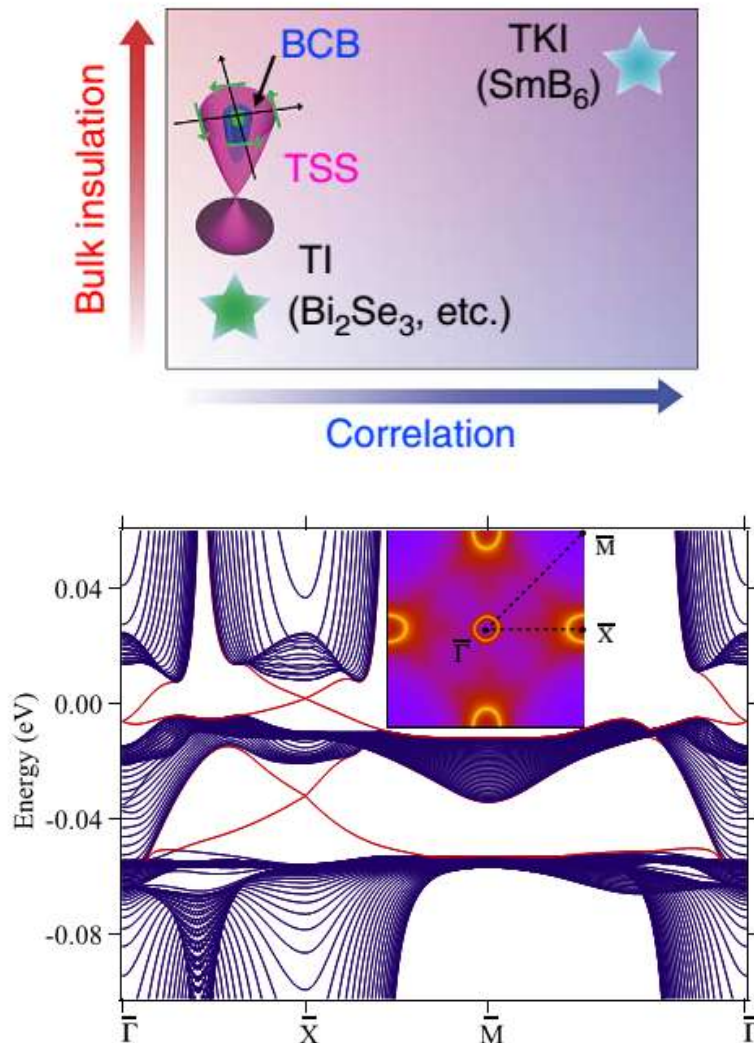
experimental data, the value of η is estimated to be $\sim 10^{-4}$ for BSTS1 and BSTS2. Here, because of imperfect insulation of bulk states, about 15% of the injected spins contribute to the spin-electricity conversion effect [11].

Note that, since the spin pumping induces spin polarization directly on the Fermi level of the surface state, the voltage generation is obviously dominated by the surface spin polarization, in contrast to experiments with circularly polarized light [29,30] where interband excitations generates electron-hole pairs and photocurrents. Also, as already noted, the spin-electricity conversion effect in the present surface-electron system is different from the

Challenge: Conduction from the
Unavoidable bulk states

Inverse Edelstein in TI

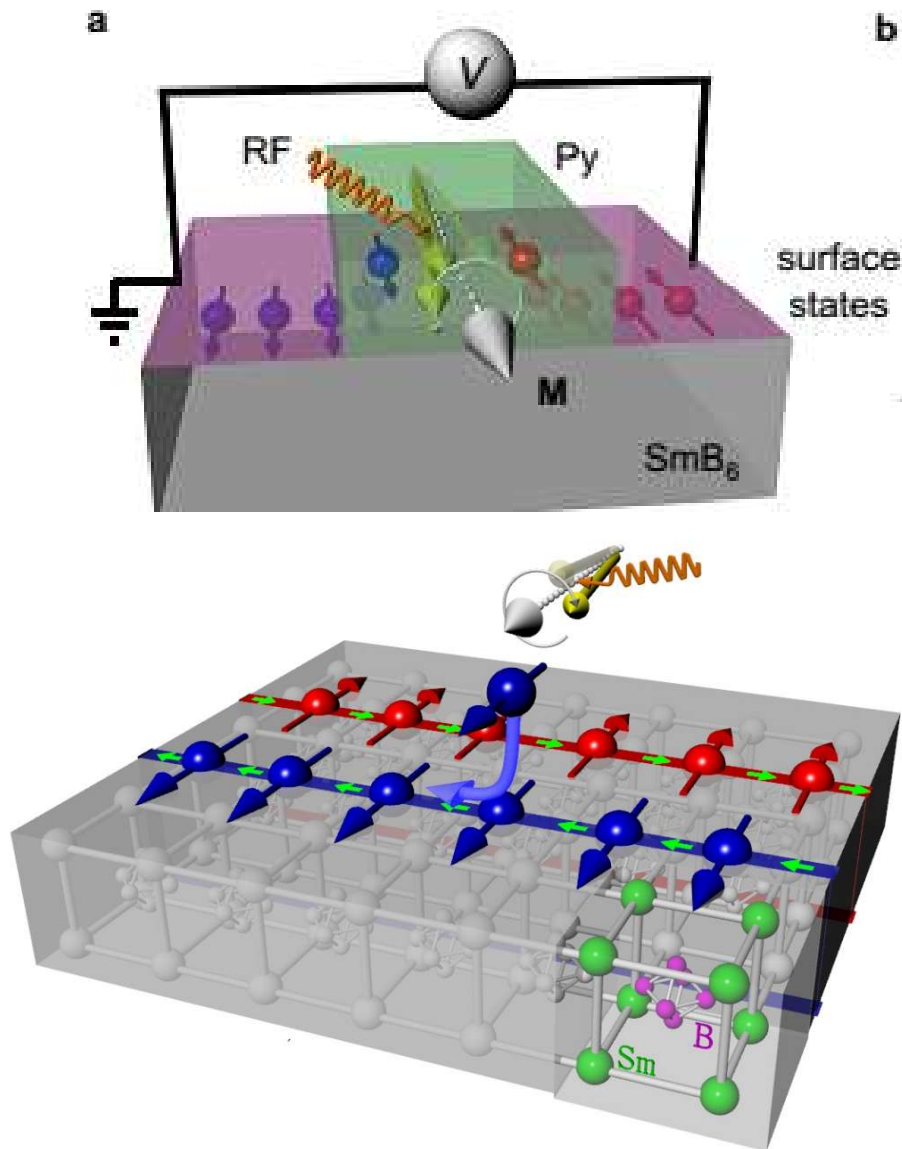
SmB_6 : A topological Kondo insulator



Fu et al., PRL (2013)

Kim et al, Scientific Reports (2013)

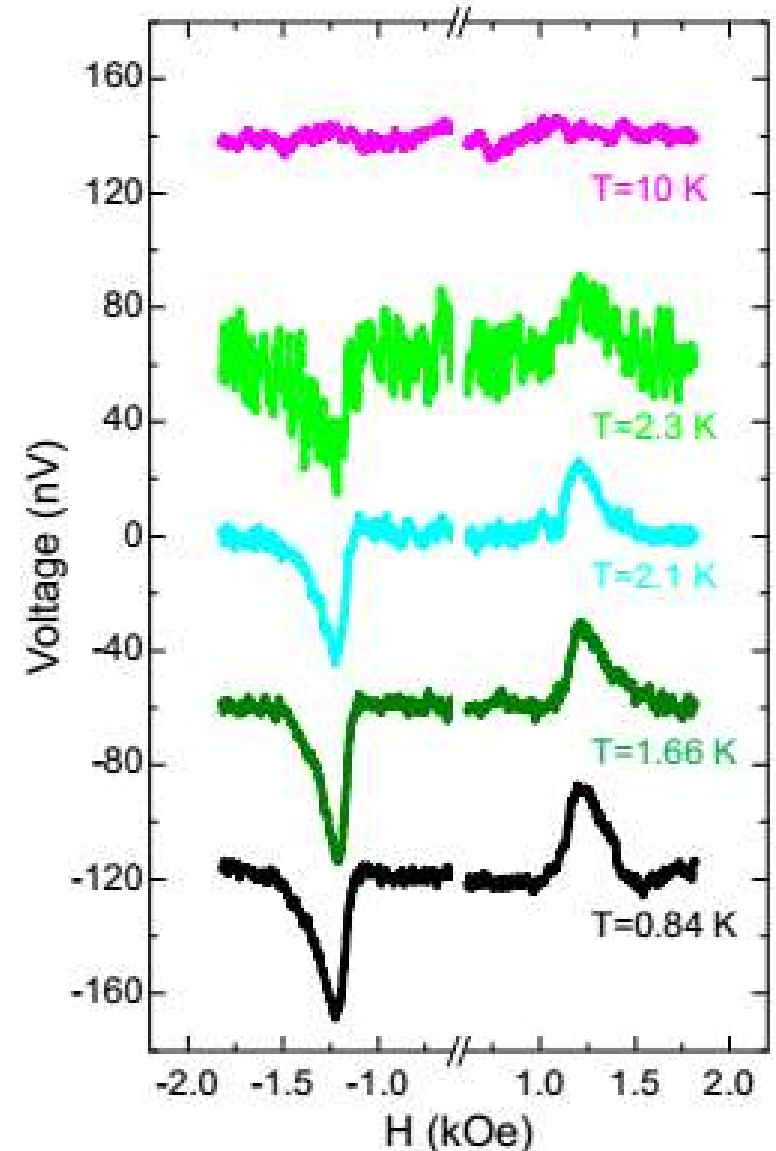
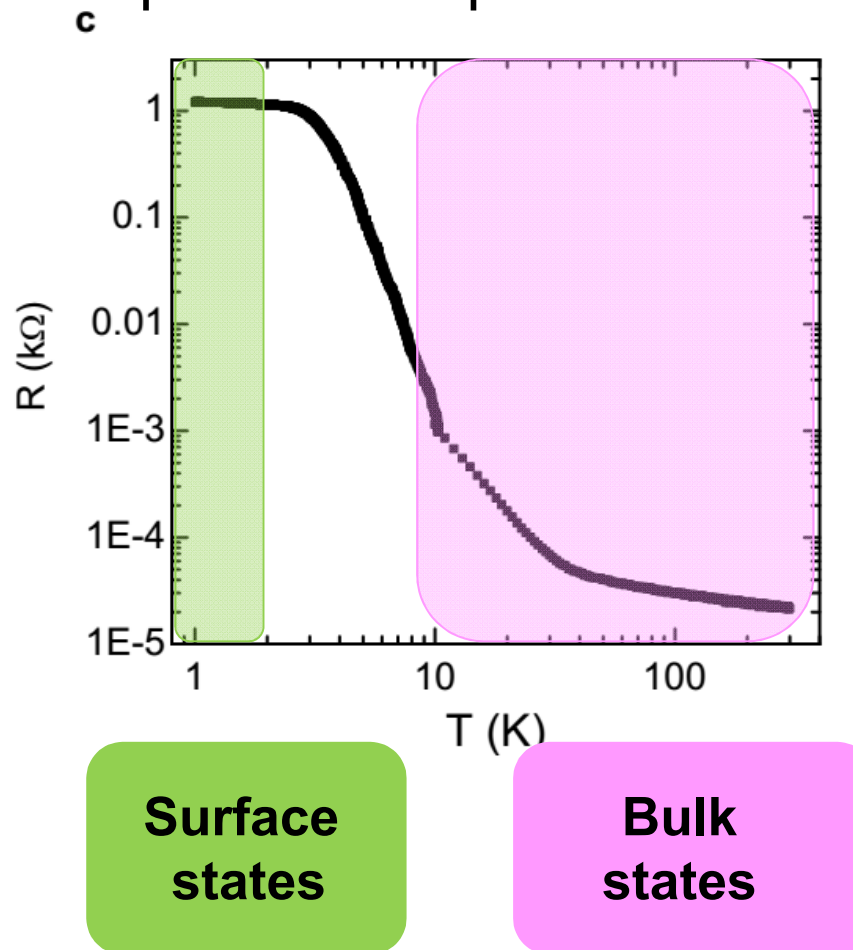
Inverse Edelstein in TI



Song, et al. Nature Commun. (2016)

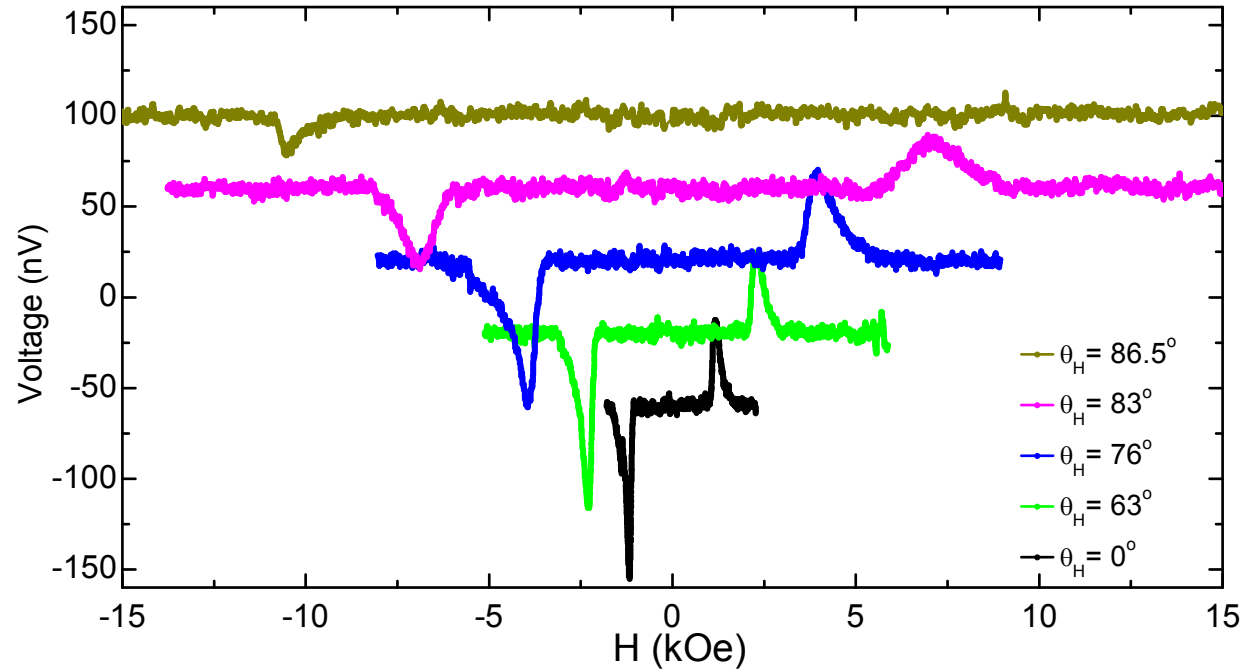
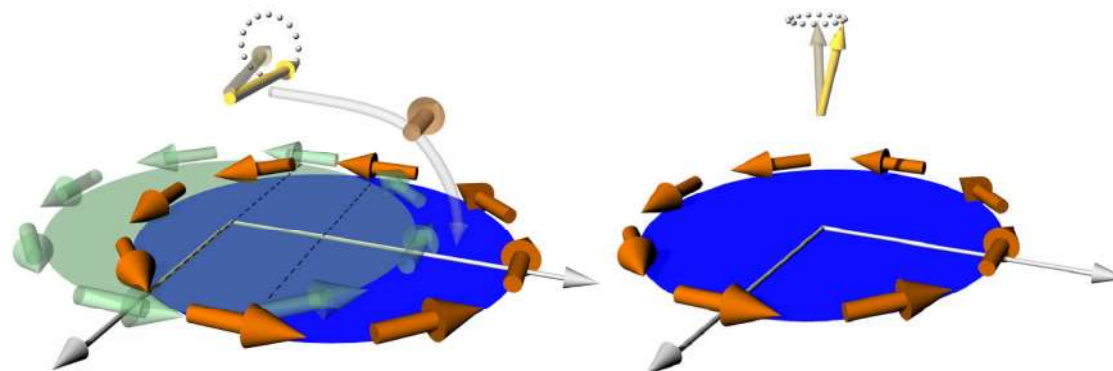
Inverse Edelstein in TI

Temperature dependence



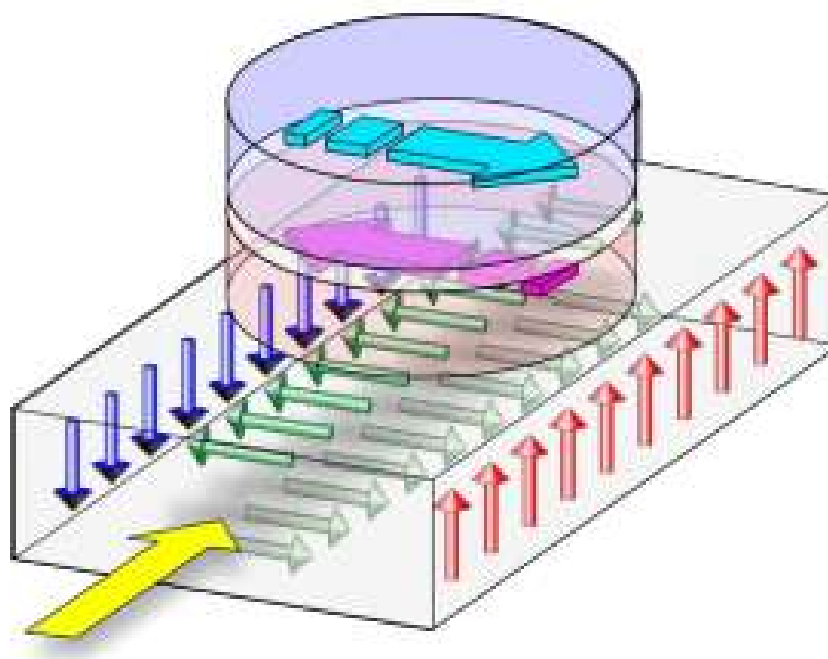
Inverse Edelstein in TI

Angle dependence



Summary of this class

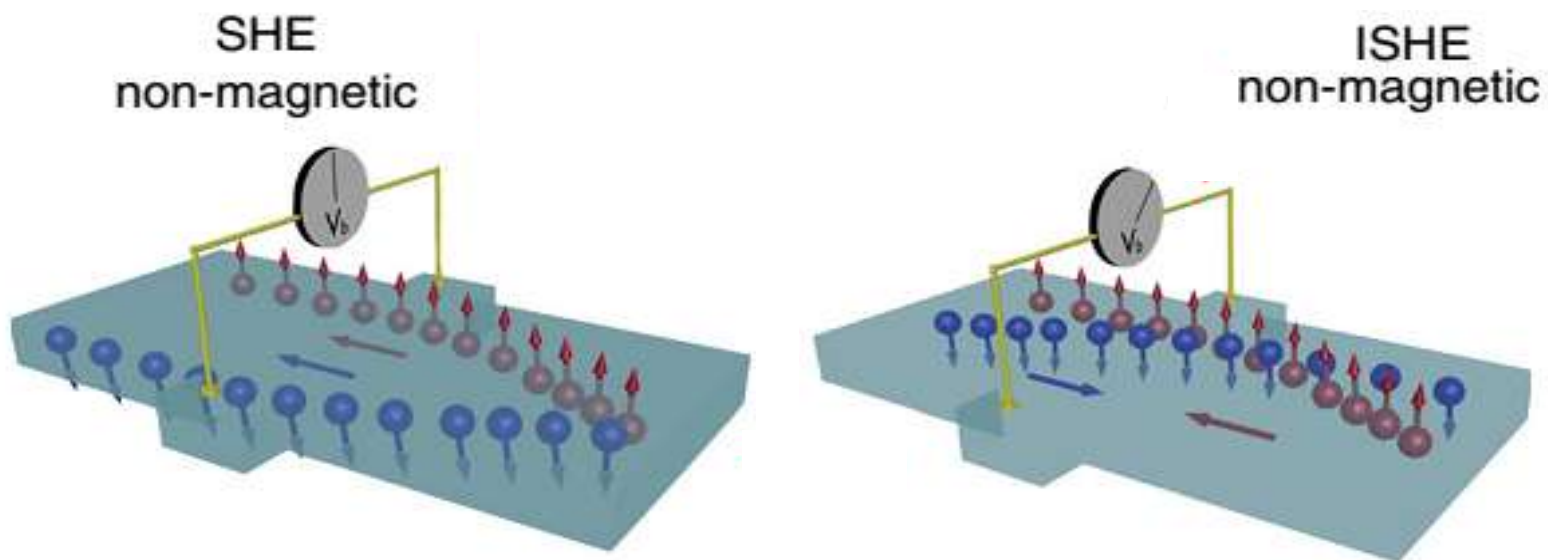
1. Spin orbit torque



$$\tau_{ST} = \frac{\hbar}{2} \hat{m} \times (\hat{\sigma} \times \hat{m})$$

Summary of this class

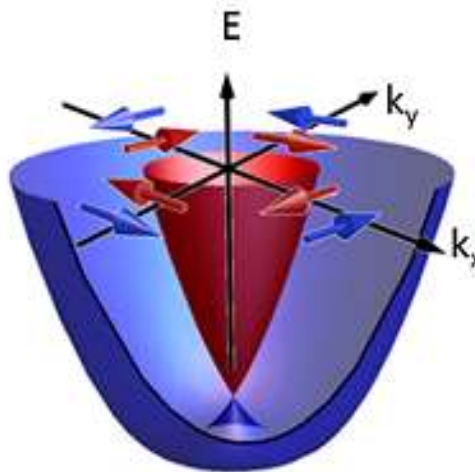
2. Spin Hall effect



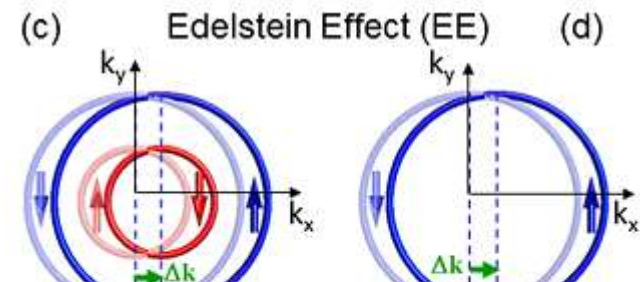
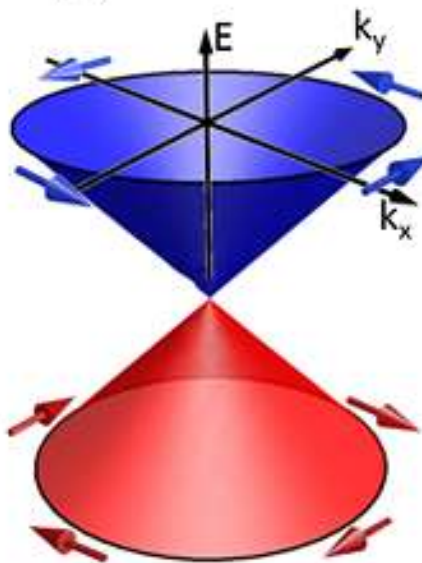
Summary of this class

3. Rashba-Edelstein effect

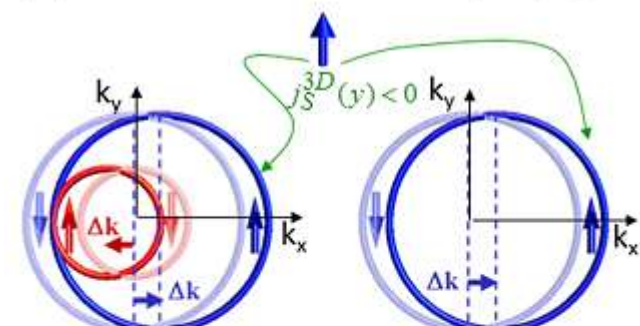
(a) Rashba Interface



(b) TI Interface



(e) Inverse Edelstein Effect (IEE) (f)



$$j_C^{2D} = \lambda_{IEE} j_S^{3D}$$

$$\lambda_{IEE} = \frac{\alpha_R \tau}{\hbar}$$

$$j_C^{2D} = \lambda_{IEE} j_S^{3D}$$

$$\lambda_{IEE} = v_F \tau$$

下一节课: Nov. 22nd

Chapter 6: Spin Caloritronics

课件下载 :

<http://www.phy.pku.edu.cn/~LabSpin/teaching.html>

谢谢！